Università degli Studi di Milano

Dottorato di Ricerca in Medicina Molecolare e Traslazionale
Dipartimento di Scienze della Salute
Ciclo XXXI

TESI DI DOTTORATO DI RICERCA
SSD MED-27

Clinical and molecular bio-markers in skull base chordomas

DOTTORANDO: Dr. Emanuele **LA CORTE**
Matricola n. **R11175**

TUTORE: Prof. Riccardo **GHIDONI**

DIRETTORE DEL DOTTORATO: Prof. Riccardo **GHIDONI**

ANNO ACCADEMICO 2017/2018

To Francesca,
my precious discovery of this PhD and lovely companion of life

To my family, Mommy and Daddy, Bros Gabri, Sis Giuli, Grandmas Chicca and Dora,
founders and supporters of my achievements

To all chordoma patients,
hoping for a definitive cure soon

SOMMARIO

Introduzione. *I cordomi della base cranica sono tumori rari e a lenta crescita derivanti dalla notocorda. La loro morbilità è principalmente legata alla loro invasione locale e alla resistenza ai trattamenti. A causa del loro aspetto eterogeneo e del loro comportamento clinico-molecolare non completamente compreso, l'obiettivo principale del presente lavoro è quello di identificare marcatori clinici e bio-molecolari come fattori prognostici specifici che potrebbero essere utilizzati per la corretta gestione di tali pazienti. Il raggiungimento di una firma prognostica dettagliata dei cordomi del basicranio è di fondamentale importanza per poter personalizzare il trattamento di ciascun paziente. Inoltre, l'analisi degli sfingolipidi sta emergendo come un nuovo approccio in molti tumori e non è mai stata applicata nei cordomi. L'obiettivo principale è lo studio del comportamento biologico del cordoma e il ruolo della produzione di ceramidi in questo contesto di proliferazione e invasione locale.*

Pazienti e Metodi. *È stata eseguita una revisione retrospettiva di tutti i pazienti diagnosticati e trattati per cordoma della base cranica presso la Fondazione IRCCS Istituto Neurologico "Carlo Besta" tra il gennaio 1992 ed il dicembre 2017. Sono stati raccolti dati clinici, radiologici, chirurgici e patologici. È stata eseguita una raccolta prospettica di campioni chirurgici congelati per analizzare le specie di ceramidi. Gli sfingolipidi sono stati estratti dai tessuti congelati; i ceramidi e i diidroceramidi sono stati valutati mediante cromatografia liquida e spettrometria di massa. L'analisi di sopravvivenza è stata eseguita secondo il metodo di Kaplan-Meier. I confronti univariati sono stati condotti usando i test di Mann-Whitney, Chi-square e il test esatto di Fisher. Sono state condotte analisi di regressione e correlazione lineari. Utilizzando un modello di regressione logistica, i predittori statisticamente significativi sono stati pesati sulla base dei loro odds ratio al fine di sviluppare una scala personalizzata - la Peri-Operative Chordoma Scale (POCS).*

Risultati. *Ottantasette pazienti sono stati trattati chirurgicamente per cordoma del basicranio. Settantotto pazienti sono stati dichiarati eleggibili per la revisione. I pazienti erano 38 maschi (48.7%) e 40 femmine (51.3%). Il follow-up medio era di 69 mesi (intervallo, 3-233). Sono stati eseguiti centoquattordici interventi chirurgici. La presenza di deficit motori si è rivelata essere un fattore prognostico significativo correlato a una PFS peggiore (p=0.0480). La presenza di calcificazioni ha mostrato una correlazione con risultati migliori di OS rispetto al tumore privo di calcificazioni (p=0.0420). Il grado di impregnazione contrastografica alla RM si è rivelato essere un fattore prognostico significativo in termini sia di OS che di PFS (p≤0.0001 e 0.0010, rispettivamente). Il coinvolgimento del forame giugulare e delle cisterne anteriori al tronco encefalico si sono rivelati due fattori prognostici significativi correlati con una riduzione di PFS (p=0.0130 e p=0.0210, rispettivamente). La dislocazione del tronco cerebrale rappresentava un fattore prognostico significativo correlato a peggiore OS e PFS nella coorte di cordomi recidivi (p=0.0060 e 0.0030, rispettivamente). L'estensione della resezione tumorale rappresentava un forte fattore prognostico secondo la PFS nella coorte di cordomi primari (p=0.0200). I pazienti operati da un chirurgo esperto (definito come il chirurgo che ha eseguito più di 10 procedure chirurgiche per cordoma del basicranio nella presente serie) hanno avuto un outcome migliore in termini di PFS nella coorte di pazienti primari (p=0.0340). Lo sviluppo di complicanze post-operatorie in pazienti con cordoma primario rappresentava un importante fattore prognostico correlato sia ad OS che a PFS (p≤0.0001 e 0.0360, rispettivamente). Nella coorte di cordomi recidivi, ∆KPS*

correlava sia a OS che a PFS (p=0.0010 e 0.0180, rispettivamente). Inoltre, il trattamento radioterapico postoperatorio correlava ad un aumento di OS e PFS (p=0.0020 e p=0.0100, rispettivamente). I seguenti fattori si sono rivelati predittori statisticamente significativi sia di PFS che di OS nel modello di regressione logistica: il grado di impregnazione contrastografica alla RM (intenso o lieve/nessuno), la presenza di deficit motori preoperatori (si o no) e lo sviluppo di complicanze post-operatorie (si o no). Una scala è stata sviluppata con score compresi tra 0 e 17 (Nagelkerke's pseudo R^2=0.656). Le specie totali di ceramidi e diidroceramidi nei cordomi primari erano 808.4±451.4 pmol/mg di proteine (522.5-1760.2) e 30.7±16.4 pmol/mg (17.6-62.4), rispettivamente. Le specie totali di ceramidi e diidroceramidi nei cordomi recidivi erano 1488.1±763.8 pmol/mg (540.7-2787.5) e 67.2±45.5 pmol/mg (9.0-145.6), rispettivamente. Le specie totali di ceramidi erano significativamente più elevate nei cordomi recidivi sottoposti a precedente resezione chirurgica e radioterapia rispetto ai cordomi primari (p=0.0496). Le specie totali di ceramidi e diidroceramidi nel gruppo "intensa impregnazione contrastografica" erano 1597.6±737.8 pmol/mg (592.7-2787.5) e 69.1±45.0 pmol/mg (17.8-145.6), rispettivamente. Le specie totali di ceramidi e diidroceramidi nel gruppo "nessuna o lieve impregnazione contrastografica" erano 664.7±120.4 pmol/mg (522.5-826.0) e 31.5±13.6 pmol/mg (17.6-53.6), rispettivamente. Ceramidi e diidroceramidi totali erano significativamente più alti nei cordomi ad "intensa impregnazione contrastografica" rispetto ai cordomi "nessun o lieve impregnazione contrastografica" (p=0.0290 e p=0.0186, rispettivamente). Analizzando l'associazione tra livelli di ceramidi e MIB-1 all'interno di ciascun paziente con cordoma della base cranica, i livelli di ceramidi totali hanno mostrato un'associazione forte (r=0.7257, r^2=0.5267) con la colorazione MIB-1 (p=0.0033). Analizzando l'associazione tra i livelli di diidroceramidi e MIB-1 all'interno di ciascun paziente con cordoma della base cranica, i livelli totali di diidroceramidi hanno mostrato anche un'associazione forte (r=0.6733, r^2=0.4533) con MIB-1 (p=0.0083). Tra le singole specie di ceramidi, Cer C24: 1 (r=0.8814, r^2=0.7769, p≤0.0001), DHCer C24: 1 (r=0.8429, r^2=0.7104, p=0.0002) e DHCer C18:0 (r=0.9426, r^2=0.8885, p≤0.0001) hanno mostrato una correlazione significativa con il MIB-1.

***Conclusioni**. L'analisi clinica ha dimostrato che la sintomatologia preoperatoria (deficit motori e a carico dei nervi cranici), la posizione anatomica (forame giugulare, dislocazione del tronco encefalico), le caratteristiche chirurgiche (estensione della resezione tumorale ed esperienza del chirurgo operatore), la presenza di complicanze postoperatorie e il declino del KPS si sono rivelati fattori prognostici significativi. Inoltre, il grado d'impregnazione contrastografica alla RM è stato significativamente correlato sia a OS che a PFS. È stata sviluppata in via preliminare la Peri-Operative Chordoma Scale (POCS) per aiutare il clinico nella gestione personalizzata del paziente che si sottoporrà a potenziali terapie adiuvanti. L'analisi di sfingolipidi, invece, ha evidenziato come i ceramidi possano rappresentare un promettente bio-marcatore nei cordomi. In particolare, i ceramidi a catena lunga e molto lunga, come Cer C24:1 e DHCer C18:0, possono concorrere ad una prolungata sopravvivenza del tumore, aggressività e l'effettiva comprensione del loro ruolo biologico potrà far luce sui possibili meccanismi di radio-resistenza, tendenza a recidivare del cordoma e allo sviluppo di agenti che possano avere come target il metabolismo dei ceramidi. Tali risultati dovrebbero essere validati in futuri studi clinici, in vitro e in vivo più ampi per confermare questo intricato legame tra il comportamento aggressivo del cordoma e dei ceramidi.*

ABSTRACT

Introduction. *Skull base chordomas are rare slow-growing neoplasms that arise from notochord. Their morbidity is mainly related to highly aggressive local invasion and resistance to treatments. Due to its heterogeneous appearance and not fully understood clinical and molecular behaviors, the main goal of the present work is to identify clinical and bio-molecular markers as specific prognostic factors that could be used for the management of skull base chordoma patients. Achieving a detailed prognostic signature of skull base chordomas is of paramount importance to personalize the treatment to each specific patient. Moreover, sphingolipids analysis is emerging as a new approach in many cancers and it has never been applied in chordomas. Our aim is to investigate chordoma biological behavior and the role of ceramides production in this context of proliferation and invasion.*

Patients and Methods. *A retrospective review of all the patients diagnosed and treated for a skull base chordoma at the Fondazione IRCCS Istituto Neurologico "Carlo Besta" between January 1992 and December 2017 has been performed. Clinical, radiological, surgical and pathological data have been collected. A prospective collection of frozen surgical specimens has been performed to analyze ceramides species in chordomas. Sphingolipids were extracted from frozen tissues and total ceramides and dihydroceramides were evaluated by liquid chromatography and mass spectrometry. Survival analysis was performed according to Kaplan-Meier method. Univariate comparisons were conducted using Mann-Whitney, Chi-square and exact Fisher test. Simple linear regression and correlation with computation of Pearson coefficients analyses were conducted. Using a logistic regression model, statistically significant predictors were rated based on their odds ratios in order to build a personalized grading scale – the Peri-Operative Chordoma Scale (POCS).*

Results. *Eighty-seven consecutive patients were surgically treated for a skull base chordoma during the period of recruitment. Seventy-eight patients were eligible for the retrospective review. There were 38 males (48.7%) and 40 females (51.3%). The mean follow-up was 69 months (range, 3–233). One-hundred-fourteen surgical operations were performed in the initial recruitment or recurrent setting. The presence of motor deficits in skull base chordoma revealed to be a significant prognostic factor correlating with a worse PFS (p=0.0480). Calcification on KM analysis showed a correlation with better outcomes (OS) compared with tumor lacking any calcification on CT scan (p value=0.0402). The degree of MR contrast enhancement revealed to be a significant and strong prognostic factor in terms of OS and PFS (p≤0.0001 and 0.0010, respectively). Jugular foramen involvement represented a significant prognostic factor with a worse PFS in the cohort of primary skull base chordomas (p=0.0130). The presence of chordoma in the pre-brainstem cistern revealed to be a significant prognostic factor with a worse PFS in the cohort of recurrent skull base chordomas (p=0.0210). Brainstem dislocation represented a significant prognostic factor correlating with a both worse outcome in terms of OS and PFS in the cohort of recurrent skull base chordomas (p=0.0060 and 0.0030). Extent of resection represents a strong prognostic factor according to PFS in the cohort of primary skull base chordomas (p=0.0200). Patients operated by an experienced chordoma surgeon did better in terms of prolonged PFS in the cohort of primary patients (p=0.0340). Development of post-operative complications in primary skull base chordoma patients represented an important prognostic factor related to both OS and PFS (p≤0.0001 and 0.0360, respectively). In the cohort of*

recurrent chordomas, ΔKPS correlated to both OS and PFS (p=0.0010 and 0.0180, respectively). Moreover, post-operative radiation treatment correlated with prolonged OS (p=0.0020) and PFS (p=0.0100). The following factors were found to be statistically significant predictors of both PFS and OS in the logistic regression model: MR contrast enhancement (intense vs mild/no), preoperative motor deficit (yes vs no) and the development of any post-operative complications (yes vs no). A grading scale was obtained with scores ranging between 0 and 17 (Nagelkerke's pseudo R^2=0.656). The mean total ceramides and dihydroceramides species in primary chordomas were 808.4±451.4 pmol/mg (522.5-1760.2) and 30.7±16.4 pmol/mg (17.6-62.4), respectively. The mean total ceramides and dihydroceramides species in recurrent chordomas were 1488.1±763.8 pmol/mg (540.7-2787.5) and 67.2±45.5 pmol/mg (9.0-145.6), respectively. Total ceramides species were significantly higher in recurrent chordomas that underwent previous surgical resection and radiation therapy in comparison to the primary chordomas (p=0.0496). The mean total ceramides and dihydroceramides species in "intense enhancement" group were 1597.6±737.8 pmol/mg (592.7-2787.5) and 69.1±45.0 pmol/mg (17.8-145.6), respectively. The mean total ceramides and dihydroceramides species in "no or mild enhancement" group were 664.7±120.4 pmol/mg (522.5-826.0) and 31.5±13.6 pmol/mg (17.6-53.6), respectively. Total ceramides and dihydroceramides were significantly higher in "intense enhancement" chordomas in comparison to the "no/mild enhancement" chordomas (p=0.0290 and p=0.0186, respectively). Analyzing the association between ceramides level and MIB-1 within each skull base chordoma patient, total ceramides level showed a strong association (r=0.7257, r^2=0.5267) with MIB-1 staining (p=0.0033). Analyzing the association between DHCer level and MIB-1 within each skull base chordoma patient, total DHCer level showed also strong association (r=0.6733, r^2= 0.4533) with MIB-1 staining (p= 0.0083). Among the single ceramides species Cer C24:1 (r=0.8814, r^2=0.7769, p≤0.0001), DHCer C24:1 (r=0.8429, r^2=0.7104, p=0.0002) and DHCer C18:0 (r=0.9426, r^2=0.8885, p≤0.0001) levels showed a significant correlation with MIB-1 staining. Final candidate predictive factors that well fitted the regression model were: cer24:1 (r=0.824, p≤0.001), and DHCer C18:0 (r=0.748, p=0.002).

***Conclusion**. Our clinical analysis showed that pre-operative clinical symptoms (motor and cranial nerve deficits), anatomical location (jugular foramen, pre-brainstem cisterns and brainstem dislocation), surgical features (extent of tumor resection and surgeon's experience), development of post-operative complications and KPS decline represent significant prognostic factors. The degree of MR contrast enhancement significantly correlated to both OS and PFS. We also preliminarily developed the Peri-Operative Chordoma Scale (POCS) to aid the practitioner in the personalized management of patients undergoing potential adjuvant therapies. Our lipid analysis showed ceramides as promising tumoral bio-markers in skull base chordomas. Long and very long chain ceramides, such as Cer C24:1 and DHCer C24:1, may be related to a prolonged tumor survival, aggressiveness and the understanding of their effective biological role will hopefully shed lights on the mechanisms of chordoma radio-resistance, tendency to recur and use of agents targeting ceramide metabolism. Such results should be validated in future larger clinical, in-vitro and in-vivo studies to confirm such intricate link between ceramides and chordoma aggressive behavior.*

LIST OF ABBREVIATIONS

18F-FDG-PET	*Fludeoxyglucose positron emission tomography*
3D-CRT	*Three dimensional conformal radiation therapy*
BCL-2	*B-cell lymphoma 2*
BEH	*Bridged ethylene hybrid*
BMP-4	*Bone morphogenetic protein 4*
Bry	*Brachyury*
BSA	*Bovine serum albumin*
CAD	*Collisionally activated dissociation*
CD	*Cluster of differentiation*
CDG	*Clavien-Dindo grading*
CDK	*Cyclin-dependent kinase*
CDKN2A	*Cyclin-dependent kinase Inhibitor 2A*
CE	*Collision energy*
Cer	*Ceramides*
CerS	*Ceramides synthase*
CH	*Chordoma*
CK	*Cyberknife*
Cl1	*Superior third of clivus*
Cl2	*Middle third of clivus*
Cl3	*Inferior third of clivus*
CN	*Cranial nerve*
CNAO	*Centro Nazionale di Adroterapia Oncologica*
CSF	*Cerebrospinal fluid*
CT	*Computed tomography*
CVJ	*Craniovertebral jucntion*
DAB	*3,3'-Diaminobenzidine*
DDT	*Diagnostic delay time*
DHCer	*Dihydroceramides*
DP	*Declustering potential*
DSS	*Disease-free survival*
EDTA	*Ethylenediaminetetraacetic acid*
EEA	*Endoscopic endonasal approach*
EGFR	*Epidermal growth factor receptor*
EMA	*Epithelial membrane antigen*
EMT	*Epithelial mesenchymal transition*
ENT	*Ear, Nose, and Throat specialist*
EOR	*Extent of resection*
ER	*Endoplasmic reticulum*
ERK	*Extracellular signal–regulated kinase*
ESI	*Electrospray ionization*
EZH2	*Enhancer of zeste homolog 2*

GAB-1	*GRB2-associated-binding protein 1*
Gd	*Gadolinium*
GlcCer	*Glucosylceramides*
GLI	*Glioma-associated oncogene*
GP	*Graph pad*
GRB2	*Growth factor receptor-bound protein 2*
GS	*Gas settings*
GTR	*Gross total resection*
GY	*Gray*
H&E	*Hematoxylin and eosin*
HPLC	*High Performance Liquid Chromatography*
HRP	*Horseradish peroxidase*
ICA	*Internal carotid artery*
IGFB2	*Insulin like growth factor binding protein 2*
IHC	*Immunohistochemistry*
IS	*Internal standard*
JF	*Jugular foramen*
KM	*Kaplan-Meier*
KPS	*Karnofsky performance status scale)*
LC	*Liquid chromatography*
LC3	*Microtubule-associated protein 1A/1B-light chain 3*
LOH	*Loss of heterozygosity*
LOS	*Lenght of stay*
MAM	*Mitochondria-associated ER membranes*
MCA	*Middle cerebral artery*
MMP	*Matrix MetalloProteinases*
MR	*Magnetic resonance*
MRM	*Multiple technical reaction monitoring*
MS	*Mass spectrometry*
mTOR	*Mammalian target of rapamycin*
NAXL	*Naso-axial line*
NBPF1	*Neuroblastoma breakpoint family*
Nc	*Notochord*
NGFR	*Nerve growth factor receptor*
NICU	*Neurointensive care unit*
NOS	*Not otherwise specified*
NPIPB15	*Nuclear pore complex interacting protein family member B15*
NPL	*Naso-palatine line*
Nt	*Neural tube*
OR	*Odds Ratio*
OS	*Overall survival*
PBS	*Phosphate-buffered saline*
PC	*Phosphatidylcholine*

PCR	*Polymerase Chain Reaction*
PD-1	*Programmed cell death protein 1*
PD-L1	*Programmed death-ligand 1*
PDGFR-B	*Platelet derived growth factor receptor beta*
PFS	*Progression-free survival*
PG	*Pituitary gland*
PI3K	*Phosphatidylinositol-3-kinases*
PR	*Partial resetion*
PSI	*Proteomic Standard Initiative*
pSTAT3	*Phospho-STAT3*
PTCH	*Patched*
PTEN	*Phosphatase and tensin homolog*
q-PCR	*Quantitative polymerase chain reaction*
RARRES2	*Retinoic Acid Receptor Responder 2*
RBE	*Relative biological effectiveness*
RPL	*Rhino-palatine line*
RT	*Radiation therapy*
RT-PCR	*Reverse transcription polymerase chain reaction*
S1P	*Sphingosine 1-phosphate*
SAMD5	*Sterile alpha motif domain 5*
SASH1	*Sterile alpha motifs- and SH3 domain-containing protein 1*
SEER	*Surveillance, Epidemiology, and End Results*
SEM	*Standard error mean*
SHH	*Sonic Hedgehog Homolog*
SK	*Sphingosine kinase*
SM	*Sphingomyelin*
Smase	*Sphingomyelin phosphodiesterase*
SMO	*Smoothened*
SNP	*Single-nucleotide polymorphism*
SPT	*Serine palmitoyltransferase*
STAT3	*Signal transducer and activator of transcription 3*
STR	*Subtotal resection*
STROBE	*Strengthening the Reporting of Observational Studies in Epidemiology*
SUFU	*Suppressor of fused homolog*
SWI	*Susceptibility weighted imaging*
TBX	*T-box*
TERT	*Telomerase reverse transcriptase*
TGF	*Transforming growth factor*
TIL	*Tumor-infiltrating lymphocytes*
TrkA	*Tropomyosin receptor kinase A*
TRKR	*Tyrosine kinases receptor*
UV	*Ultraviolet*
WHO	*World Health Organization*

TABLE OF CONTENTS

INTRODUCTION

SKULL BASE CHORDOMA

Chordoma is a rare tumor that arises from embryonic notochordal cells remnants. Although it can potentially occurs at any point along the vertebral column, the sacro-coccygeal and the skull base areas represent the most common locations[21,30,203]. Given the growth predilection in the clivus, the most frequent symptoms are cranial nerve deficits, such as sixth or third nerve palsies. The median survival is estimated at 7 years from the time of diagnosis[21,39,40,174]. "Maximally safe surgical resection" and adjuvant high-dose radiation therapy represents the actual gold standard treatment[24,40,174]. The management of skull base chordoma patients is really challenging due to the need of preserving neurological functions and overall quality of life while maximizing tumor resection. The lethality of skull base chordomas is largely related due to their tendency to recur and locally progress, although systemic metastases have been reported in 12.5% of cases[174,203]. Proximity to vital neurovascular structures and locally aggressive behavior, apart from their histological grade, characterize chordoma as a malignant tumor[174,197,203]. The clinical course of chordomas is usually featured by a slow growth often impacting neurological functions, which lead to worse quality of life and death. Their growth pattern is characterized by encasement of neurovascular structures, dural penetration, bone infiltration and brainstem adhesions which makes chordomas a very challenging tumor[21,40,203]. Large retrospective studies on skull base chordomas in the last years highlighted a trend toward the improvement of the survival time mainly due to advancement of technology and surgical techniques[40,80,97]. They included the development of endoscopic technique, refinements of microsurgical open skull base techniques and the use of more accurate radiation therapy delivery modalities. Although these great improvements, chordoma is still a malignant tumor that strongly impact patient's quality of life with a 5-year

overall survival (OS) and 5-year progression free-survival (PFS) rates of 78.4% and 50.8%, respectively[174]. Previous studies have highlighted that tumor morbidity and mortality seems to be affected not only by clinical variables, such as extent of resection, tumor location and post-operative radiation therapy, but also by biological features[21,30,41,179]. Although morphology and basic immunohistochemical profiling of chordoma cells have been well characterized in the medical literature, its underlying molecular and genetic mechanisms are still not well and clearly understood. To date, no chemotherapeutic agent showed its role as first-line therapy for chordomas. Precision medicine with molecular target therapies is emerging as a promising and innovative approach to directly inhibit specific molecules and their pathways known to be involved in skull base chordomas[30,68,171–173].

Historical notes

The first pathological description of a "jelly-like" mass at the spheno-occipital synchondrosis has been made by the German pathologist Rudolf Virchow in 1846[191]. Hubert von Lushka, a German anatomist, found a similar "*soft, lobulated mass, which had grown from the inside of the bone at the lower limit of the back of the cuff, and with perforation of the dura mater tissue*" in an autopsy performed in 1856[110]. Based on these observations, Virchow introduced the term "*ecchondrosis physaliphora*" (ancient Greek-derived term "*phusallìs*" meaning bubble and "*-phore*" meaning to hold), to describe such pathological entity characterized by vacuolated cells resembling a plant-like pattern and their putative cartilaginous origin from spheno-occipitalis synchondrosis (Fig. 1).

Two other skull base chordoma cases were described in 1857 by German pathologists Friedrich von Zenker and Karl Ewald Hasse[63,215]. In 1858, the

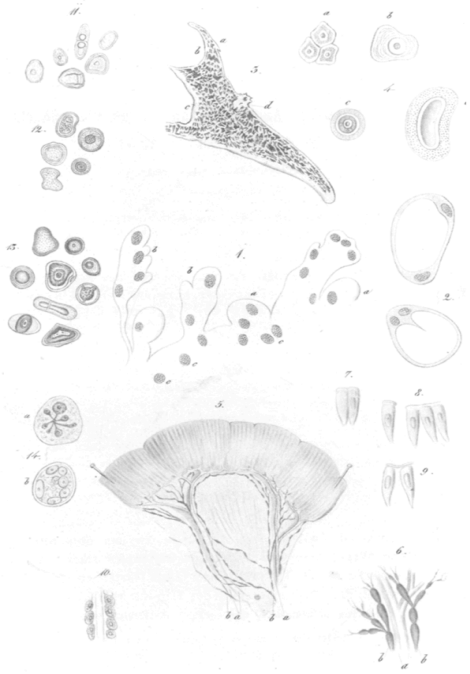

Figure 1. Original drawing of skull base "ecchondrosis physaliphora" from Hubert von Lushka [adapted from Lushka H, 1857].

Virchow's doctoral advisor Johannes Peter Muller rejected the cartilaginous hypothesis of tumor origin and hypothesized that notochordal remnants, mainly located at the skull base, odontoid process and coccyx, could degenerate into chordoma[128]. Unfortunately, such theory was discarded by Virchow and Lushka and not validated until 1894, when the German pathologist Moritz Wilhelm Hugo Ribbert re-proposed Muller's notochord theory. He was the first to introduce the term "*chordoma*", highlighting its origin from the *chorda dorsalis*[54,155]. He performed several experiments on rabbits with repeated punctures of intervertebral pulposus nucleus that leaded to the development of subsequent reactive proliferative tissue resembling the notochordal remnants[149]. Ribbert also identified chordomas in ten patients after performing 500 consecutive autopsies[148]. In 1923, Stewart and Burrow proposed to differentiate the benign intradural small gelatinous mass found behind the clivus as "*ecchordosis physaliphora*" (abandoning the Virchow's term "*ecchondrosis*" due to the notochordal origin) and the more invasive form as "*chordoma*"[15]. The first-ever clinical description of a spheno-occipital chordoma patient determining compression of the pons was given by a Swiss physician C. Klebs in 1864[87]. The American neurosurgeon Harvey Cushing performed the first surgical removal through a transsphenoidal approach of a skull base chordoma (Fig. 2) in 1909[35].

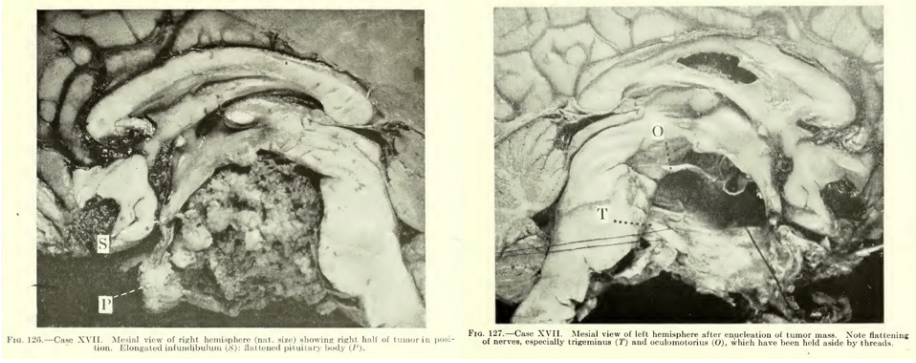

Fig. 126.—Case XVII. Mesial view of right hemisphere (nat. size) showing right half of tumor in position. Elongated infundibulum (*S*); flattened pituitary body (*P*).

Fig. 127.—Case XVII. Mesial view of left hemisphere after enucleation of tumor mass. Note flattening of nerves, especially trigeminus (*T*) and oculomotorius (*O*), which have been held aside by threads.

Figure 2. Original pictures of the first skull base chordoma patient surgically treated by Dr. Harvey Cushing [adapted from Cushing H, 1912] .

Embryology

Since the first description by Muller in 1858, many other scientists proved that chordoma specifically arises from vestigial remnants of notochord.
The notochord is a flexible rod-like midline structure that features all the members of the *Chordata* phylum and plays both a structural support and inducer role for the right development of the embryo. It originates during the third week of development (namely "early gastrula stage") from the dorsal organizer that soon after becomes the chordamesoderm, the dorsally-positioned segment of mesoderm. Progenitor notochordal cells move forward to the pre-chordal plate reaching the endodermal layer to constitute the notochordal plate (Fig. 3). The notochordal plate after detaches itself from the endoderm giving finally rise to an elongated stack of vacuolated cells with a thick extracellular sheet, the definitive notochord (Fig. 3)[154].

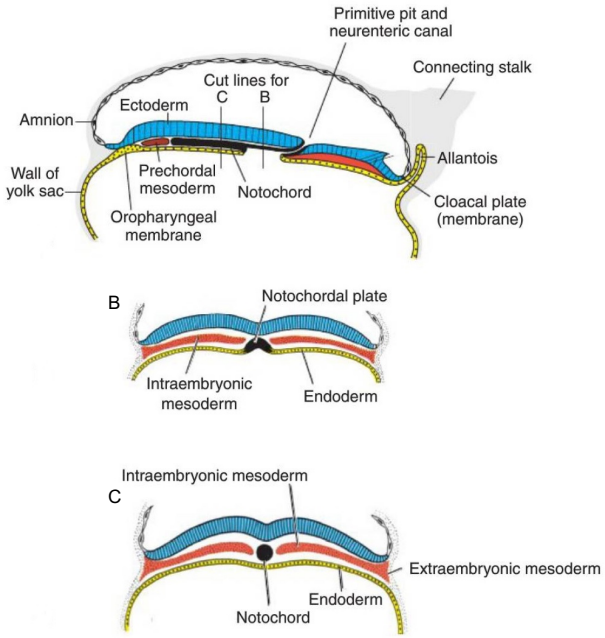

Figure 3. Schematic drawings that show the notochord development [adapted from Sadler TW, Langman's Medical Embriology, 30th edition, 2015].

The notochord extends along the entire length of the future vertebral axis, from the pre-chordal plate caudal to the oropharyngeal membrane toward the cloacal membrane. Specifically, the rostral notochord has a hook-like appearance and is present for a short distance on the posterior aspect of the basilar cartilage, then travels forward and upward obliquely on the ventral surface, where it may be attached at some point to the pharyngeal epithelium, and extends backward to end into the dorsum sellae (Fig. 4)[144].

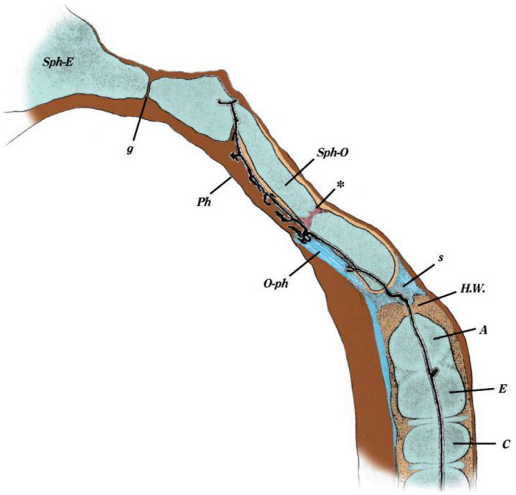

Figure 4. Graphycal illustration showing the course of the notochord within the osseous and cartilaginous structures of the developing skull base [adapted from Ramesh T et al., 2017].

The notochord is composed by an internal layer of vacuolated cells encircled by an epithelial-like cells layer and an external peri-notochordal basement membrane. Such membrane is formed by an inner basal lamina, a medial layer made of collagen running parallel to the notochord and another external layer of a loosely-organized perpendicular matrix. The typical structural flexibility but solid of the notochord is created by the delicate counterbalance between the hydrostatic pressure derived from vacuolated cells and the rigid outer layer[175].

The notochord regresses during the late fetal period and its remnants become the *nuclei pulposi* of the mature intervertebral disks[114].

The notochord, apart from its important role as supporting structure of the developing embryo, plays a crucial role as inducer of the adjacent structures. Bone morphogenetic protein-4 (BMP-4), member of TGF family protein, is a molecule secreted from the dorsal organizer and induces the mesoderm ventralization[154]. On the other hand, chordin, noggin and follistatin are important repressor of BMP-4 activity and are secreted by the dorsal organizer and are responsible for the mesoderm dorsalization and formation of notochord and para-axial mesoderm[154].

Brachyury (from Ancient Greek "*brakhus*" meaning short and "*ourà*" meaning tail) or *T gene* ("T" stands for tail) is a member of T-box gene family (*TBX*) that encodes a transcription factor with a common DNA-binding domain involved in notochordal cell migration and formation, mesoderm dorsalization, cell cycle control and cell proliferation[131]. In 1927 Nadine Dobrovolskaïa-Zavadskaïa, a Russian pioneer developmental geneticist working in Paris at the Pasteur Laboratory, characterized for the first time a loss-of-function mutation affecting a gene locus by observing mice developing with a short tail[132]. Animals harboring a homozygous mutation of *Brachyury* early died because of a failed formation of the notochord and posterior structures such as the neural tube[92]. The first gene cloning of *Brachyury* has been conducted in 1990 and showed encoding a protein having a specific DNA-binding palindromic sequence TCACACCT, called *TBX*[67]. Brachyury has also been shown to be a diagnostic marker of chordoma and important factor in epithelial-mesenchymal transition (EMT) in hepatocellular carcinoma[195].

Sonic Hedgehog (Shh) is a protein encoded by the *SHH* gene and plays a key role in the embryo development and structure differentiation (Fig. 5)[25]. In the absence of Shh ligand, the Patched (PTCH) receptor inhibits the Smoothened (Smo) receptor, allowing suppressor of fused (SUFU) to bind

and inactivate GLI transcription factors. Shh binds to PTCH and activates Smo, thus inactivates SUFU and, in turn, causes GLI1, GLI 2 and GLI3 to be translocated into the nucleus where they activate target genes such as PTCH1 and Engrailed. Shh acts as a morphogen because it has a cell-fate determining activity through its diffusion gradient governing the pattern of development of midline structures such as the vertebral columns, brain and spinal cord. Shh is firstly expressed in the notochord and in the ventral plate and regulates the differentiation of somites into sclerotomes and motor neuron differentiation in the ventral neural tube, respectively (Fig. 5)[25,103]. Removal of *SHH* from the notochord abolished Shh expression in the floor plate and resulted in the loss of vertebral structures and nuclei pulposi. Experiments showed how de-regulation of Shh pathway signal is crucial to the ectopic development of motor neuron cells[188].

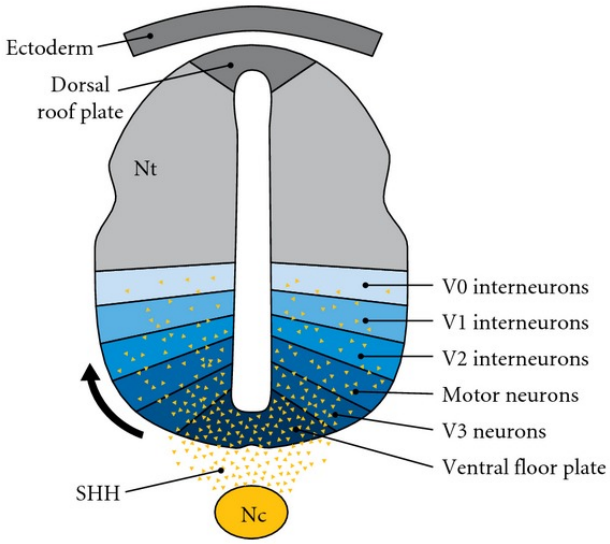

Figure 5. Formation of different cell types at the ventral portion of the neural tube (Nt). Sonic hedgehog (SHH), secreted from notochord (Nc) and ventral plate, is responsible for generating interneurons and motor neurons of the ventral floor plate [adapted from Lee RW et al., 2011].

Epidemiology

Chordoma is considered a rare tumor because its incidence is less than 6 cases per 100.000 according to the European Commission[145]. Based on SEER (Surveillance Epidemiology and End Results) population-analysis, an American cancer registry maintained by National Cancer Institute, the overall age-adjusted incidence rate is estimated to be 0.089 per 100.000 persons[23,115]. Chordoma represents the fourth most common malignant bone tumor among the whole population with a rate of 8.35-8.4%, after osteosarcoma (28.8%), chondrosarcoma (28.3%) and Ewing's sarcoma (15.5%)[10,42]. Skull base chordoma represents 41.1% of all chordomas, whereas mobile spine and sacral bone are involved in 27.4% and 31.5 % patients, respectively[23,220]. Childhood chordoma are relatively rare, representing around 6.3% cases of all primary chordoma cases and the skull base is the most affected location in 61.6% patients[101,115]. The mean age at presentation of skull base chordomas is 47.4 years, so presenting earlier in life compared to the mobile spine (56.6 years) and sacrum (62.7 years) chordomas[23,220]. There is a slight predominance of males in skull base chordoma (54.1%)[220]. There is no difference between males and females in 5 years (71.9% vs 75.4%) and 10-years survival (57.8% vs 59.3%)[23]. Regarding skull base chordoma population ethnicity, 83.4% are white, 4.8% black and 11.8% other[220]. According to the SEER study done in the period 1973-1995, the mean OS in skull base chordoma was 6.94 years, in sacral and mobile spine chordomas were 6.48 and 5.88 years, respectively[115]. The predicted 5-years, 10-years and 15-years survival in cranial chordoma were 64.7%, 46.6 % and 48.4%[115]. According to the most recent SEER population study done in the period 1973-2013, the mean OS in skull base chordoma is 13.5 years, whereas in sacral and mobile spine chordomas are 7.25 and 7.91 years, respectively[23]. The estimated 3-years, 5-years and 10-years survival rates are 80.9%, 73.5% and 58.7%, respectively. In another recent study,

the estimated disease-specific survival (DSS) at 5-years and 10-years is 73% and 64%, respectively[102]. On the ground of such studies, the location is a significant prognostic factor and the skull base chordoma group has a better survival outcome ($p \leq 0.001$)[23]. Moreover, the more recent SEER population analysis studies showed a better outcomes trend in skull base chordomas, mainly due to advancement of minimally invasive and maximally effective skull base surgery techniques and better radiation delivery modalities[220].

Pathology

Skull base chordoma macroscopically appears as a lobulated and gelatinous mass with a color ranging from whitish-greyish to yellowish (Fig. 6). The tumor has generally a soft and friable consistency and barely presents in its context some calcifications or bone dystrophic sequestration. It has an infiltrating pattern, extending beyond the cortical surface of the bone and invading surrounding structures such as mucosa, submucosa, muscle and dura mater. It may have a variable content of neo-formed vascularization[12,54,174].

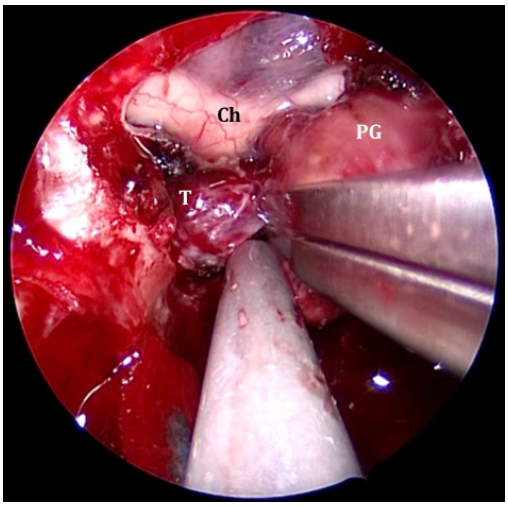

Figure 6. Intraoperative endoscopic view of chordoma and its delicate relations with pituitary gland and chiasmatic apparatus. The tumor presents itself as a lobulated greyish mass. Ch, *chiasm*; PG, *pituitary gland*.

According to the 4th Edition of WHO Classification of Tumours of Soft Tissue and Bone, chordomas are classified in classical chordoma or NOS (not otherwise specified), chondroid chordoma and de-differentiated (biphasic) chordoma (Fig. 7)[203]. Chordoma histology is characterized by the constant presence of vacuolated cells with eosinophilic cytoplasm and eccentric nuclei, the so-called physaliphorous cells, that are arranged in sheets within a myxoid matrix and separated by fibrous septa[135,203].

Chondroid chordomas are characterized by the presence of physaliphorous cells interspersed within a matrix that resembles neoplastic hyaline cartilage. They represent around 20% of all skull base chordomas. The differential diagnosis is with chondrosarcoma[135,203]. A de-differentiated chordoma is characterized by a biphasic presentation of a classical chordoma next to a region characterized by spindle-shaped cells, thus, an undifferentiated pleomorphic sarcoma or osteosarcoma. It may occur in association or at the location of a previously resected conventional chordomas[64,119,136]

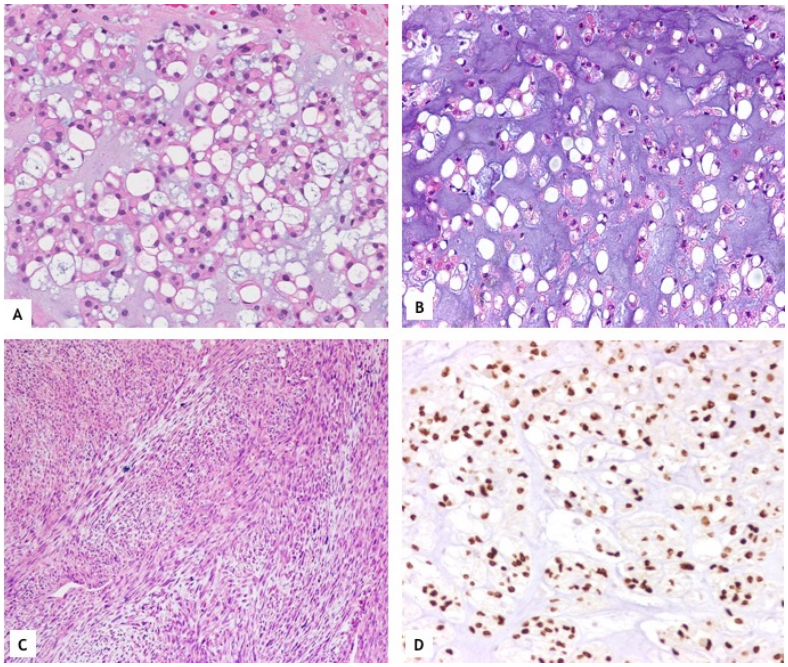

Figure 7. A) Photomicrograph showing conventional chordoma (40x) [adapted from Wasserman JK, 2018]; B) Photomicrograph showing chondroid chordoma (40x); C) Photomicrograph showing de-differentiated chordoma (20x); D) Photomicrograph showing chordoma strongly expressing nuclear immmunoreactivity for Brachyury (anti-Bry, 40x).

Two other histopathological variants of chordomas, apart from the WHO classification, have been described: cellular and poorly-differentiated variants[69,199]. The “cellular variant” is featured by abundant tumor cells with scarce myxoid stroma whereas the “poorly-differentiated” chordoma is, on

the other hand, composed of tightly packed and small atypical epithelioid cells arranged to form nests and sheets, with absence of any physaliphorous cells and with a fibrous background[69]. Chordomas with rhabdoid cells have been also described and may represent a continuum spectrum between poorly-differentiated and de-differentiated chordoma[69,136]. Although some authors described in the past medical literature the “atypical variant” as a mixed highly-cellular and poor-differentiated chordoma there are not well and shareable established criteria and its term use is not recommended anymore[69]. Its description relies on the presence of atypical cellular features such as hyperchromatic nuclei, nuclear pleomorphism and prominent nucleoli, extensive necrosis, epithelioid cells and high mitotic index[181,199].

Chordomas, apart from its peculiar histology, are identified by the expression of featuring immune-markers such as S-100, Epithelial Membrane Antigen (EMA) and cytokeratin. Recently, Brachyury has been routinely employed as a useful diagnostic marker to help into the differential diagnosis (Fig. 7) (i.e. chondrosarcoma, clear cell renal carcinoma and signet ring cell carcinoma metastasis)[178,195,199].

Radiology

The two current and more commonly employed radiological techniques to diagnose skull base chordomas are computed tomography (CT) and magnetic resonance (MR).

CT is useful to evaluate the tumor involvement of the surrounding skull base bone and to disclose the presence of any calcification and/or bone sequestration. Chordoma presents itself as isodense/hypodense lesion in comparison to the surrounding brain parenchyma. In the pre-operative planning, volumetric CT scans with 3D reconstructions are vital to evaluate the CVJ and, therefore, to predict any post-operative instability and to evaluate the rhinosinusal structures in chordomas amenable to an anterior midline approach. CT angiography is required if the tumor has intimate relations with the major brain vessel of Willis circle (such as internal carotid artery and vertebral artery) and to plan the potential vessel sacrifice with/without a flow replacement bypass.

MR is the radiological modality of choice to deeply study the nature and exact location of the tumor and its intricate relationships (Fig. 8). On T1-weighted images, chordomas generally present as hypointense lesion and there are rarely hyperintensities related to recent intratumoral hemorrhages; on T2-weighted images chordomas are generally hyperintense, but some tumor may present itself as hypointense/isointense and such radiological feature seems to correlate to a lesser myxoid matrix and a worse prognosis. The significance of the degree of contrast enhancement is still debated in the current literature and there is no current agreement of its prognostic role. Pamir et al. proposed to classify chordomas in different categories according to the intensity of contrast enhancement (no, mild, intense) and pattern (heterogeneous and homogenous) to better differentiate them from chondrosarcomas[138]. Diffusion-weighted MR is an advanced technique that can be used to assess tumor cellular density and could be useful to

differentiate chordomas from chondrosarcomas[56,129,211]. Dynamic Contrast-Enhanced MR Perfusion Imaging represents another advanced MR technique that can estimate tumor plasma volume and vascular permeability and it can be useful to monitor chordoma growth, response to radiation therapy and distinguishing it from other spinal lesions[157].

Although there is, to our knowledge, no studies evaluating the role of nuclear imaging in skull base chordomas, ^{18}F-FDG-PET could be useful in the staging and diagnosis of systemic involvement/metastases and may become an important tool in the follow-up of chordoma patients[173].

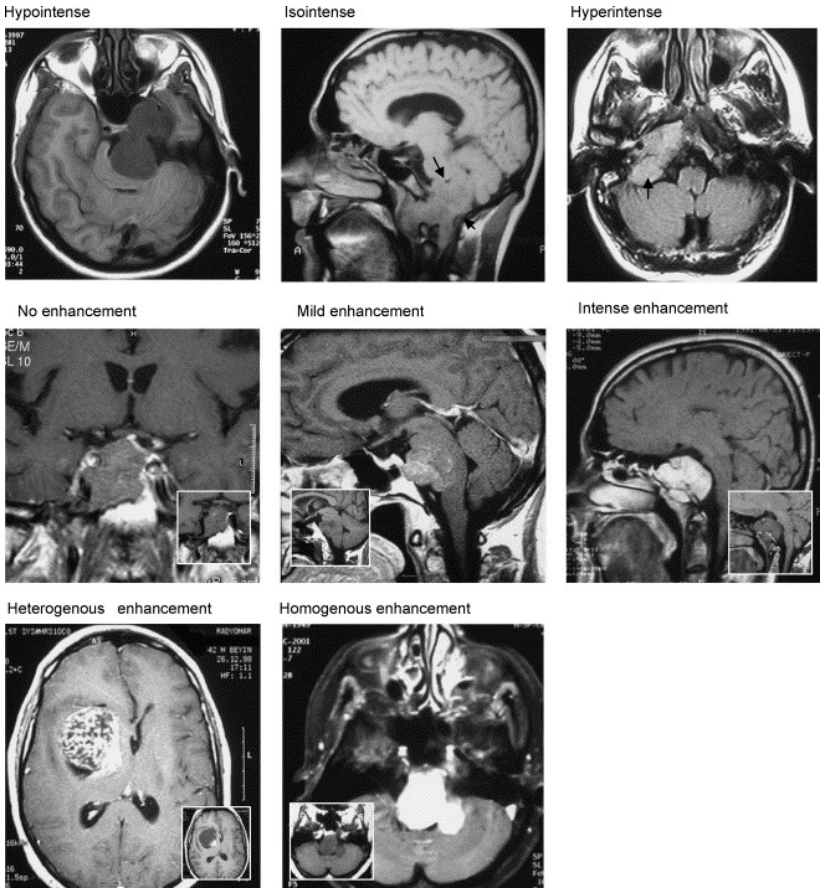

Figure 8. Different radiological MR features of skull base chordomas [adapted from Pamir M et al., 2006]

Surgical anatomy and treatment

The clivus of Blumenbach represents the central portion of the skull base extending from the sella turcica to the foramen magnum (Fig. 9)[98,147]. It is derived from the fusion of the synchondrosis between the body of the sphenoid bone and the basilar portion of the occipital bone at around 25 years. The endocranial surface is smooth and concave in a lateral-to-lateral direction and is continuous to the petrosal portions of temporal bones through the petro-clival fissures. Petro-clival fissure extends from anterior lacerum foramen and petrous apex anteriorly and superiorly to the jugular foramen (posterior lacerum foramen). The extracranial surface is rough and presents the median pharyngeal tubercle, where pharyngo-basilar fascia attaches. Clivus takes anterior relations with vomer bone and sphenoid body and laterally with the petrous temporal bones through petro-clival fissures.

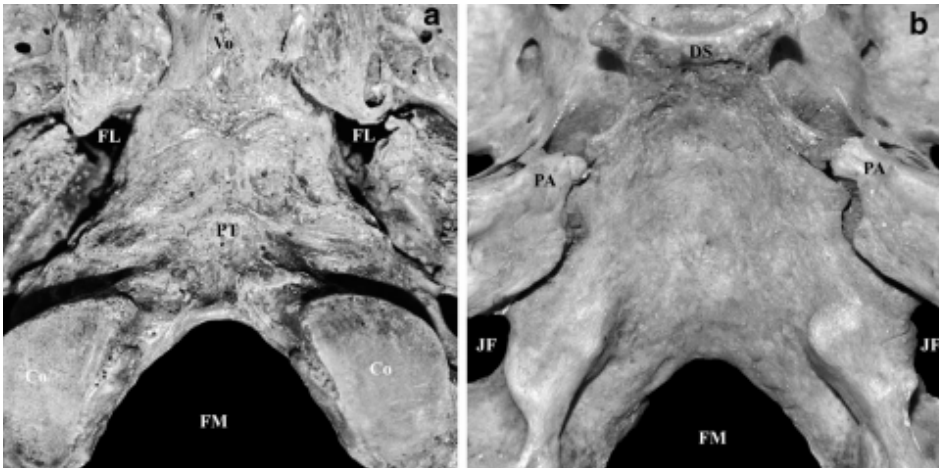

Figure 9. Extracranial (left) and intracranial (right) osseous structures and anatomical subdivision of the clivus. Co, *occipital condyle*; DS, *dorsum sellae*; FL, *foramen lacerum*; FM, *foramen magnum*; JF, *jugular foramen*; PA, *petrous apex*; PT, *pharyngeal tubercle*; Vo, *vomer* [adapted from La Corte et al., 2018].

Skull base chordomas could be approached by different corridors and the choice of the right corridor depends on the primary location and extension of the tumor (Fig. 10)[6]. Our surgical philosophy has been summarized in a recent publication[99]. Chordomas poses intrinsic challenges due to their anatomical location that are also dominated by different surgical specialties (neurosurgery, ENT, maxillofacial); therefore, a multidisciplinary skull base team is crucial to better address a such complex tumor. Surgical approaches are chosen by the need of maximally and safely resect the tumor with a limited morbidity.

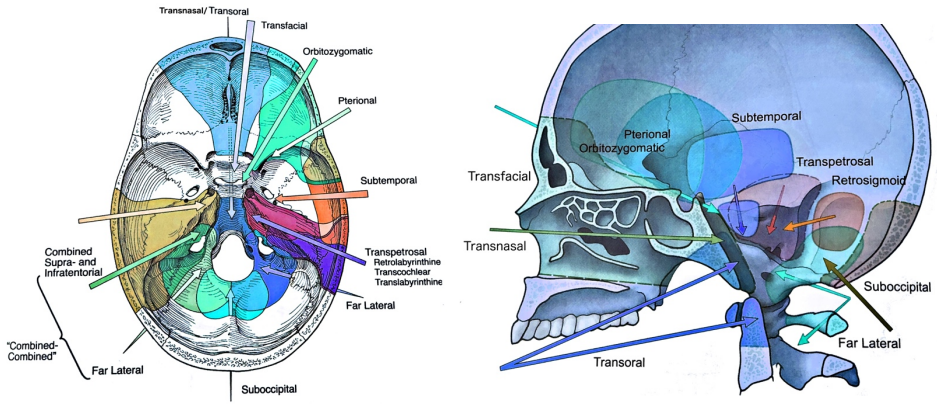

Figure 10. Surgical approaches to the clivus and craniovertebral junction [adapted from Bambakidis et al., 2012].

In the present dissertation, we will mainly present the key steps of the most commonly employed surgical technique in our series of skull base chordomas: the endoscopic endonasal approach (Video 1-4). For a detailed and technical description of craniotomical and endoscopic approaches to the skull base, please refer to the major neurosurgical textbooks[147,164,204].

The main approach to the clivus and anterior cranio-vertebral junction (CVJ) has been the microscopic transoral-transpharyngeal[33,75,116]. This approach could be linked to the mandible (mandibulotomy), tongue (glossotomy), hard and soft palate (palatotomy) and maxillae splitting (maxillotomy). Such extensions may increase the surgical complexity and exposure but also

concomitantly increase morbidity and the rate of cosmetic complications[82,116,213]. Minimally invasive techniques such as the endoscopic endonasal approach (EEA) to the clivus and cervical spine contributed to advance surgical outcomes of such challenging region, such as a reduction of morbidities, a faster patient recovery and a wider, closer and brighter view of the surgical area[53,192–194]. The main limit of EEA is its caudal exposure due to the presence of nasal and palate bony and soft structures superiorly and inferiorly, respectively. Thus, pre-operative planning of the feasibility of the EEA is fundamental to select the best approach to address a particular pathology. The *nasopalatine line* (NPL) has been described as a good predictor of the inferior limit of the EEA. Several studies affirmed that it overestimated the inferior limit of EEA by an average of 13mm[1,10]. In response, we proposed a second line as a more accurate predictor of the inferior limits of the EEA, namely the *nasoaxial line* (NAxL), whose starting point is the mid-distance of nasal aperture. However, NAxL has been defined in cadaver dissections and it was unclear if it accurately predicted the lower limits of the EEA to the CVJ in practice. Therefore, we proposed a new line, the *rhinopalatine line* (RPL) that appears to correlate most accurately with our previous described surgical results (Fig. 11)[96]. RPL is defined as the line, in the midsagittal plane, that crosses the 2/3 point of the distance from the *rhinion* to the anterior nasal spine of the maxillary bone and the the posterior nasal spine of palatine bone. It is then extended posteriorly and inferiorly to end at the cervical spine. The use of the RPL may assist surgeons in choosing suitable candidates for the skull base chordomas amenable to an EEA and in selecting those who are better approached trough the transoral approach (Fig. 12).

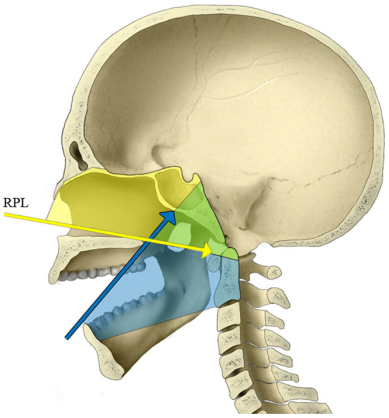

Figure 11. Illustration depicting the surgical exposures of EEA and ETA to the skull base [adapted from La Corte et al, 2018].

The yellow arrow denotes the rhinopalatine line (RPL), which estimates the lower limit of the EEA and the area shaded in yellow depicting the portions of the skull base exposed by this approach. The blue arrow denotes the upper limit of the ETA, with the area shaded in blue depicting the portions of the skull base and cervical spine exposed by this approach. The area in green represents the overlapping area of the skull base that can be accessed by both endoscopic approaches. These rostro-caudal limits of each approach should be considered in choice of endoscopic approach to pathology of the lower skull base.

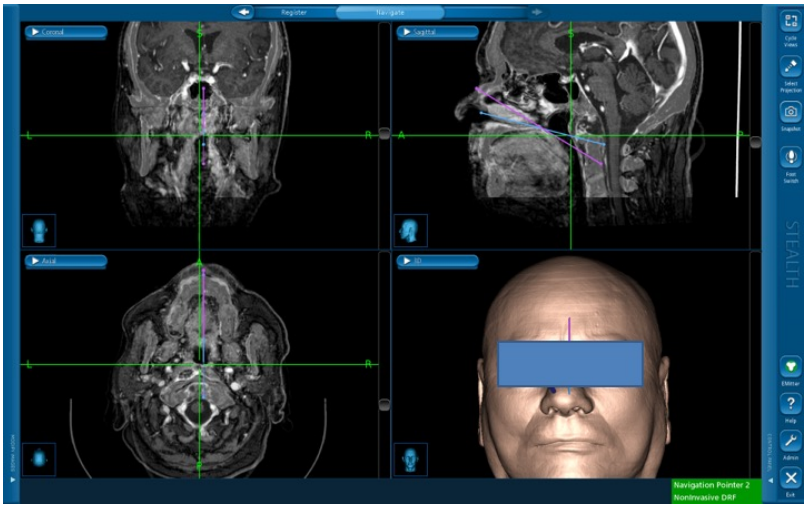

Figure 12. Neuro-navigator snapshot showing the surgical trajectories to a cranio-vertebral junction chordoma. The light blue line represents the trajectory predicted by the rhinopalatine line (RPL); the pink line represents the trajectory predicted by the nasopalatine line (NPL), the green lines represent the actual surgical inferior limit, corresponding exactly to the RPL.

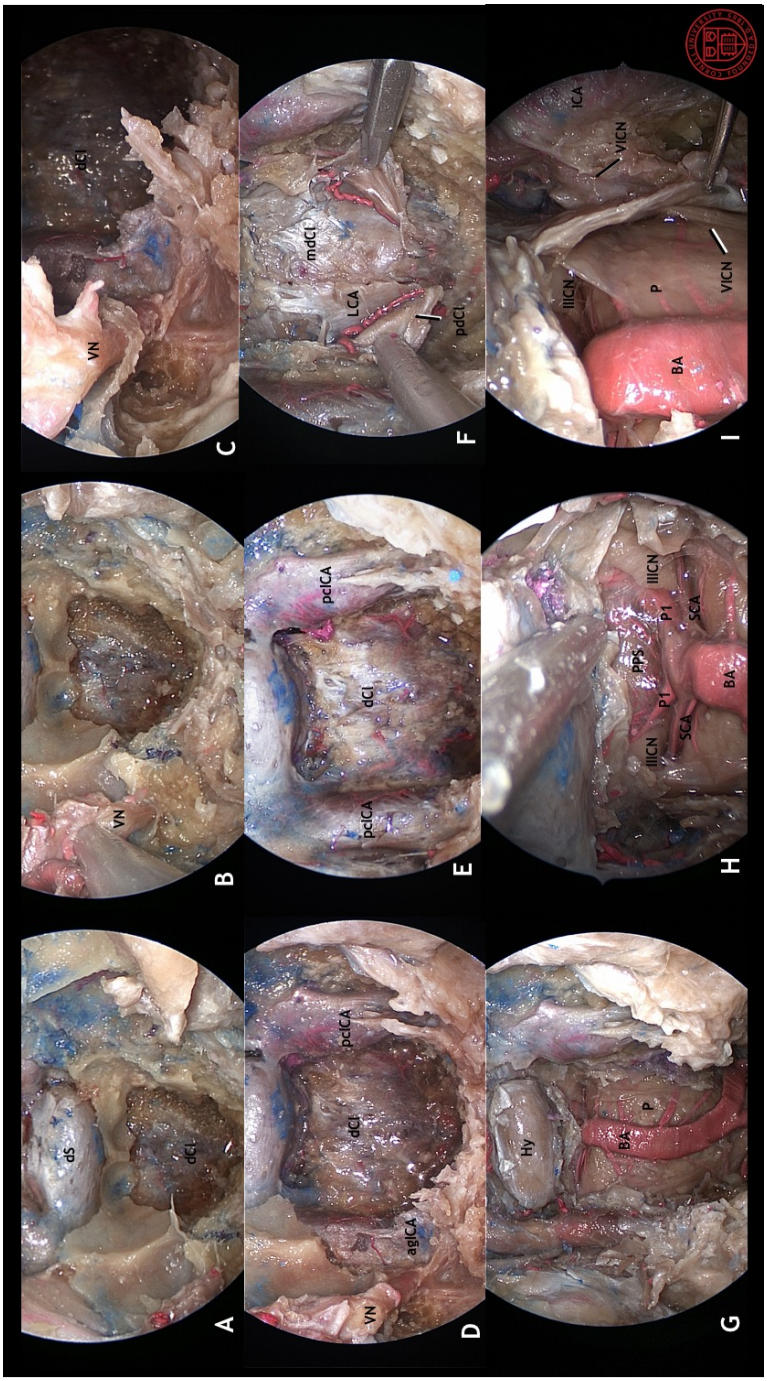

Figure 13. Surgical anatomy of the transclival corridor. Anatomical dissections have been performed at the Weill Cornell Medicine Lab, New York. The transclival represents the superior corridor that leads to the sphenoidal portion of the clivus and posterior fossa.

The surgical key steps of the transclival corridor (Fig. 13) are described as follows: A) After getting access to the sphenoid sinus, the inferior wall of the sphenoid body is drilled down towards the clivus and clivectomy performed. The lateral limits of this surgical window are represented by the two paraclival internal carotid artery. B) The vidian nerve represents one of the main anatomical landmarks in the endoscopic skull base surgery of chordomas[83,143,189]. It is identified to safely localize the anterior genu of ICAs. C) Drilling around the vidian canal to leave a bony surrounding it to leave the vidian nerve intact. D) and E) An extensive drilling of the clivus has been carried out to bilaterally expose the ICAs. The vidian nerve points towards the anterior genu of right ICA. F) Exposure of the space between the periosteal and actual clival dura mater. The lateral clival arteries are, therefore, identified. G) Removal of the clivus dura mater and exposure of posterior fossa contents such as mesencephalon, pons with related vascular arteries such as basilar, anterior inferior cerebellar artery and vertebral arteries. H) Angled and focused view of mesencephalon, posterior perforated substance, basilar artery apex with P1 segments, superior cerebellar artery SCA and III cranial nerves. I) Angled and focused view of pre-pontine cistern and the course of the sixth cranial nerve. The abducens nerve represents the most affected cranial nerve in skull base chordoma patients.

Abbreviations: agICA, *anterior genu of internal carotid artery*; BA, *basilar artery*; dCl, *dura mater of clivus*; dS, *dura mater of sella*; Hy, *pituitary gland*; ICA, *internal carotid artery*; LCA, *lateral clival artery*; mdCl, *inner meningeal dura layer of clivus;* P, *pons*, pcICA, *paraclival segment of internal carotid artery*; PPS, *posterior perforated substance*; P1, *first segment of posterior cerebral artery*; pdCl, *periosteal dura mater layer of clivus*; SCA, *superior-cerebellar artery*, VN, *vidian nerve*; IIICN, *oculomotor nerve*; VICN, *abducens nerve*.

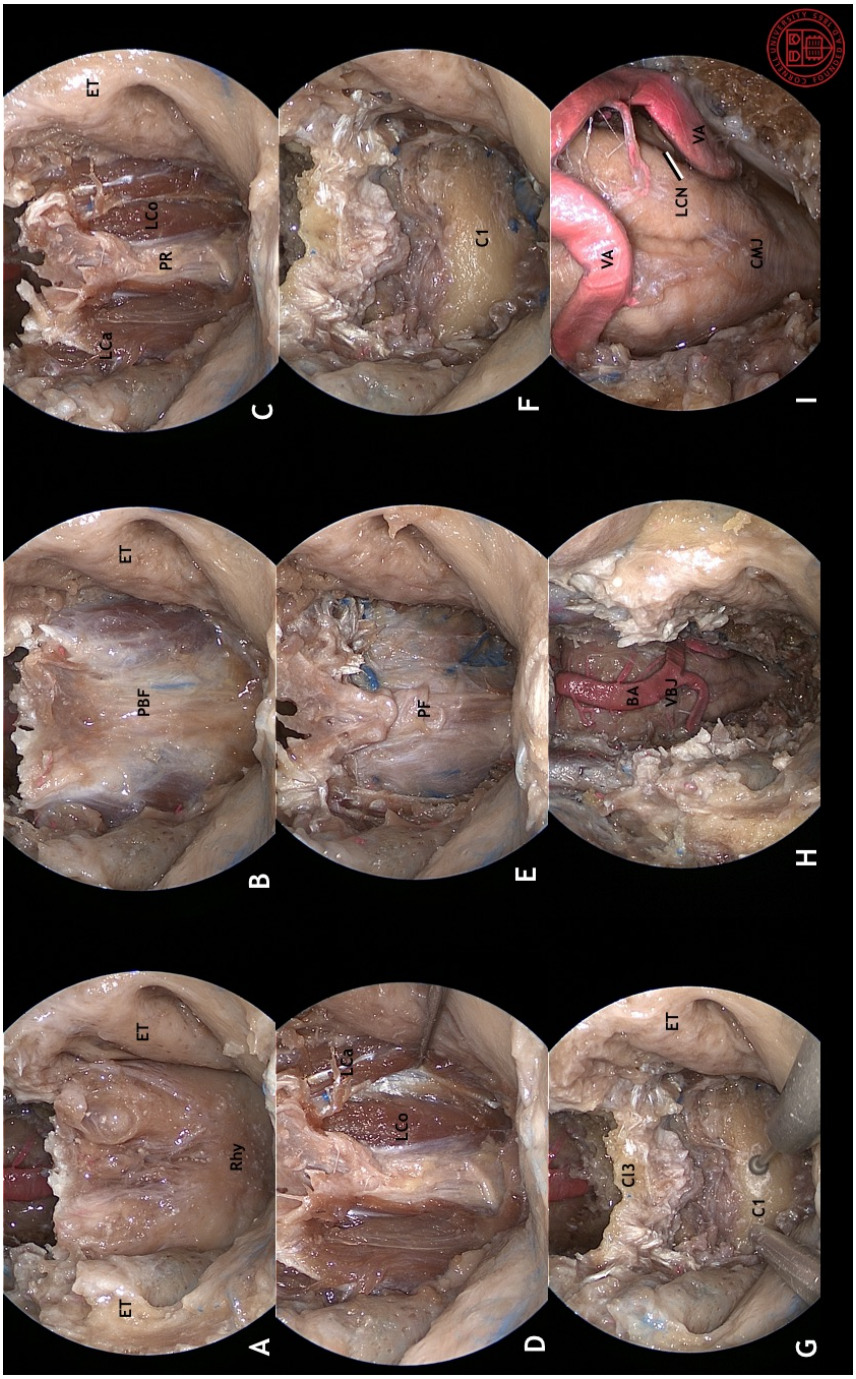

Figure 14. Surgical anatomy of the trans-rhinopharyngeal corridor. Anatomical dissections have been performed at the Weill Cornell Medicine Lab, New York. The trans-rhinopharyngeal represents the inferior corridor that leads to the foramen magnum and cranio-vertebral junction area.

The surgical key steps of the trans-rhinopharyngeal corridor (Fig. 14) are described as follows: A) The rhinopharynx mucosa is exposed, the two Eustachian tubes and torus tubarius represent the most lateral approach of this module, but they can be resected to laterally extent the surgical window[125,189]; B) The mucosa is removed and the underlying pharyngobasilar fascia is exposed; C) and D) The pharyngobasilar fascia is removed and the underlying pre-vertebral muscle layers is revealed. Pre-vertebral muscles are the medial longus colli and the lateral longus capitis muscles. A median strong fibrous band, the pharyngeal raphe, is visible right posteriorly to the pharyngobasilar fascia. E) The atlo-occipital membrane is exposed and then F) removed to expose the bony complex of cranio-vertebral junction. The anterior arch of C1 is visible together with its ligamentous structures. G) The drilling of the anterior arch of C1 has been carried out, together with the inferior segment of the clivus and C2 dens and removal of cervico-medullary junction dura mater. H) The posterior fossa content has been exposed, such as the pons, medulla and cervical portion of the spinal cord. The vasculature of the pons and cervico-medullary is exposed. I) Angled and focused view of the medulla showing the intimate relations of the vertebral arteries and their perforators. The left lower cranial nerve complex is also visible laterally to the left vertebral artery.

Abbreviations: BA, *basilar artery*; C1, *atlas*; Cl3*, inferior third of clivus*; CMJ, *cervico-medullary junction*; ET, *Eustachian tube*; LCa, *longus capitis muscle*; LCo, *longus colli muscle*; LCN, *lower cranial nerves*; PBF, *pharyngobasilar fascia*; PF, *prevertebral fascia*; PR, *pharyngeal raphe*; Rhy, *rhynopharynx*; VA, *vertebral artery*; VBJ, *vertebro-basilar junction*.

Video 1. Surgical video of an upper third clivus chordoma.

Video 2. Surgical video of a middle third clivus chordoma.

Video 3. Surgical video of a lower third clivus chordoma.

Video 4. Surgical video of a pontine recurrent chordoma.

Radiation therapy

There are no clear guidelines and high-level of evidence on the best available treatment of skull base chordomas. The current gold-standard therapeutical strategy includes a maximally safe resection followed by adjuvant radiation treatment[30,41,174]. Skull base chordomas are really challenging tumors because of their proximity of dose-limiting organs such as the optic tract and brainstem and their radioresistance[54,55,165]. However, the use of modern technologies, such as heavy-particles therapy also called as hadron therapy, led to deliver a more precise dose distribution than the past radiation modalities. Hadron therapy uses nuclear particles such as proton, neutrons or carbon ions to deliver the dose to the tumor. Such therapy appears to be more effective than photon-based therapy, due to its ability to deliver higher doses of radiation with a discrete sparing of surrounding vital and dose-limiting regions[2,55,77,130,135,201]. The physical properties of heavy-particles and their clinical usefulness are explained by the phenomenon of "Bragg peak"; the majority of the dose is delivered at a predictable depth and less dose is delivered outside the target volume (Fig. 15)[47].

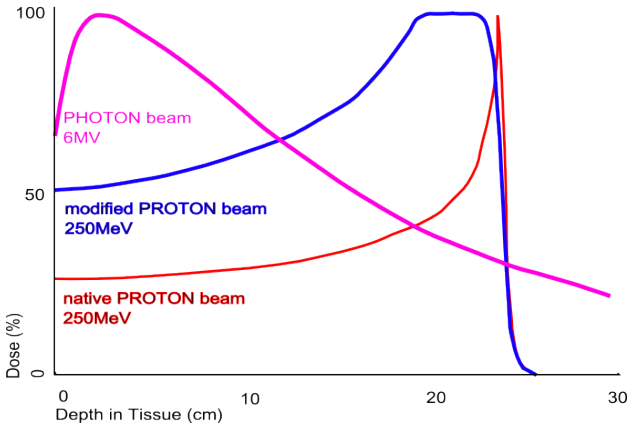

Figure 15. Graph showing the Bragg peak of proton beam compared to the dose produced by photon beam [adapted from Dr. Miller A, Wikipedia].

Carbon ion therapy has a greater relative biological effectiveness than photons or protons and shows a less degree of sensitivity to oxygen and other radioresistance features, making them a potentially attractive choice for the treatment of chordomas but further studies are needed to understand its implications and applications (Fig. 16)[41,130,133,137]. Although many studies on protons and charged particles therapy showed promising results, there is no high-level scientific evidence on its clinical efficacy and therefore particle therapy should be currently considered experimental, until further randomized controlled studies will be conducted[41,80]. Other radiation modalities use photons to deliver the dose to the tumor and include stereotactic radiosurgery (Gamma-knife or Cyber-knife) and Three-Dimensional Conformal Radiation Therapy (3D-CRT) and may have a role in treating small residual post-operative chordomas[174].

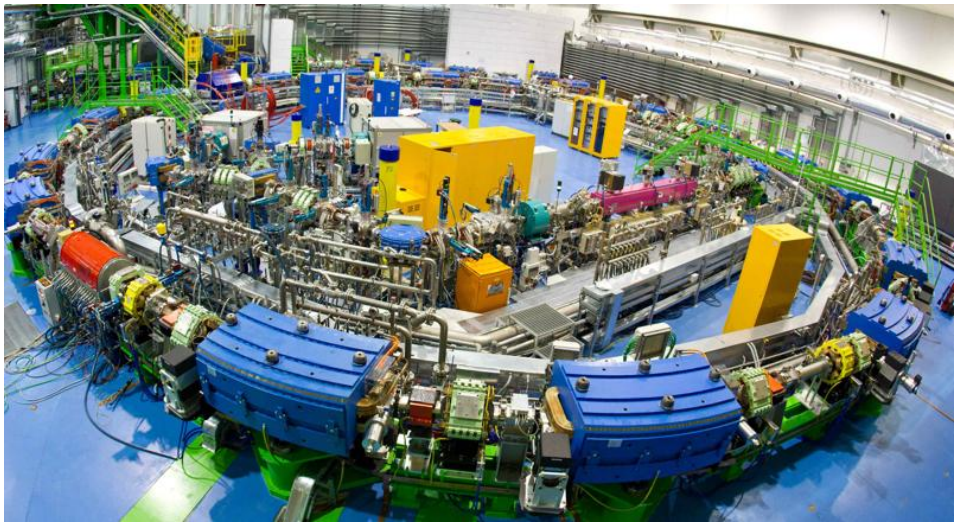

Figure 16. Picture of the synchrotron, where the heavy particles are accelerated, installed at CNAO, Pavia, Italy.

Medical treatment

There is no current approved medical treatment for advanced chordoma[30,174]. Classical cytotoxic chemotherapy is generally inactive for such tumors and may have a dismal role in the de-differentiated subtype and pediatrics. Irinotecan represents the only drug that has been tested in a phase-2 trial, which resulted in 1/15 patients having an objective response[27]. Small retrospective series and case reports showed responses to anthracyclines, cisplatin, alkylating agents and etoposide[38,49]. Brachyury, PDGFRB, PI3K/mTOR, EGFR, and MET represent some relevant therapeutic targets that have been discovered in chordoma[41,179,180,202]. There is also somewhat preclinical evidence that their inhibition can have a slight activity in the tumor control[74,167,179,180,207]. The first described target-therapy has been with imatinib mesylate in a patient with an advanced chordoma[20]. Afterwards, a multi-institutional, non-randomized, phase-2 study of imatinib in patients with advanced chordoma presented an objective partial response in only one case out of 50 patients[173]. Additionally, a retrospective study showed that the combined mTOR and PDGFRB inhibitor therapy (sirolimus+ imatinib) could work more than the single imatinib alone[171]. A phase-2 study (imatinib+everolimus) in advanced chordomas is still in progress (EUDRACT-2010–021755–34). Some case reports reported a somewhat activity of EGFR inhibitors (such as cetuximab, erlotinib, and gefitinib), and a phase-2 study of lapatinib has been conducted in EGFR-positive advanced chordoma[160,172].

Despite some innovations put forward in the last ten years in deciphering chordoma biology, therapies still offer a limited value to the patient and there is a common need to develop new therapeutic strategies (Tab. 1)[30,39,41,207].

Table 1. Overview of the current clinical trials on chordomas patient [adapted from Chordoma Foundation website[29]].

Mechanism	*Therapy*	*Type*	*Sites & Trial ID*
Therapeutic vaccine targeting Brachyury plus radiation	GI-6301	Phase 2	National Cancer Institute NCT02383498
CDK4/6 inhibitor	Palbociclib	Phase 2	University of Heidelberg (DE) NCT03110744
PD-1 inhibitor plus radiation	Nivolumab	Phase 1	Memorial Sloan Kettering, Johns Hopkins NCT02989636
EGFR inhibitor	Afatinib	Phase 2	University of Leiden (NL), Istituto dei Tumori (IT), University College London (UK) NCT03083678
EZH2 inhibitor	Tazemetostat	Phase 2	Multi-center NCT02601950

Cytogenetics, transcriptomics and functional studies

The pathological mechanisms driving chordomagenesis are still far way to be completely understood[207].

The majority of chordomas are diploid, whereas tumors presenting with an abnormal karyotype present with a survival reduction[1]. Common chordoma cytogenetics abnormalities are loss of heterozygosity (LOH) of chromosomes 1p36, 9p, 10q and 17p[36,71,109,120,207]. Specifically, loss or rearrangement of 1p36 represents the most frequent chromosomal aberration in sporadic chordomas and it also has a prognostic significance and it has been linked to hereditary familiar chordomas[109,150]. Moreover, *CDKN2A* gene is located the locus 9p21, and it is mainly involved in the regulation the cell cycle arresting the cells in G1 phase[57].

A recent study provided a genomic and transcriptomics characterization of skull base chordomas and showed chromosomal abnormality in 1p, 7, 10, 13, and 17 regions and recurrent somatic variants including *MUC4*, *NBPF1*, *NPIPB15* single nucleotide variations and *SAMD5-SASH1* gene fusion[153]. Furthermore, the presence of the germline functional SNP rs2305089 in the *T* gene is associated with chordomas and may help in not-skull base chordoma prognostication[30,84].

Several gene expression studies have been conducted in chordomas and they generally showed a clustering with cartilaginous neoplasms including chondrosarcomas[65,163]. Chordoma tumours showed higher expression levels of extracellular matrix such as collagen II, SOX9, podoplanin, fibronectin, metalloproteinase MMP-9 and MMP-19, CD24 antigen, insulin growth factor binding protein 2 (IGFB2), retinoic acid receptor responder 2 (RARRES2), cytokeratins than chondroid tumors[65,163]. Expression of tyrosine kinases receptors (TRKR) has been analyzed using IHC, western-blotting and RT-PCR techniques showing that platelet-derived growth factor receptor beta (PDGFR-β) was expressed in mostly every chordomas[43,180]. Such finding

provided the rationale for the development of the first phase II clinical trial of imatinib mesylate in chordomas[21,46]. In a study of 21 chordomas, EGFR has been reported to be over-expressed in 67% and in a bigger study of 284 chordomas in 86.1% by immunohistochemistry[43,181]. c-MET and c-KIT (CD117) were detected in 66% and 33% of specimens[43]. In the latter study c-KIT was highly expressed in in 31 tumors (20.9%) and expressed in 61/80 primary chordomas (76.2%) and in 127/148 chordomas (85.8%)[181]. The active phosphorylated forms of ERK, AKT and STAT3, indicative of tyrosine kinase activity, were detected in 86%, 76% and 67% of cases[43]. PSTAT3 was expressed in 79 primary chordomas (71.2%) and in 227/287 (79.1%) of all chordomas in another study[181]. The expression of nerve growth factor receptor (TrkA) and nerve growth factor (NGF) was significantly higher in chordomas than in notochordal cells[140]. Several studies have reported a high protein expression (90-100%) of the transcription factor Brachyury. This gene is normally expressed in undifferentiated embryonic notochord and it regulates stem cell genes and EMT process[74,132]. The overexpression is due mostly by an amplification at locus 6q27 where is located the *Brachyury* gene[132,195,210]. β-catenin and other cell–matrix adhesion molecules such as N-cadherin are intensely expressed in clival chordomas and may act as responsible for their tumor aggressiveness and local invasion[185]. Impaired expression of tumor suppressor gene *PTEN*, involved in the negative regulation of PI3K/Akt/mTOR pathway, has also been found in chordomas and may suppresses apoptosis, promotes cell growth and drives cellular proliferation[142,162]. Sonic hedgehog pathway (SHH) represents an important developmental pathway and it is directly involved in the correct embryonic development of notochord and central nervous system structures[25,103]. Only one brief letter showed the potential activation of such pathway in chordomas[22]. Moreover, SHH is located at the chromosome 7p12 and copy number variation studies showed gains and partial polysomies of chromosome 7 in chordomas[13,159].

CERAMIDES

Structure and metabolism

Ceramide (Cer) represents the structural core of every sphingolipid, a family of complex lipids that are involved in the architecture and fluidity of cellular membranes[8,58,59]. Sphingolipids have been discovered in brain extracts and named by J.L.W. Thudichum in 1884 recalling the myth of the Sphynx due to their unknown and enigmatic biological role. Cer is composed of a sphingosine base and a fatty acid varying in length from C14 to C26; the most common is behenic acid (Fig. 17)[48]. Cer, then, serves as the metabolic and structural precursor for complex sphingolipids, such as sphingomyelin (SM), Cer-1-phosphate and glucosylceramides (GlcCer)[8].

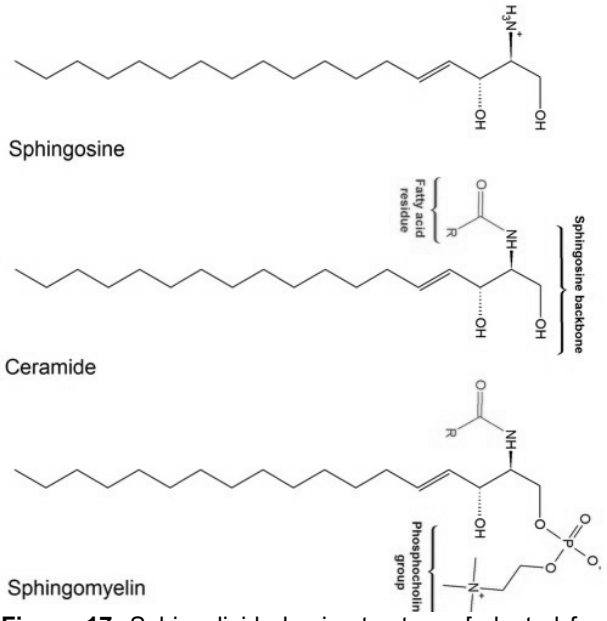

Figure 17. Sphingolipids basic structures [adapted from LHcheM, Wikipedia].

Endogenous Cer could be generated through two main pathways (Fig. 18):

- *De novo* biosynthesis pathway that occurs on the cytoplasmic face of the endoplasmic reticulum and begins with the condensation of serine and palmitoyl-CoA by serine-palmitoyl transferase (SPT) to generate 3-Ketosphinganine which is, then, transformed to dihydrosphingosine by 3-Ketosphinganine reductase. The acylation of dihydrosphingosine to dihydroceramide is carried out in humans by six different ceramides synthases (CerS). CerS introduce fatty acids with varying lengths and degrees of unsaturation. Specifically, CerS1/4 produce Cer C18 and to a lesser extent Cer C20, whereas CerS5/6 selectively produce Cer C16 and to a lesser extent Cer C12 and Cer C14. In turn, ceramide is formed by the desaturation of dihydroceramide;

- *Salvage* pathway that occurs on the acidic subcellular compartments, lysosomes and endosomes, and it is derived by the catabolism of complex sphingolipids through different specialized hydrolases that finally form glucosylceramide and galactosylceramide. In turn, they are hydrolyzed by specific β-glucosidases and galactosidases to regenerate ceramide. Sphingomyelin (SM) can be hydrolyzed by one of several sphingomyelinases (SMases), such as acid, neutral and alkaline SMases.

In sphingolipid biosynthesis pathways, Cer can be also phosphorylated by ceramide kinase, glycosylated by glucosyl or galactosylceramide synthases, or receive a phosphocholine group from phosphatidylcholine (PC) to synthetize SM through the action of SM synthases[8,59].

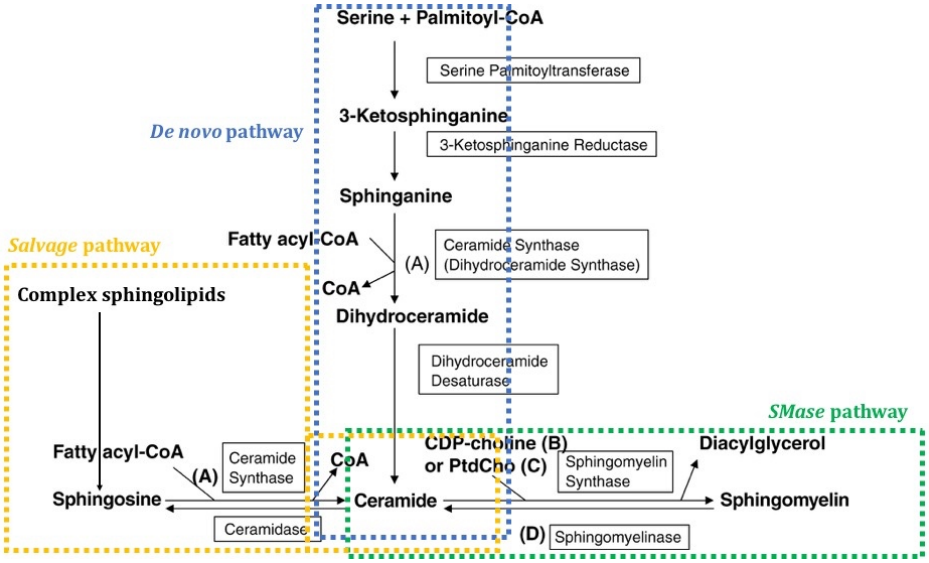

Figure 18. Ceramide metabolism pathways [adapted from Xu et al., 2005].

Ceramides may be catabolized by many ceramidases to generate sphingosine, which may be recycled into sphingolipid pathways or phosphorylated by sphingosine kinases (specifically SK1 or SK2). The product sphingosine-1-phosopate (S1P) can be dephosphorylated to regenerate sphingosine through the action of intracellular S1P phosphatases or acting as second messenger or extracellular ligand[8].

Ceramides and programmed cell death

Ceramides and other metabolites, such as DHCer and S1P, act as fundamental bioactive signaling lipids regulating cell growth, differentiation, senescence, apoptosis and autophagy[8,9,59]. Recent knowledge shows an intricate and balanced connection between sphingolipids species and cell fate determination, particularly in the response to stress and stimuli such as pro-inflammatory cytokines, oxidative stress, UV and γ-radiation and chemotherapeutic agents. Cer species are found to be critical for the induction of distinct autophagy pathways: protective autophagy and autophagy-associated cell death, with completely opposing functions in the cellular fate (Fig. 19)[9,81,146,217].

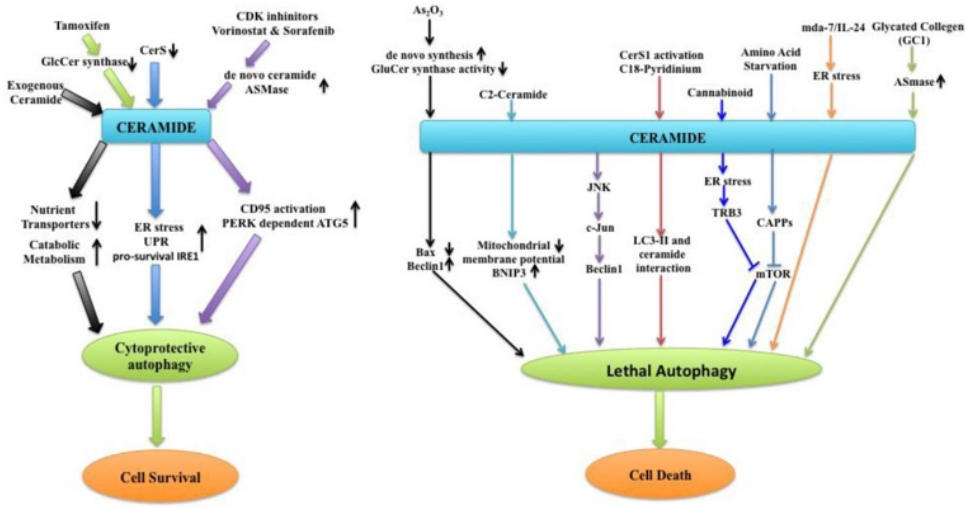

Figure 19. Signaling pathways of cytoprotective and lethal autophagy that are regulated by ceramides [adapted from Jiang W et all, 2014].

Autophagy and apoptosis have been depicted as the two-main programmed cell death biological mechanisms. There is an enigmatic and complex balance between survival and autophagy-related cell death depending on various biological situations[104]. For example, autophagy may function as a stress response to promote cell survival and to suppress apoptosis[95,122]. However, in other examples, autophagy may serve as a mechanism for caspase-dependent or independent cell death[168,214].

Cer is an apoptosis inducer through the activation of the mitochondrial pathway. In some cell types, increased Cer levels arrest cell growth and promote cell apoptosis[90,161] On the other hand, S1P promote cell survival and blocks cell apoptosis[170]. Moreover, dhCer also shows anti-apoptotic effects to promote cell survival during hypoxia through the induction of autophagy and controlling the 'switch' between Cer-mediated apoptosis and cytoprotective autophagy in response to stress[37,176].

Many studies also showed that Cer are autophagosome membrane essential components[169,208]. *De novo* biosynthesis occurs in the ER and might be a driving force for the formation of the autophagosome[62]. A recent paper noted that Cer directly interacts with microtubule associated protein light-chain3 (LC3) on mitochondrial membranes to induce deadly autophagy via an increase of intracellular mitophagy[166]. Moreover, Cer with different fatty acid chain lengths produced by CerS1-6 might have distinct biological functions in the regulation of cell death in various different stress conditions and tissue types. For example, changes between Cer C18 and C16 may play distinct roles in inducing autophagy versus cell death in cardiomyocytes[152].

AIM OF THE WORK

Precision medicine is an emerging approach for disease treatment and prevention that takes into account individual variability in genes, environment and lifestyle for each patient[32]. This approach includes the use of targeted therapy to each patient starting from a detailed phenotypical and genotypic assessment. Such a rationale appears particularly promising in the modern era of oncology, where some tumors may express a defined molecular signature that could be potentially targeted by new therapeutic options. In the present project, we propose to delineate a precision approach to better characterize such rare intracranial tumor.

The main goal of the present work is to identify clinical and molecular bio-markers as specific prognostic factors that could be used for the proper management of skull base chordoma patients. Achieving a detailed clinical and molecular signature of skull base chordomas is of paramount importance to personalize the treatment to each specific patient. The chance to recognize specific pathways involved in chordoma biology will allow us to identify potential candidates for new molecular targeted-therapies and improving the disease clinical history. The implementation of biomarkers to routine laboratory is therefore required. Moreover, an innovative lipid approach will be employed to better characterize skull base chordomas and elucidate new pathways that can be related to specific tumoral radio-resistance features. The present work has been divided in two different phases to better assess and validate the biomarkers:

1. A retrospective review gathering clinical, radiological, surgical and pathological data by querying Institutional tumor registries;
2. A prospective phase based on the collection of clinical-radiological features and frozen surgical specimens to perform a bio-molecular analysis with LC-MS/MS to evaluate and quantify ceramides and dihydroceramides species in skull base chordoma.

PATIENTS AND METHODS

Study design and population

A retrospective review of all the patients diagnosed and treated for a skull base chordoma at the Fondazione IRCCS Istituto Neurologico “Carlo Besta” between January 1992 and December 2017 has been performed. The two queried sources used for the present study were the prospectively collected Institutional Tumor Registry and Neuropathological Tumor Database. All patients of any ages harboring a histopathology-confirmed skull base chordoma have been included in the study. The exclusion criteria were the following: incomplete clinical data and impossibility to determine the surgical outcome, insufficient and not adequately representative tissue specimen to confirm the diagnosis of chordoma, the non-primarily skull base location of the tumor. Institutional review board approval was obtained for the present study and consent obtained from the patients. Eighty-seven consecutive patients were surgically treated for a skull base chordoma during the period of recruitment. Seventy-eight patients were eligible for the retrospective review. Nine patients were excluded from the analysis due to incomplete clinical data (n=8) and different location (n=1). Data were reported according to the STROBE guidelines for observational studies.

The gathered clinical variables were the following: gender, age at the time of surgery, tumor location and extension, type (primary/recurrent), radiological features, pre- and post-operative symptoms, previous treatments, surgical approach, intra-operative findings, extent of resection, surgical complications, pre- and post-operative patient functional status, histological subtype, type of adjuvant treatment, progression free-survival (PFS) and overall survival (OS).

Surgical anatomy

The location of chordomas was reported as skull base and non-skull base, according to previous papers[14,54,55]. Skull base chordomas included tumors localized in the clivus and/or in the first two cervical vertebras, whereas non-skull base chordomas included tumors localized in the region extending from the third cervical vertebra to the sacro-coccygeal region and these were not the focus of the present project. The recruited skull base chordomas were further classified accordingly to their primary anatomical location in upper, middle and inferior clival location (Cl1, Cl2, Cl3) and cranio-vertebral junction types[40,54,164]. The secondary extensions of skull base chordomas to the surrounding anatomical structures were the following: supra-sellar space and/or 3rd ventricle, optic-carotid cistern and/or Sylvian fissure, sphenoidal sinus and/or other paranasal sinuses, cavernous sinus, middle cranial fossa, petrous apex, cerebello-pontine angle cistern, jugular foramen, occipital condyle, rhynopharynx and/or para-pharyngeal space, pre-brainstem cistern with/without brainstem dislocation.

Radiological assessment

The diameters of tumor were drawn from the three anatomical planes and the volume was then calculated using an ellipsoid model "(ABC)/2" equation in the available computerized digital images. The signal intensity of the lesion on T1-weighted and T2-weighted images were collected by using the intensity of the brain as reference, and determined as "hypo-", "iso-" or "hyper-" when the intensity of the lesion was lower, equal or higher than that of the central nervous system structures. The degree (absent, mild, intense) and pattern (homogenous, heterogeneous) of contrast enhancement on MR images were also evaluated[138]. The presence of bone erosion and/or calcifications was evaluated on the available CT scans. In cases where

imaging was not available, the dimensions and radiological features were gathered from the clinical and radiological chart notes. The extent of resection (EOR) was confirmed by comparison of pre-operative and 3 months post-operative contrast-enhanced MR images. EOR was categorized as 100% (GTR), ≥ 85% and < 100% (STR), and < 85% (PR). The radiological features were evaluated by an independent reviewer blinded to the patient clinical outcomes.

Clinical assessment

The pre-operative clinical symptoms were divided in the following categories: cranial nerve deficits, endocrinopathy, headache and/or cervical pain, motor, sensory and cerebellar deficits. The disease history was defined as the period from the starting clinical presentation to the surgical intervention. The type of chordoma was defined as primary or recurrent tumor in relation to the previous treatments (surgery and or radiation therapy) and radiological/clinical evidence of disease progression. A stable tumor was defined as residual tumor. An intentional diagnostic biopsy was not considered as a previous treatment, thus patients with a biopsy and absence of a disease progression were considered primary tumors.

Surgical technique

Since the present case series involved many surgeons from the same Institution, surgical approaches have been chosen in relation to each surgeon's personal experience. The EEA has been introduced at our Institution in 1993, but a routinely use has been started from 2005. The philosophy of our contemporary surgical technique is to achieve maximally safe resection and it is summarized in our recent publication[99].

Surgical outcomes

Patients were assessed by clinical, laboratory, and radiological evaluation throughout the hospital stay, and at 3 months, 6 months, 1 year, and every 1 year subsequently, for any new clinical features, tumor regrowth and adjuvant treatments. The medical and surgical complications were graded according to the Clavien-Dindo grading classification system (CDG)[28]. The functional status was assessed by KPS score. Clinical outcomes were assessed at discharge and at the last follow-up through office visits and/or telephone interviews. Progression-free (PFS) and overall survival (OS) were calculated from the date of treatment. OS was defined as the period from the first surgical treatment to all-causes death or at the end of observation. PFS was defined as the period from the surgical treatment until the clinical and/or radiological evidence of any tumor re-growth.

Pathology

Chordomas were classified accordingly to the 4th Edition of WHO Classification of Tumours of Soft Tissue and Bone in: chordoma NOS (not otherwise specified), chondroid chordoma and “de-differentiated” chordoma[203]. Tumor specimens collected from the operating room were fixed in Carnoy’s solution, de-hydrated in absolute ethanol and paraffin-embedded, then sectioned at 2 µm. For the histological analysis, slides were re-hydrated and stained with hematoxylin-eosin (H&E) according to the standard method. Since October 2015, apart from the routinely collection for histological analysis purposes, part of the surgical tissues, chosen by the pathologist, was also directly snap-frozen in liquid nitrogen at the time of surgery and stored at -80°C until use for other purposes.

Immunohistochemistry

The chordoma tissue samples were investigated by immunohistochemistry (IHC) for the expression of markers routinely employed for diagnostic purposes, such as cytokeratin (AE1-AE3), vimentin, EMA, S-100. Additionally, we investigated the following markers: Brachyury (mouse monoclonal anti-Brachyury, dilution 1:100, Abcam, UK), p53 (mouse monoclonal anti-p53, 1:50, DAKO, Denmark), beta-catenin (mouse monoclonal anti-beta-catenin, 1:100, BD Biosciences, USA), filamin-A (mouse monoclonal anti-filamin, 1:200, Fitzgerald Industries, USA), GAB-1 (mouse monoclonal anti-GAB-1, 1:50, Abcam, UK), EGFR (mouse monoclonal anti-EGFR, 1:100, ThermoFisher Scientific, USA), PDGFR-beta (rabbit polyclonal anti-PDGFR-beta, 1:200, Santa Cruz Biotechnology, USA), c-MET (rabbit polyclonal anti-c-MET, 1:50, Santa Cruz Biotechnology, USA), c-kit/CD117 (rabbit polyclonal anti-CD117, 1:200, DAKO, Denmark), PTEN (mouse monoclonal anti-PTEN, 1:100, Santa Cruz Biotechnology, USA), YKL-40/GP-39 (goat polyclonal anti-YKL-40/GP-39, 1:250, Santa Cruz Biotechnology, USA), TERT (mouse monoclonal anti-h-TERT, 1:200, Merck Millipore, Germany), MIB1/ki67 (mouse monoclonal anti-Ki67 clone MIB1 1:100, DAKO, Denmark), BCL2 (mouse monoclonal anti-BCL2 1:50, DAKO, Denmark), p62 (mouse monoclonal anti-p62 1:200, BD Biosciences, USA). Antigen retrieval was performed in a EDTA buffer solution (pH 9.0) and 98°C in PT Link pre-treatment module (DAKO, Denmark) or in citrate-buffer solution (pH 6.0) in the microwave. Endogenous peroxidase activity was blocked using 3% H2O2 (Sigma-Aldrich, USA) for 20 min. Nonspecific binding was blocked in normal goat serum (1:20, Dako, Denmark) or in bovine serum albumin (BSA, 1:20, Santa Cruz Biotechnology, USA). Sections were then incubated with primary antibodies according to the reference working concentration and were subsequently incubated with anti-mouse or anti-rabbit Envision® HRP-peroxidase conjugated or anti-goat

biotin (1:300) and streptavidin system (1:300) as secondary antibodies (DAKO, Denmark) for 1 hour at room temperature. Detection was performed using the 3'-3'-diaminobenzidine substrate system (DAB Substrate Chromogen System, DAKO, Denmark). Sections were finally counterstained with hematoxylin. Staining was evaluated by two observers blinded to clinical outcome of patients and it was considered as positive when they exhibited a moderate to strong staining in at least 20% of tumor cells. The degree of staining was also semi-quantitatively graded according to the percentage of stained cells. In skull base chordoma, expression of the employed markers was scored as follows: "-" (<5%), "+/-" (5-20%), "+" (20-50%) and "++" (>50%). For statistical analysis, "-" and "+/-" were grouped together as "negative" and "+" and "++" were grouped together as "positive".

TERT promoter sequencing

DNA for *TERT* promoter sequencing was extracted form paraffin-embedded tumors using phenol-chloroform method. Paraffin tumor blocks were cored, choosing an area rich of tumor cells from H&E slides, and de-waxed in xylene and absolute ethanol. Then, tissues were digested over-night in proteinase-K (20mg/ml) at 55°C. DNA was extracted from digested tissues by phenol-chloroform and absolute ethanol, and then measured by Nanodrop® spectrophotometer (ThermoFisher Scientific, USA). PCR sequencing analysis was performed using customized primers for *TERT* promoter, including the C250 and C228 hotspots, according to the following thermal profile: denaturation (5', 95°C), annealing (62°C, 30''), elongation (72°C, 30'') for 35 cycles and final elongation (7', 72°C) using Taq Fast as polymerization enzyme (Roche, Switzerland). PCR products were then sequenced using Sanger method on a capillary sequencer (ABI3130 Life Technologies, USA) and analyzed by Sequencing Analyzer (Life Technologies, USA) and Chromas Lite programs (Technelysium, Australia).

Sphingolipids analysis with LC-MS/MS

Ceramides and dihydroceramides species were extracted from frozen samples and assessed using liquid chromatography–mass spectrometry (LC-MS/MS)[117]. Tumor samples were added with 100 µL of PBS + 0.1% protease inhibitor and homogenized in TissueLyser (Qiagen, Hilden, Germany) for 3 min at 50 oscillations/s. Total protein concentration was measured by Bradford dye-binding method. Samples were added with 10 µL of IS (Cer C12 20 mM) and 850 µL of a methanol/chloroform mixture (2:1, v/v), then sonicated for 30 min. Afterwards, there were incubated overnight in an oscillator bath at 48 °C. Once at room temperature, samples were added with 75 µl of KOH 1 M in methanol and incubated at 37 °C for 2 hours. To bring the pH at a neutral level, 75 µl of acetic acid 1 M was added in methanol. The phase was evaporated under a stream of nitrogen. The residuals were dissolved in 150 µl of methanol and then centrifuged for 10 min at 13000 rpm. 10 µL were directly injected in LC-MS/MS. The analytical system consisted of a HPLC coupled to a tandem mass spectrometer. The LC system was a Dionex 3000 UltiMate instrument with autosampler, binary pump and column oven (Thermo Fisher Scientific, USA). Separation was attained on a reversed-phase BEH C-18 10 x2.1 x1.7 µm analytical column preceded by a security guard cartridge. Linear gradients were obtained between eluent A (water + 2 mM ammonium formate + 0.2% formic acid) and eluent B (methanol + 1 mM ammonium formate + 0.2% formic acid). The column was equilibrated with 80% (B), increased to 90% (B) in 3 min, held for 3 min, increased to 99% (B) in 9 min, held for 3 min, back to the initial conditions in 2 min and kept for 2 min at 80% (B). The flow rate was 0.3 mL/min, the autosampler and the column oven were kept at 15°C and 30°C, respectively. The tandem mass spectrometer was an AB Sciex 3200 QTRAP instrument with electrospray ionization TurboIonSpray™ source (AB Sciex S.r.l., Milano, Italy). Instruments were managed with the proprietary

manufacturer's software and according to the manufacturer's instructions. The analytical data were processed using Analyst software (version 1.2). The ion spray voltage was set at 5.5 kV and the source temperature was set at 300 °C. Nitrogen was used as a nebulizing gas (GS 1, 45 psi), turbo spray gas (GS 2, 50 psi) and curtain gas (25 psi). The collision-activated dissociation (CAD) was set to a low level. The dwell time was set at 0.1 s, and the MS scan was performed in positive ion modes (ESI+). MS/MS experiment were conducted using nitrogen as collision gas. Compound-dependent parameters (CE, DP) were optimized via direct infusion. Multiple reaction monitoring (MRM) mode was used. Quantitative analysis was performed interpolating each peak area of analyte/area IS with calibration curve of each sphingolipids. The sphingolipids amount was normalized by total protein content, expressed in milligram, in each sample. Six-point calibration curve was evaluated by spiking increasing amounts of the analytes in water in the concentration range of 0-40 pmol/vial. Linearity was observed for each analyte in the whole range (R^2>0.99).

Statistical analysis

Descriptive statistics was used to analyze the pre-, peri- and post-operative clinical data. Categorical values were described with percentages and continuous variables were described with means, standard deviations and ranges. Statistical analysis between different groups was performed to determine if significant differences existed between means of clinical and radiological outcome data. Survival analysis was performed according to Kaplan-Meier method. Univariate comparisons were conducted using Mann-Whitney, Chi-square and exact Fisher tests. Simple linear regression and correlation with computation of Pearson coefficients analyses were conducted. The level of significance was set according to GP style as follows: *, p≤0.05; **, p≤0.01; ***, p≤0.001, ****, p≤0.0001.

Clinical prognostic factors with p values ≤ 0.05 on univariate analysis were subject to multivariate analysis using a Spearman's rank model correlating with OS and PFS. Ceramides and dihydroceramides total and single species were subjected to multiple linear regression analysis using a Pearson correlation model with MIB-1 as regression model target. To evaluate the ceramides and dihydroceramides also as independent prognostic factors, a set of linear regression analyses were conducted with OS and PFS as regression model targets. The following statistical analyses were performed to preliminarily build a personalized outcome grading scale, the Peri-Operative Chordoma Scale (POCS). Firstly, a logistic regression model was built to investigate the strength of the relationship between the putative clinical predictors and surgical outcomes (OS and PFS). The peri-operative factors that resulted statistically significant at the preliminary clinical analysis were as follows: jugular foramen involvement, MR contrast enhancement, presence of preoperative motor deficits and CN deficits, tumor involvement of pre-brainstem cisterns, pre-operative brainstem dislocation, personal surgical expertise, development of postoperative complications, entity of tumor resection and ΔKPS. We used the Cox&Snell and Nagelkerke pseudo-R^2 to evaluate the goodness of fit of the model. Secondly, we rated the significant predictors after rounding their ORs to the closest even number. All the independent variables were entered into the equation first and each one was deleted, one at time, if they did not contribute to the regression equation by the backward elimination method. Final candidate predictive factors that well fitted the model were: MR contrast enhancement, presence of preoperative motor deficits and development of postoperative complications. The presence or absence of these factors were initially considered in a simplified version of POCS, namely POCS-beta. Therefore, for each patient, a corresponding total score was calculated based on the sum of all predictors' scores. The ANOVA test was performed to compare the mean scale scores between the changes in surgical outcomes measure.

Finally, we attempted to validate the ability of POCS in determining surgical outcomes by using chi-square analysis. Statistical analyses were run on SPSS v.18 (IBM Inc., Armonk, NY) and GraphPad (GraphPad Software, Inc.).

RESULTS

CLINICAL ANALYSIS

Demographics

Seventy-eight patients were included in the present study for the clinical retrospective analysis. There were 38 males (48.7%) and 40 females (51.3%). The female/male ratio was 1:1.1. The mean age at the time of surgery was 49.7±18.8 years (range, 10-85). One-hundred-fourteen surgical operations were performed in the initial recruitment or recurrent setting. Staged-operations were performed in eleven patients (14.1%), in 2-stages in ten and in 3-stages in one patient. The mean follow-up period calculated from the first treatment performed at our Institution of the present cohort series was 69 months (3-233). Sixty (76.9%) patients presented with primary tumors and eighteen (23.1%) patients were recurrent tumors which showed a clear evidence of disease progression. The patients which have already undergone previous treatments in other Institutions were the follows: ten patients only surgical treatment, two only radiation therapy, five surgery and radiation and one patient surgery, radiation and chemotherapy with tyrosine kinase inhibitors (Imatinib). Of the recurrent chordomas, eleven patients (61.1%) had only one recurrence after previous treatments, four patients (22.2%) had 2 previous recurrences and three patients (16.7%) had three previous recurrences.

Pre-operative signs and symptoms

The most common pre-operative symptom was cranial nerve deficit, presenting mostly with diplopia caused by any oculomotor nerve deficit. Cranial nerve deficits were specifically present in 65 cases (83.3%) with the general following frequencies: CN 1=0 (0%), CN 2=14 (21.5%), CN 3=14

(21.5%), CN IV=6 (9.2%), CN V=12 (18.5%), CN VI=46 (70.8%), CN VII= 7 (10.8%), CN VIII=4 (6.1%), CN IX-X-XI=17 (26.1%), CN X11=10 (15.3%). Patients presented with headache and/or cervicalgia in 28 cases (35.9%), cerebellar signs in 16 cases (20.5%), long tracts motor deficits in 15 cases (19.2%), body sensory deficits in 5 cases (6.4%), trigeminal neuralgia in 3 cases (3.8%), endocrinopathy in 2 cases (2.6%) and only one (1.3%) patient with obstructive hydrocephalus and raised ICP symptoms. In primary tumors group, 49 cases (81.7%) presented with cranial nerve deficit, 24 (40%) with headache and/or cervicalgia, 13 (21.7%) with cerebellar deficit, 11 (18.3%) with motor deficit, 4 (6.7%) with sensory deficit, 1 (1.7%) with endocrinopathy. In recurrent tumor patients, 16 cases (88.9%) presented with cranial nerve deficit, 4 (22.2%) with headache and/or cervicalgia, 3 (16.7%) with cerebellar deficit sign, 4 (22.2%) with motor deficit, 1 (5.5%) with sensory deficit, 1 (5.5%) with endocrinopathy. There was no statistically significant difference in terms of clinical presentation between primary and recurrent tumors. The presence of motor deficits (Fig. 20) in the cohort of primary skull base chordomas revealed to be a significant prognostic factor correlating with a worse PFS (p=0.0480).

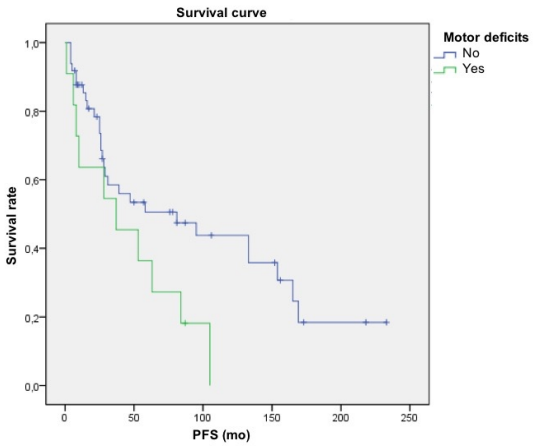

Figure 20. Kaplan-Meier survival curve for PFS according to preoperative motor deficits in primary skull base chordomas (p=0.0480).

Significantly, the presence of motor deficits (Fig. 21) represented an important prognostic factor with a worse PFS also in the cohort of recurrent skull base chordomas (p=0.0160).

Moreover, the presence of any pre-operative cranial nerve deficits (Fig. 22) represented a significant prognostic factor with a worse PFS in the cohort of recurrent patients (p=0.0260).

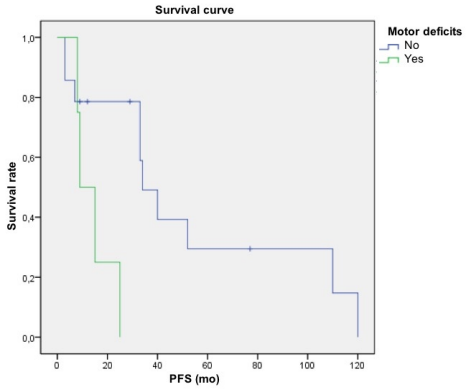

Figure 22. Kaplan-Meier survival curve for PFS according to preoperative motor deficits in recurrent skull base chordomas (p=0.0160).

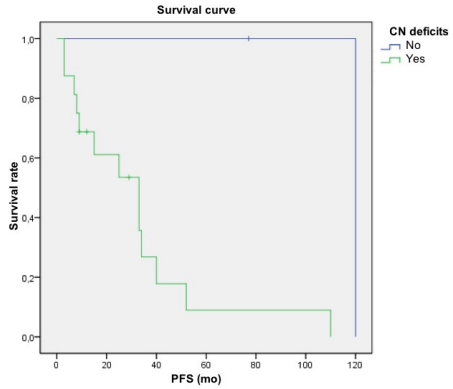

Figure 21. Kaplan-Meier survival curve for PFS according to preoperative cranial nerve deficits in recurrent skull base chordomas (p=0.0260).

The mean diagnostic delay time (DDT), defined from the onset of symptoms or evidence of radiological/clinical disease progression to surgical intervention, was 10.3 ± 13.5 months (1-97). The mean DDT for primary tumors was 10.4 ± 10.9 months (1-66) and for recurrent tumors was 13.2 ± 21.9 (1-97). The mean pre-operative KPS at our institutional admission was 84.5 ± 9.8 (50-100). The mean pre-operative KPS in primary tumors was 85.8 ± 8.3 (60-100) and in recurrent tumors was 80 ± 12.8 (50-100) and was not significantly different (p=0.0523).

Radiological features

The mean tumor volume was 20.8 (1.6-126.0) cm^3 and the mean maximum diameter was 3.1 (0.7-7.2) cm. The mean tumor volume for first operations was 17.7 (1.6-78.7) cm^3 compared with 31.3 (4.4-126.6) cm^3 for recurrent tumors (p=0.0548). The mean maximum diameter for first operations was 3.0 (0.7-6.3) cm compared with 3.6 (1.7-7.2) cm for recurrent tumors (p≤0.05).

The typical imaging features (based on >50% volume) of skull base chordomas were the following: intermediate to low signal intensity on T1-weighted MRI, high signals on T2-weighted MRI and a heterogeneous enhancement on post-contrast administration T1-weighted MRI.

The presence of any calcification on appropriate imaging (CT and/or SWI-MR were available in sixty-two cases) was investigated and twenty-eight patients (45%) presented intra-tumoral calcification. Calcification on KM analysis (Fig. 23) showed a correlation with better outcomes (OS) compared with tumor lacking any calcification on CT scan in primary skull base chordomas (p=0.0420).

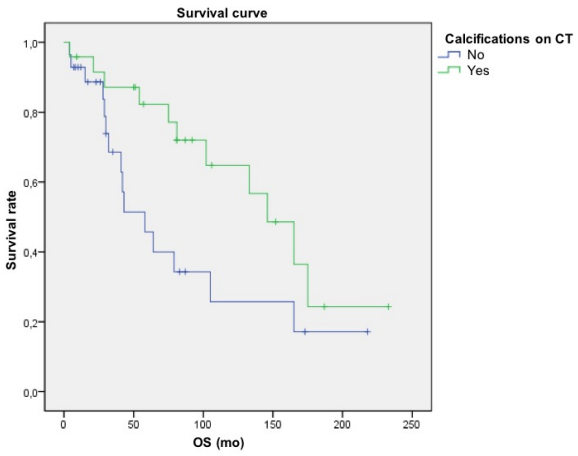

Figure 23. Kaplan-Meier survival curve for OS according to presence of calcification in primary skull base chordomas (p=0.0420).

The degree of contrast enhancement in chordoma is scarcely described in the existing literature and it is not considered in the modern clinical and radiological patient management as prognostic factor in skull base chordomas[138,156]. In our series (MR imaging post-gadolinium T1-weighted features were available and retrieved from 67 cases), thirty-nine patients (58.2%) presented with an intense contrast enhancement, twenty-two (32.8%) with mild enhancement and six (9%) with no enhancement. The degree of MR enhancement revealed to be a significant prognostic factor in terms of OS and PFS in the cohort of primary skull base chordoma patients (Fig. 24).

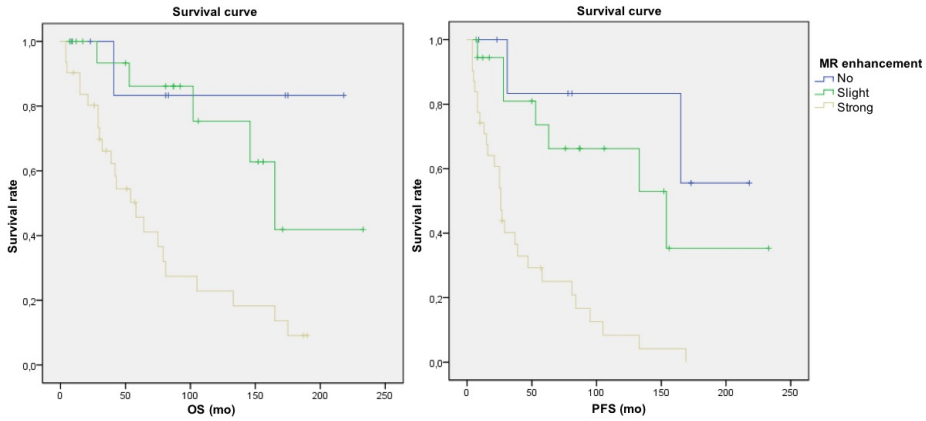

Figure 24. Kaplan-Meier survival curves for OS (left) and PFS (right) according to the degree of MR enhancement in primary skull base chordomas ($p \leq 0.0001$ and 0.0010, respectively).

Tumor location

Fifty-seven (73.1%) skull base chordomas involved the upper third of the clivus, fifty-nine (75.6%) involved the middle third, thirty-one (39.7%) involved the lower third and eighteen (23.1%) involved the first two cervical vertebra. In a pluri-recurrent case the tumor arose primarily in the ponto-cerebellar angle, presumably due to surgical trajectory seeding. The secondary extensions of skull base chordomas to the surrounding

anatomical structures were the following: supra-sellar space and/or 3rd ventricle (19 cases, 24.3%), optic-carotid cistern and/or Sylvian fissure (3, 3.8%), sphenoidal sinus and/or other paranasal sinuses (18, 23.1%), cavernous sinus (34, 43.6%), orbit (1, 1.3%), middle cranial fossa (7, 8.9%), petrous apex (23, 29.4%), cerebello-pontine angle cistern (8, 10.2%), jugular foramen (11, 14.1%), occipital condyle (12, 15.4%), rhynopharynx and/or para-pharyngeal space (11, 14.1%), pre-brainstem cistern (42, 53.8%), brainstem dislocation (24, 30.8%), extension toward the lower cervical vertebral column (2, 2.6%%). In two cases (2.6%) the tumor was completely intradural, in fourteen cases (18%) completely extradural and in 62 cases (79.4%) were extradural extending into the intradural space.

Jugular foramen involvement (Fig. 25) represented a significant prognostic factor with a worse PFS in the cohort of primary skull base chordomas (p=0.0130). The presence of chordoma in the pre-brainstem cistern (Fig. 26) revealed to be a significant prognostic factor with a worse PFS in the cohort of recurrent skull base chordomas (p=0.0210). Brainstem dislocation (Fig. 27) represented a significant prognostic factor correlating with a both worse

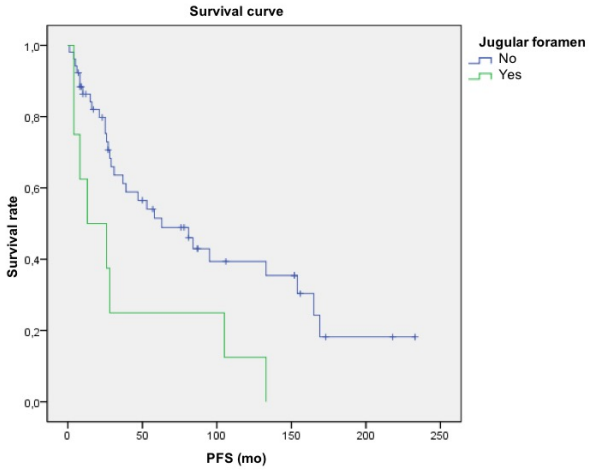

Figure 25. Kaplan-Meier survival curve for PFS according to jugular foramen involvement in primary skull base chordomas (p=0.0130).

outcome in terms of OS and PFS in the cohort of recurrent skull base chordomas (p=0.0060 and 0.0030).

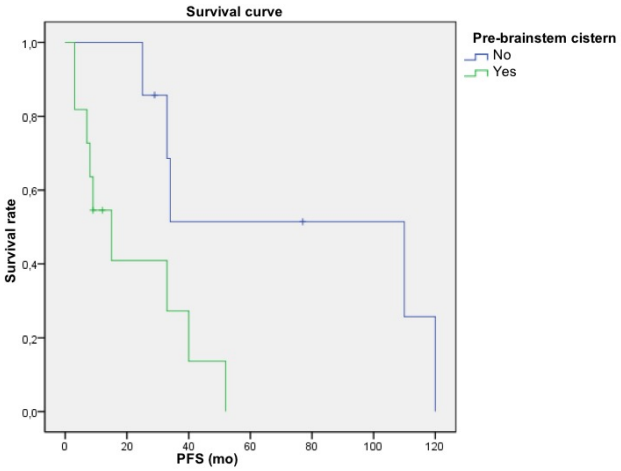

Figure 26. Kaplan-Meier survival curve for PFS according to preoperative radiological involvement of any pre-brainstem cistern in recurrent skull base chordomas (p=0.0210).

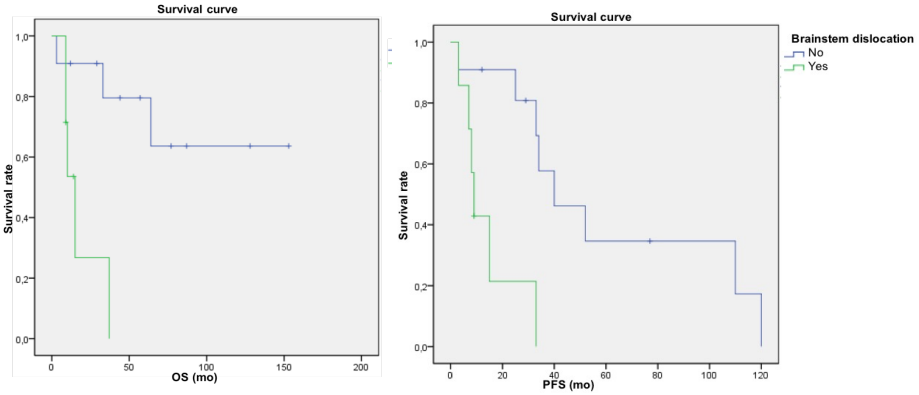

Figure 27. Kaplan-Meier survival curves for OS (left) and PFS (right) according to preoperative radiological brainstem dislocation in recurrent skull base chordomas (p value: 0.0060 and 0.0030, respectively).

Surgical features

One-hundred-fourteen surgical operations were performed in the initial recruitment or recurrent setting (Fig. 28). Staged operations were performed in eleven patients (14.1%), in 2-stages in ten and in 3-stages in one patient. An *anterior* skull base approach was performed in 76 patients (66.7%), specifically the most common approach was endoscopic endonasal approach performed in 41 patients (54%), followed by extended sub-frontal approach performed in 13 patients (17.1%), a microsurgical transsphenoidal approach in 9 patients (11.8%), a microsurgical transsphenoidal approach with a trans-facial/maxillary extension in 9 patients (11.8%), a microsurgical endoscopic-assisted transsphenoidal approach in 3 patients (3.9%), and a combined EEA-extended sub-frontal approach in one patient (1.4%). An *anterolateral* skull base approach was performed in 17 patients (14.9%), specifically the most common approach was frontotemporal orbitozygomatic approach in 9 patients (52.9%), sub-temporal trans-zygomatic approach with anterior petrosectomy in 5 patients (29.4%), lateral supraorbital approach in one patient (5.9%), subtemporal trans-tentorial in one patient (5.9%), a combined subtemporal transtentorial with far lateral approach in one patient (5.9%). A *lateral/posterolateral* skull base approach was performed in 19 patients (16.7%), specifically the most common approach was far-lateral approach performed in 12 patients (63.3%), a petro-occipital trans-sigmoid approach was performed in 3 patients (15.9%), a posterior petrosal approach in one patient (5.2%), a combined transpetrosal-far lateral approach in one patient (5.2%), an extreme-lateral supracerebellar infratentorial approach in one patient (5.2%) and a two-stage combined petro-occipital transsigmoid with an anterior skull base endoscopic endonasal approach was performed in one patient (5.2%). In two CVJ chordomas extending into lower cervical vertebrae bodies an anterolateral transcervical approach was performed.

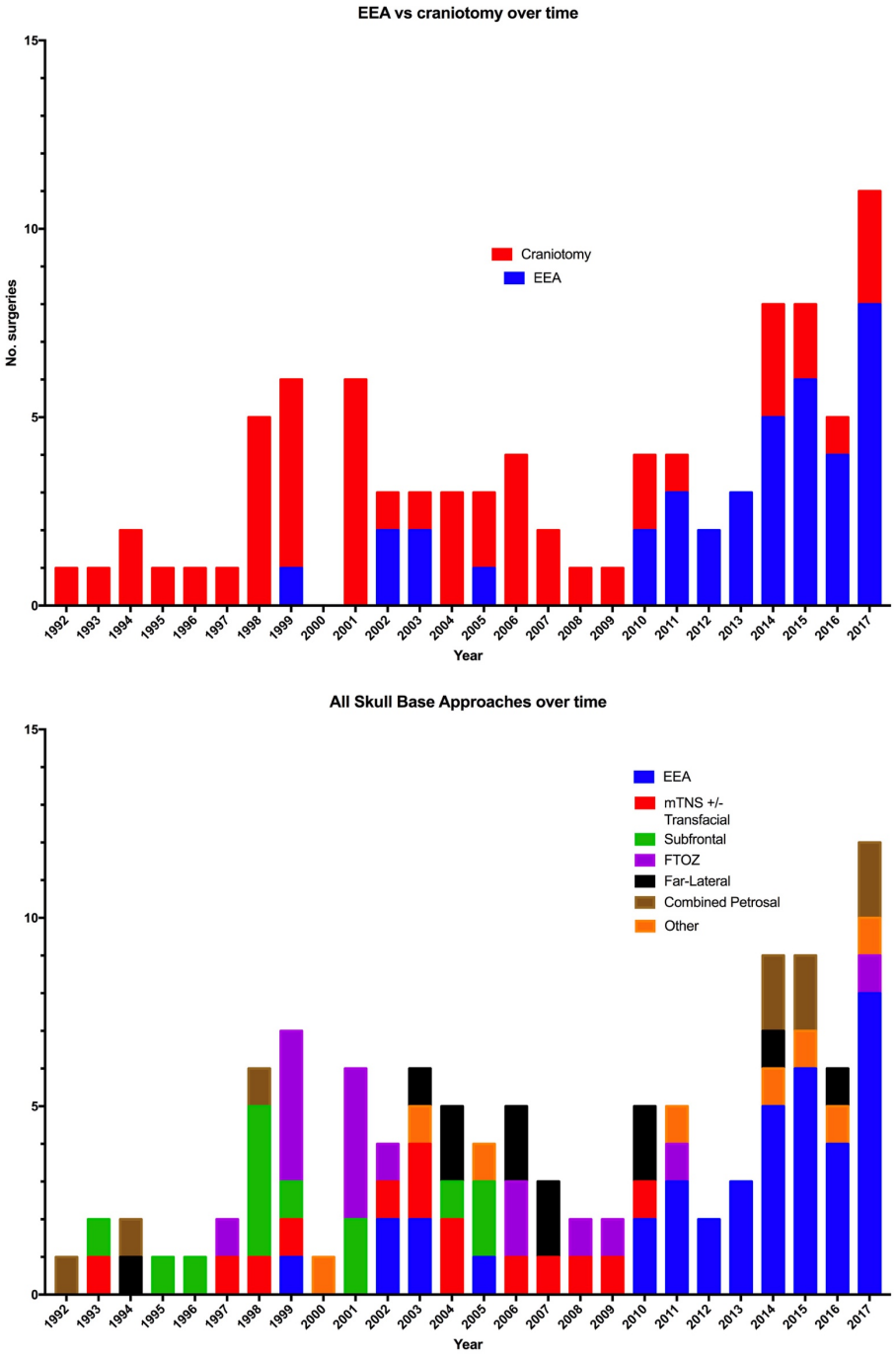

Figure 28. Histograms showing the type of employed surgical approach (above, EEA vs craniotomy; below, details of the craniotomical approach).

Gross total chordoma resection was achieved in 15 patients (19.2%), subtotal in 38 (48.8%) and partial in 25 (32%). GTR was achieved in 12 patients (20%) and STR in 27 patients (45%) and PR in 21 (35%) among the primary and in 3 (16.7%), 11 (61.1%) and 4 (22.2%), respectively, in recurrent patients who had undergone prior treatments. Analyzing the EOR in relation to the first period (1991-2004), GTR was achieved in 0 patients (0%) and STR in 11 patients (45.8%) and PR in 13 (54.2%) and in the second period (2005-2017) GTR was achieved in 15 (27.8%), 27 (50%) and 12 (22.2%), respectively ($p \leq 0.05$). Extent of resection (Fig. 29) represented a strong prognostic factor according to PFS in the cohort of primary skull base chordomas ($p=0.0200$).

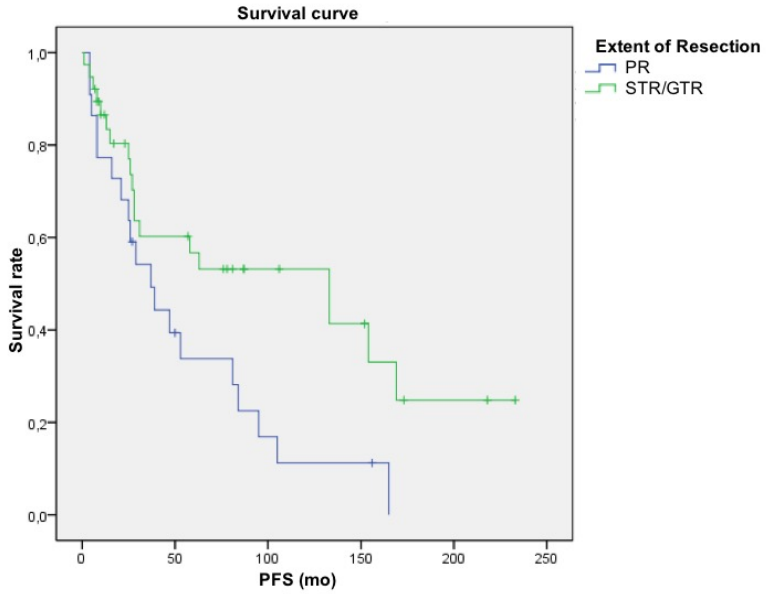

Figure 29. Kaplan-Meier survival curve for PFS according to extent of surgical resection in primary skull base chordomas ($p=0.0200$).

Interestingly, patients operated by an experienced surgeon (defined as the surgeon who performed more than 10 skull base chordoma surgical procedures in the present series) did better in terms of prolonged PFS in the cohort of primary patients (p=0.0340). Surgeon's experience represents, therefore, a significant clinical predictor of better outcomes (Fig. 30).

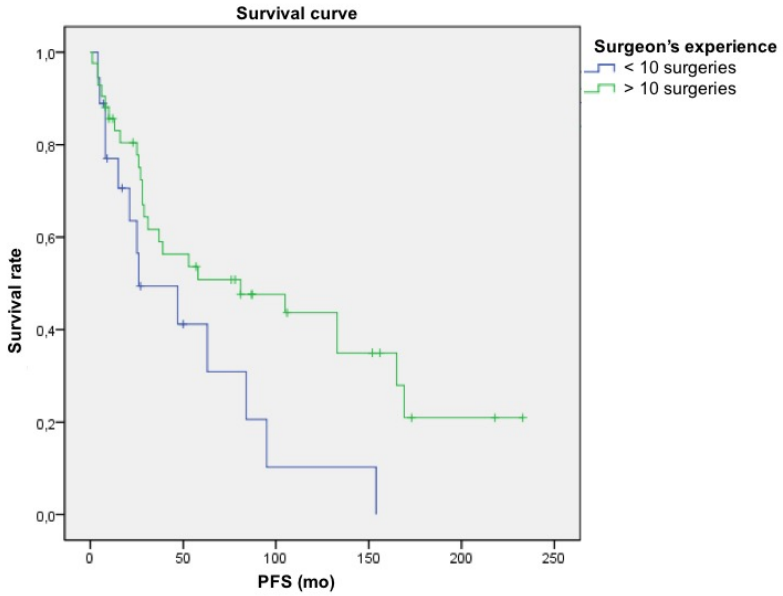

Figure 30. Kaplan-Meier survival curve for PFS according to the individual surgeon's experience in primary skull base chordomas (p=0.0340).

Post-operative complications

There were 4 peri-operative deaths (3.5%). The medical and surgical complications were graded according to the Clavien-Dindo Grading classification system (CDG)[28]. Complications (Fig. 31) were defined as any deviation from the normal peri-operative course (CDG≥1). The rate of complications requiring a surgical procedure and/or a Neuro-Intensive Care Unit (NICU) transfer (CDG 3 and 4) was 24.6% (28). The majority of complications (21.9%) were treated without any invasive treatment (CDG 1 and CDG2). CDG 1 (17, 14.9%) included patients with a worsening or new

neurological deficit (mainly CN and motor deficits), CDG 2 (8, 7.0%) included patients with panhypopituitarism treated with hormonal replacement therapy and meningitis and urinary tract infection treated with antibiotics. CDG 3a (6, 5.2%) included patients with CSF leaks treated with external spinal drainage, whereas, CDG 3b (8, 7.0%) included patients with CSF leaks treated with revision surgery and/or lumbar peritoneal drainage. CDG 4a (1, 0.9%) included a patient with post-operative hematoma surgically evacuated with no need of respiratory aid, whereas, CDG 4b (9, 7.8%) included patients with hematomas surgically evacuated and/or hydrocephalus treated with external ventricular drainage and ventricular peritoneal shunt and/or tracheostomy requiring mechanical ventilation. CDG 5 (4, 3.5%) included patients died from peri-operative brain strokes derived from intraoperative MCA rupture, brain hematomas determining midline shift and arousal disorders, hydrocephalus and post-operative ICA rupture.

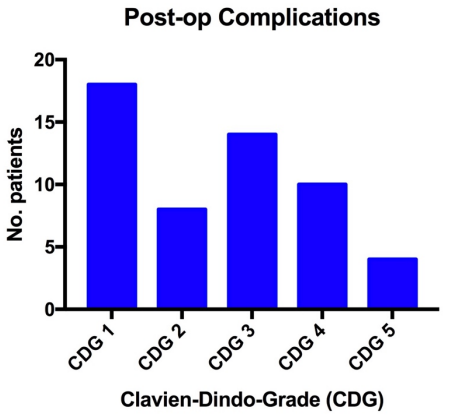

Figure 31. Histogram showing post-operative complications according to CDG scale.

The mean length of stay (LOS) was 15.8 ± 22.2 days (3-139). The mean LOS was 12.8 ± 15.0 days (3-103) for first operations and 20.4 ± 29.6 days (3-139) for recurrent tumors ($p \leq 0.05$).

Development of post-operative complications (Fig. 32) in primary skull base chordoma patients represented an important prognostic factor related to both OS and PFS ($p \leq 0.0001$ and $p = 0.0360$, respectively).

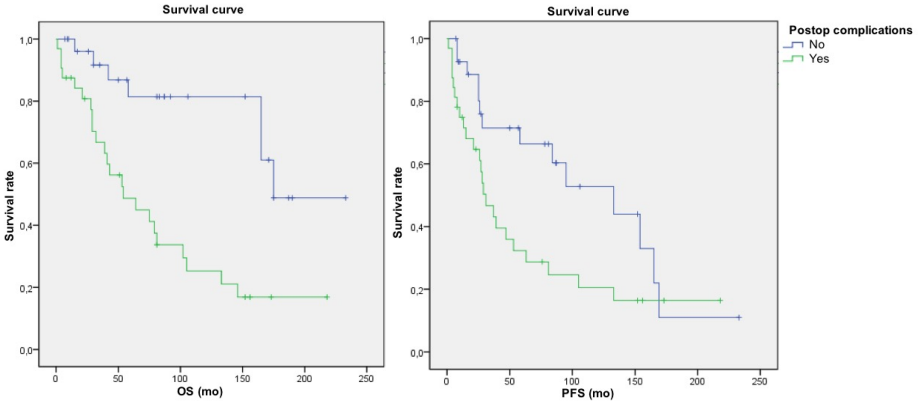

Figure 32. Kaplan-Meier survival curves for OS (left) and PFS (right) according to development of post-operative complications in primary skull base chordomas (p≤0.0001 and 0.0360, respectively).

The KPS score was used to assess functional status pre-operatively and at the discharge; the ΔKPS (KPS_{OUT} – KPS_{IN}) represented a significant clinical prognostic factor (Fig. 33) related to OS in primary skull base chordomas (p=0.0170). In the cohort of recurrent chordomas, ΔKPS correlated to both OS and PFS (p=0.0010 and 0.0180, respectively).

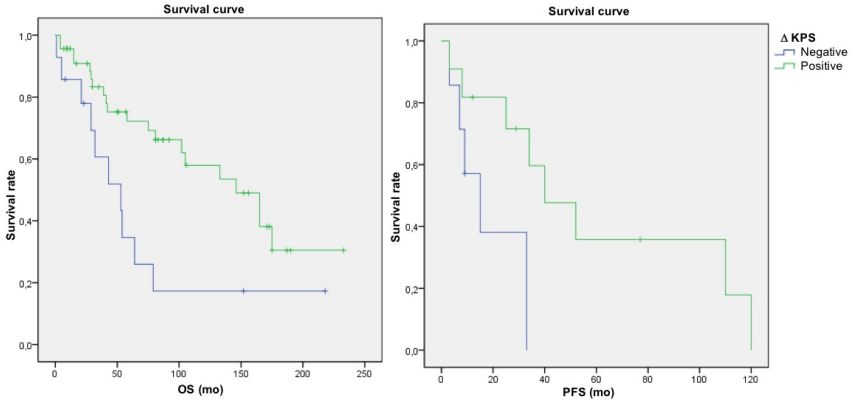

Figure 33. Kaplan-Meier survival curves for OS (left) in primary chordomas and PFS (right) in recurrent chordomas according to ΔKPS (p=0.0170 and 0.0180, respectively).

Surgical outcomes

Thirty-four patients (43.6%) died because of tumor progression and 4 (5.1%) from peri-operative complications. At the time of the last follow-up examination, 40 patients (51.2%) were still alive, of which 26 patients were alive and free of tumor or with stable tumor, whereas 3 patients were alive with noticeable tumor progression. Tumor relapse locally occurred in 14 patients (17.9%). The mean OS time after surgery was 69 months (3-233), whereas the mean PFS time was 54.1 months (4-247). The mean OS after tumor relapse was 42.6 months (3-132) whereas the mean OS for primary tumor was 42.9 months (1-139).

Adjuvant treatments

Radiation therapy data were available for 69 patients in our cohort. Fifty-five patients received post-operative radiation therapy. Ten patients did not receive any post-operative radiation therapy. Four recurrent patients presented at our Institution with a previous radiation treatment. Re-radiation treatment with carbon ions was performed in 7 pluri-recurrent patients. Three pluri-recurrent patients received post-operative chemotherapy with tyrosine kinase inhibitor (imatinib mesilate) with negligible beneficial effects on controlling local disease. The radiation treatment employed photon particles in 15 patients and hadron particles in 38 patients, whereas two were unknown. The radiation therapy modality included 3D-conformal radiation therapy (CRT) in 6 patients, stereotactic radiosurgery (CK) in 4 patients, CRT with a CK boost in 5 patients and 38 patients with heavy particles therapy. In the patients that have undergone hadron therapy, 18 patients received only protons, 19 patients received carbon ion and mixed proton-carbon ions in one patient.

Since 2011, every skull base chordoma patient undergoes a multi-specialist meeting with radiation oncologist for evaluation of the best treatment and the referral to the Italian Center of Hadron Particles therapy (CNAO). Regarding the patients treated at CNAO (28), the total administered dose for protons was 74 Gy (RBE, Relative Biological Effectiveness), 2 Gy(RBE) per 37 fractions, the total administered dose for carbon ions was 70.4 Gy(RBE), 4.4 Gy(RBE) per 16 fractions. For the survival statistical analysis, any post-operative radiation treatment (Fig. 34) correlated with prolonged OS (p=0.0020) and PFS (p=0.0100). Analyzing the radiation type there were non-significant difference between patients undergoing photon, proton or carbon ions in terms of OS (p=0.4750) and PFS (p=0.5960). Analyzing the radiation modality delivery, the hadron therapy conferred to patients a prolonged OS (p=0.0290) compared to non-hadron, but no difference was revealed in terms of PFS (p=0.7660).

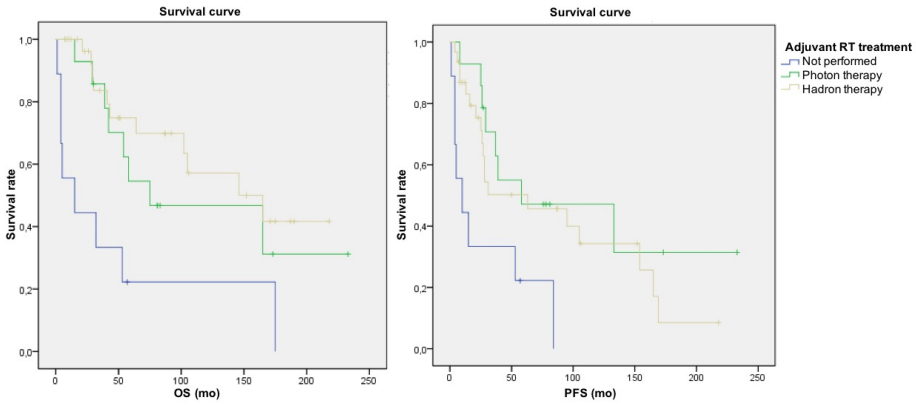

Figure 34. Kaplan-Meier survival curves for OS (left) and PFS (right) in primary chordomas according to the adjuvant radiation treatment (p=0.0020 and 0.0100, respectively).

Preliminary development of Peri-Operative Chordoma Scale (POCS)

Based on the clinical results obtained in the first section, our aim was to preliminarily construct a grading scale for each individualized patient that could be useful for practitioners to determine outcome and, thus, the better management of patients undergoing potential adjuvant therapies. The Peri-Operative Chordoma Scale (POCS) incorporates both pre-operative and peri-operative factors that can aid the surgeon to better manage the skull base chordoma patient immediately at the discharge or at first months after surgery.

The results of logistic regression analysis between the putative predictors and outcomes measures are shown in Table 2. The variable "jugular foramen tumor involvement" was excluded from the analysis because it was present in every case of the recurred patients, thus, it was a constant. Applying the backward method in the logistic regression model, it was possible to eliminate the variables that did not reach a statistically significance.

Table 2. Logistic regression predicting shorter surgical outcome measure and associations between peri-operative clinical factors in skull base chordoma patients*.

Factor	B Value (SE)	OR (95%CI)	p-value
Constant	-2.96 (1.09)	-	0.007
MR contrast enhancement			
No/Mild	Reference	-	-
Intense	3.99 (1.15)	54.2 (5.7-514.4)	0.001
Pre-op motor deficit			
No	Reference	-	-
Yes	3.16 (1.60)	23.5 (1.0-541.6)	0.049
Post-op complications			
No	Reference	-	-
Yes	2.47 (1.13)	11.8 (1.3-108.5)	0.030

*Cox&Snell pseudo R^2=0.484; Nagelkerke's pseudo R^2=0.656.

The statistically significant variables in the regression model were: MR contrast enhancement (intense vs no/mild), preoperative motor deficits (yes vs no) and the development of any post-operative complications (yes vs no) according to CDG. The OR of each significant predictor are shown in Table 2. Taken together, these entered variables into the model indicated a good fit (Cox & Snell pseudo R^2=0.484 and Nagelkerke's pseudo R^2=0.656). We, therefore, built our chordoma grading scale, namely the Peri-Operative Chordoma Scale (POCS) that is shown in Table 3.

Table 3. Peri-Operative Chordoma Scale (POCS).

Variable	Score
MR contrast enhancement	
No/Mild	0
Intense	9
Pre-op motor deficits	
No	0
Yes	6
Post-op complications	
No	0
Yes	2

The presence or absence of these factors were initially considered in a simplified version of POCS, namely POCS-beta (Tables 4 and 5). Afterwards, to rate each significant clinical predictor on the basis of their respective OR, that were divided by a value of six to create the following grade of POCS: MR contrast enhancement (value=9), preoperative motor deficits (value=6) and the development of any post-operative complications (value=2). A grading scale was obtained, with scores ranging between 0 and 17. Higher scores indicate the higher likelihood of patients to deteriorate in terms of shorter OS and PFS ($P \leq 0.001$) (Tables 6 and 7).

Table 4. POCS-beta and distribution of patients in relation to OS*.

POCS-beta	Survival (n=29)	No survival (n=29)	% of patients of no survival
0	12	1	7.7%
1	16	7	30.4%
2	0	18	100%
3	1	3	75%

*Chi-Squared: 31.8, $P \leq 0.001$

Table 5. POCS-beta and distribution of patients in relation to PFS*.

POCS-beta	No recurrence (n=21)	Recurrence (n=37)	% of patients of recurrence
0	10	3	23.1%
1	11	12	52.2%
2	0	18	100%
3	0	4	100%

*Chi-Squared: 23.2, $P \leq 0.001$

Table 6. POCS and distribution of patients in relation to OS*.

POCS	Survival (n=29)	No survival (n=29)	% of patients of no survival
0	12	1	7.7%
2	7	3	30%
6	2	0	0%
8	0	2	100%
9	7	4	36.4%
11	0	14	100%
15	0	2	100%
17	1	3	75%

*Chi-Squared: 32.7, $P \leq 0.001$

Table 7. POCS and distribution of patients in relation to PFS*.

POCS	No recurrence (n=21)	Recurrence (n=37)	% of patients of recurrence
0	10	3	23.1%
2	7	3	30%
6	1	1	50%
8	0	2	100%
9	3	8	72.7%
11	0	14	100%
15	0	2	100%
17	0	4	100%

*Chi-Squared: 27.3, $P \leq 0.001$

POCS was furtherly evaluated for testing its strength and performance in a restricted subgroup of chordoma patients of our series having a longer follow-up. We have decided to include the following patients according to the most recent and larger epidemiological study on chordomas: patients with a F-UP≥45 months when evaluating PFS (n=45) and patients with F-UP≥100 months when evaluating OS (n=31).

The preliminary analysis of POCS-beta revealed to be statistically significant to both OS (P≤0.001) and PFS (P=0.004) (Tables 8 and 9). Higher POCS scores, also in the group of patients having a larger follow-up, confirmed the higher likelihood of patients to deteriorate in terms of both OS (P≤0.001) and PFS (P=0.003) (Tables 10 and 11).

Table 8. POCS-beta and distribution of patients with a F-UP≥100 months in relation to OS*.

POCS-beta	Survival (n=11)	No survival (n=20)	% of patients of no survival
0	5	1	16.7%
1	6	2	25%
2	0	14	100%
3	0	3	100%

*Chi-Squared: 20.8, *P*≤0.001

Table 9. POCS and distribution of patients with a F-UP≥100 months in relation to OS*.

POCS	Survival (n=11)	No survival (n=20)	% of patients of no survival
0	5	1	16.7%
2	3	1	25%
6	1	0	0%
8	0	2	100%
9	2	1	33.3%
11	0	10	100%
15	0	2	100%
17	0	3	100%

*Chi-Squared: 21.2, *P*=0.004

Table 10. POCS-beta and distribution of patients with a F-UP≥45 months in relation to PFS*.

POCS-beta	No recurrence (n=13)	Recurrence (n=32)	% of patients of recurrence
0	7	3	30%
1	6	8	57.1%
2	0	17	100%
3	0	4	100%

*Chi-Squared: 18.1, *P*≤0.001

Table 11. POCS and distribution of patients with a F-UP≥45 months in relation to PFS*.

POCS	No recurrence (n=13)	Recurrence (n=32)	% of patients of recurrence
0	7	3	30%
2	4	2	33.3%
6	1	1	50%
8	0	2	100%
9	1	5	83.3%
11	0	13	100%
15	0	2	100%
17	0	4	100%

*Chi-Squared: 21.8, *P*=0.003

PATHOLOGICAL ANALYSIS

Pathology

Seventy-three cases (93.6%) were typical chordomas, 2 cases (2.6%) were chondroid chordoma and 3 de-differentiated (3.8%). Two typical chordomas at their recurrence after proton beam radiotherapy transformed into a high-grade chordoma with conventional features with foci of de-differentiated chordoma. A complete pathological examination has been performed on 17 specimens. All the detailed features are presented in Table 2.

Among all the analyzed features, the presence of high tumor infiltrating lymphocytes (TILs) correlated with a better OS outcome (Fig. 35) and represented, therefore, a significant pathological prognostic factor (p=0.0170).

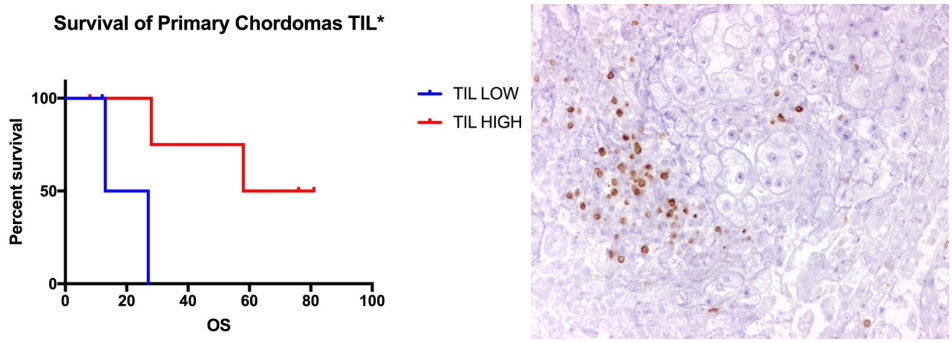

Figure 35. Left) Kaplan-Meier survival curves for OS (mo) in primary skull base chordomas according to the quantity of TILs (p=0.0170). Right) Immunohistochemical slice showing TILs within chordoma. BCL-2 selectively stains all the lymphocyte (20X).

Table 12. Morpho-pathological features.

Mitoses	
0	7 (41.2%)
<2	4 (23.5%)
>3	6 (35.3%)
Necrosis	
Yes	5 (29.4%)
No	12 (70.6%)
Hemorrhage	
Yes	8 (47.1%)
No	9 (52.9%)
Apoptosis	
Yes	4 (23.5%)
No	13 (76.5%)
Nuclear pleomorphism	
Yes	5 (29.4%)
No	12 (70.6%)
Hyperchromatic nuclei	
Yes	4 (23.5%)
No	13 (76.5%)
Prominent nuclei	
Yes	4 (23.5%)
No	13 (76.5%)
Intra-lesional Fibrous Septa	
Yes	13 (76.5%)
No	4 (23.5%)
Abundant Myxoid Matrix	
Yes	14 (82.3%)
No	3 (17.7%)
Physaliphorous cells	
High	16 (94.1%)
Low	1 (5.9%)
TIL *	
High	12 (70.6%)
Low	5 (29.4%)
Bone Infiltration	
Yes	14 (82.3%)
No	3 (17.7%)
Mucosa, Submucosa, Muscle Infiltration	
Yes	7 (41.2%)
No	10 (58.8%)
Calcifications	
Yes	3 (17.7%)
No	14 (82.3%)

* significant prognostic factor

Immunohistochemical findings

Forty-three tumors were considered eligible, after quality and quantity assessment by the pathologist, to perform further bio-molecular analysis apart from the classical diagnostic panel (Tab. 3). Brachyury is considered a diagnostic marker of chordoma and it is routinely applied in the diagnostic process. Such marker presented a very strong nuclear expression in the physaliphorous cells in 96% of samples and absent in two (4%) de-differentiated chordoma patients (Fig. 36). The expression of other markers has been evaluated according to the main related pathways involved in chordomagenesis. Beta-catenin is exclusively expressed with a membrane and cytoplasmic pattern in every analyzed sample (100%). Filamin A has never been employed in chordomas and, interestingly, presents a strong and mild expression in 90.7% and 9.3%, respectively. GAB-1 is markedly expressed in 12.9%, slightly expressed 51.6% and absent in 35.5% of chordoma samples. Regarding of the expression of some TRKs commonly involved in chordomas, c-Met, c-Kit, PDGFRß, EGFR have been studied. Specifically, c-Met was slightly expressed in 51.2%, markedly expressed in 13.9% and absent in 34.9% of cases. c-Kit was slightly expressed in 62.8%, markedly expressed in 11.6% and absent in 25.6%. PDGFRß was slightly expressed in 48.8%, markedly expressed in 9.3% and absent in 41.9%. EGFR was not expressed in 100% of the analyzed samples.

YKL-40 was slightly expressed in 11.7%, markedly expressed in 2.2% and absent in 86.1% of cases. p53 was expressed in 15% and absent in 85% of cases. TERT was slightly expressed in 37.2%, markedly expressed in 34.9% and absent in 27.9% of cases. Therefore, ATRX has been investigated and all the samples expressed it (9/9, 100%). TERT promoter target sequencing was *wild-type* with no mutation at the analyzed sequence. p62 was slightly expressed in 30%, markedly expressed in 60% and absent in 10% of cases. bcl-2 was expressed in 9.1% and absent in 90.9% of cases.

Multiple comparison tests have been performed and no immuno-histochemical markers seems to be peculiar and exclusively associated neither with the type (primary/recurrent) and within the recurrence neither recurrence with or without radiation therapy.

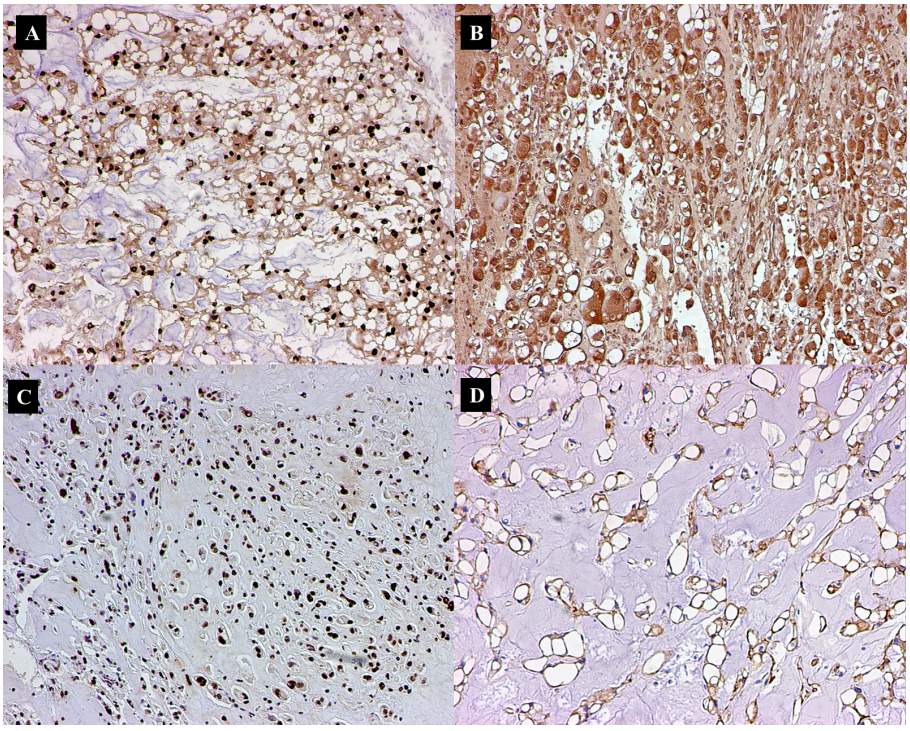

Figure 36. Immunohistochemical findings of chordomas. (A) Photomicrograph showing strong nuclear immunoreactivity for Brachyury of chordoma cells (anti-Bry, 40×). Photomicrographs showing immunoreactivity for PDGFR-beta (B), TERT (C) and beta-catenin (D). Beta-catenin's staining has a prevalent cytoplasmic membrane pattern. (anti- PDGFR-beta, anti-TERT, anti- beta-catenin, 40×).

Table 13. Immunohistochemical findings.

Brachyury (tot. 50)	
-	2 (4%)
+	48 (96%)
Beta-catenin (39)	
Membrane/Cytoplasmic	39 (100%)
Nuclear	0 (0%)
Filamin A (43)	
+	4 (9.3%)
++	39 (90.7%)
GAB-1 (31)	
-	11 (35.5%)
+	16 (51.6%)
++	4 (12.9%)
C-MET (43)	
-	15 (34.9%)
+	22 (51.2%)
++	6 (13.9%)
C-KIT (43)	
-	11 (25.6%)
+	27 (62.8%)
++	5 (11.6%)
PDGFR-b (43)	
-	18 (41.9%)
+	21 (48.8%)
++	4 (9.3%)
YKL-40 (43)	
-	37 (86.1%)
+	5 (11.7%)
++	1 (2.2%)
TERT (43)	
-	12 (27.9%)
+	16 (37.2%)
++	15 (34.9%)
ARTX (9)	
-	0 (0%)
+	9 (100%)
P53 (20)	
-	17 (85%)
+	3 (15%)
EGFR (20)	
-	100 (100%)
+	0 (0%)
p62 (10)	
-	1 (10%)
+	3 (30%)
++	6 (60%)
BCL-2 (11)	
-	10 (90.9%)
+	1 (9.1%)

SPHINGOLIPIDS ANALYSIS

Clinical features

Thirteen patients underwent sixteen surgeries and have been included in the present study for prospectively collection of sixteen chordoma samples for lipid analysis. There were 7 males (53.8%) and 6 females (46.2%). Six tumors were primary (37.5%), eight were recurrent after radiation therapy (50%), two were recurrent without radiation therapy (12.5%). These last two samples were gathered from the same patient who underwent a 2-stages surgery; to avoid any misinterpretation of biochemical values due to surgery-induced cellular stress, only the first specimen has been included in the analysis. The mean age at the time of surgery was 53.3 ± 14.4 years (36–82). The mean follow-up period calculated from the first treatment performed at our Institution of the present patient series was 13.7 months (1-51). Of the recurrent chordomas, five (50%) had only one recurrence before, three (30%) had 2 previous recurrences and two (20%) had three previous recurrences. The recurrent patients already treated with post-operative radiation therapy were as follows: five with carbon ions (62.5%) and three with proton beam therapy (37.5%).

Sphingolipids characterization and tumor type

Total and single ceramides and dihydroceramides species production have been evaluated on 15 chordomas, six primary chordomas, one recurrent without radiotherapy and eight recurrences after radiotherapy. The mean total ceramides and dihydroceramides species in chordomas were 1216.2 ± 730.7 pmol/mg protein (522.5-2787.5) and 52.6 ± 40.6 pmol/mg protein (9.0-145.6), respectively. The mean total ceramides and dihydroceramides species in primary chordomas were 808.4 ± 451.4 pmol/mg (522.5-1760.2)

and 30.7±16.4 pmol/mg (17.6-62.4), respectively. The mean total ceramides and dihydroceramides species in recurrent chordomas were 1488.1 ± 763.8 pmol/mg (540.7-2787.5) and 67.2 ± 45.5 pmol/mg (9.0-145.6), respectively. Eight ceramides subspecies were analyzed and Cer C16:0 (60.8%), Cer C24:1 (17.5%), Cer C24:0 (10.0%) were the most abundant single ceramides in skull base chordomas (Fig. 37).

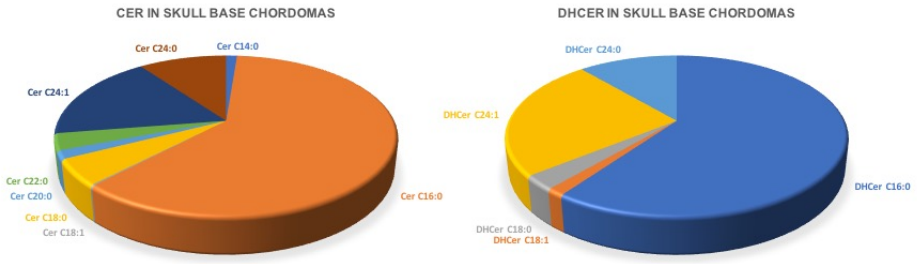

Figure 37. Graphs showing the percentages of ceramides (left) and dihydroceramides (right) single species in skull base chordomas.

In the primary chordoma group (Fig. 38), the most abundant were Cer C16:0 (66.1%), Cer C24:1 (13.8%) and Cer C24:0 (10.1%). In the recurrent chordoma group (Fig. 38), the most abundant were Cer C16:0 (58.9%), Cer C24:1 (18.8%) and Cer C24:0 (9.9%).

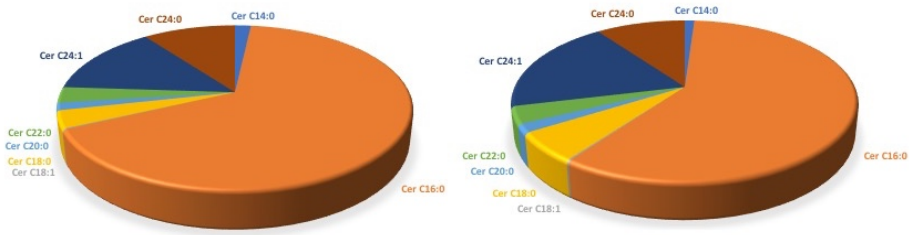

Figure 38. Graphs showing the percentages of ceramides single species in primary (left) and recurrent (right) skull base chordomas.

Five dihydroceramides (DHCer) were analyzed and DHCer C16:0 (60.5%), DHCer C24:1 (24.8%) and DHCer C24:0 (11.4%) were the most abundant single ceramides in skull base chordomas. In the primary chordoma group, the most abundant were DHCer C16:0 (70.4%), DHCer C24:1 (17.7%), DHCer C24:0 (9.5%). In the recurrent chordoma group, the most abundant were DHCer C16:0 (57.5%), DHCer C24:1 (27.0%), DHCer C24:0 (11.4%).

Figure 39. Graphs showing the percentages of dihydroceramides single species in primary (left) and recurrent (right) skull base chordomas.

Total ceramides species (Fig. 40) were significantly higher in recurrent chordomas that underwent previous surgical resection and radiation therapy in comparison to the primary chordomas (p=0.0496). When analyzing the effect of radiation therapy, the ceramides in the group of chordomas with previous radiation therapy were not significantly different from the ceramides in the group of chordomas with no previous radiation therapy (p=0.0541). DHCer levels (Fig. 40) were not significantly different between primary and recurrent chordomas (p=0.0663), and between chordoma with previous radiation therapy and chordoma without radiation therapy (p=0.1520).

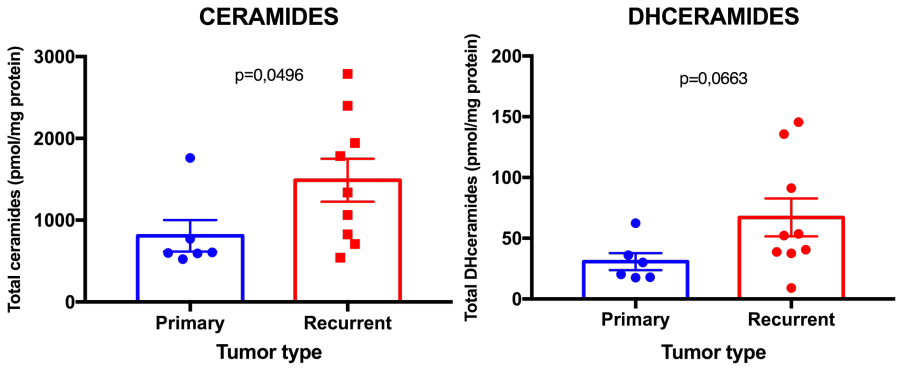

Figure 40. Bar graphs, with standard error mean (SEM), showing the content of total ceramides (left) and dihydroceramides (right) species in primary and recurrent chordomas.

Among the single ceramides species (Fig. 41), Cer C18:0 (p=0.0120), Cer C20:0 (p=0.0176), Cer C22:0 (p=0.0256) and Cer C24:1 (p=0.0076) were significantly different between primary and recurrent skull base chordomas, whereas Cer C14:0 (p=0.5287), Cer C16:0 (p=0.3884), Cer C18:1 (p=0.0663) and Cer C24:0 (p=0.0663) did not reach any statistical significance.

Among the single DHCer species (Fig. 42), DHCer C24:1 (p=0,0120) were the only one significantly different between primary and recurrent skull base chordomas, whereas DHCer C16:0 (p=0.1135), DHCer C18:1 (p=0.8913), DHCer C18:0 (p=0.0709), DHCer C24:0 (p=0.0663) did not reach any statistical significance.

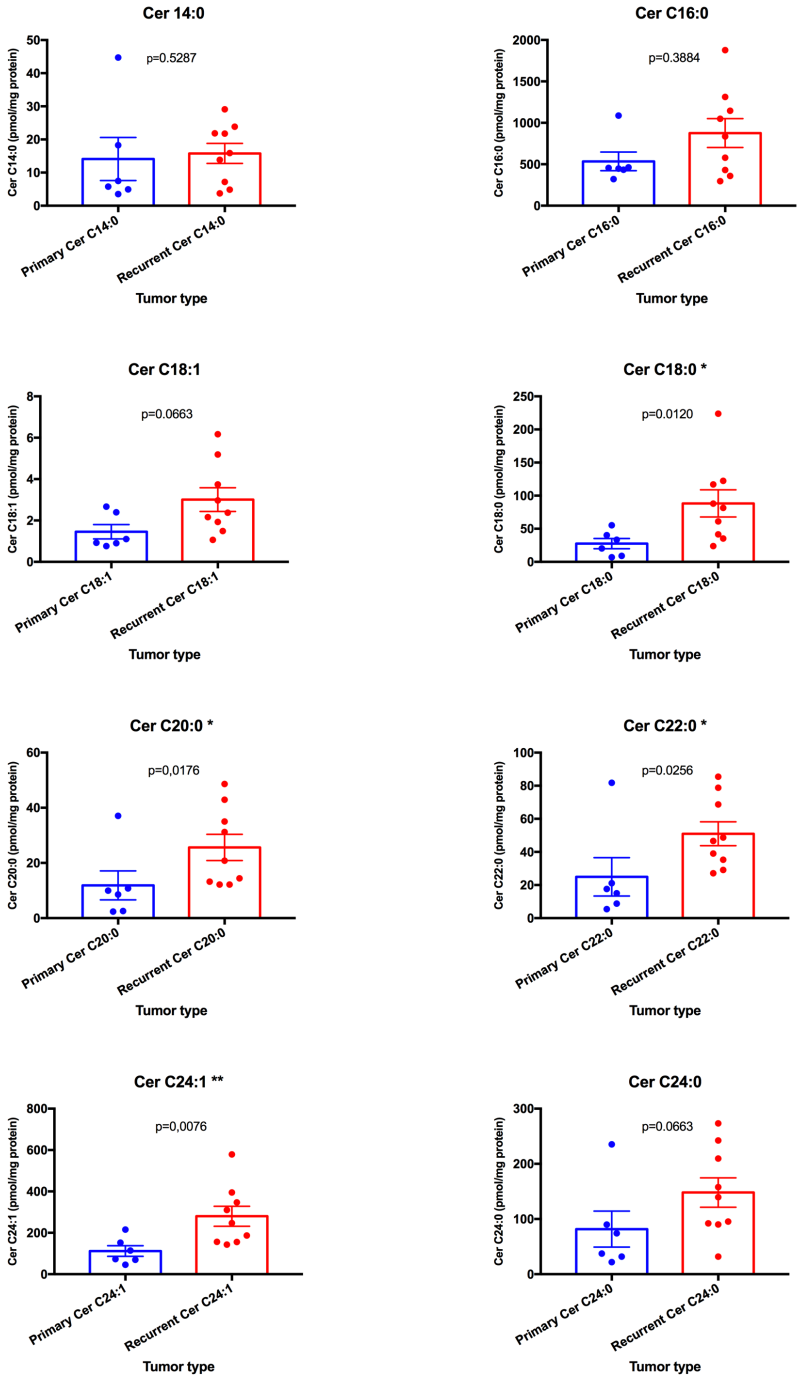

Figure 41. Bar graphs, with SEM, showing the content of single ceramides species in primary and recurrent chordomas. *, p≤0.05; **, p≤0.01; ***, p≤0.001, ****, p≤0.0001

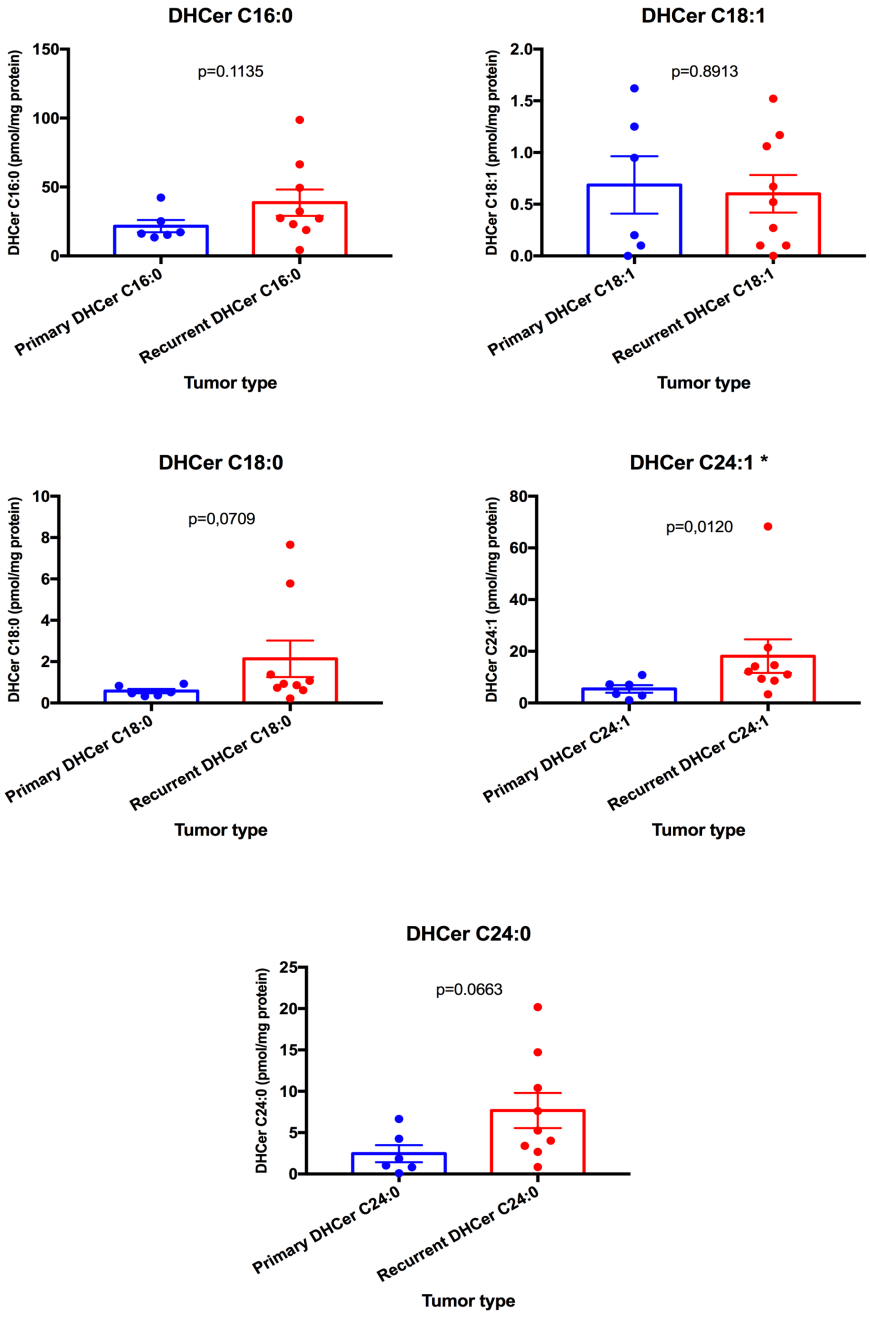

Figure 42. Bar graphs, with SEM, showing the content of single dihydroceramides species in primary and recurrent chordomas. *, p≤0.05; **, p≤0.01; ***, p≤0.001, ****, p≤0.0001

Sphingolipids characterization and MR contrast enhancement pattern

Preoperative radiological information was available in 14/15 of patients. One patient did not undergo contrast administration due to high serum creatinine. For statistical purposes, we have identified and selected two groups: chordoma exhibiting an intense post-gadolinium enhancement and chordoma with no or mild post-gadolinium enhancement.

The mean total ceramides and dihydroceramides species in "intense enhancement" group were 1597.6 ± 737.8 pmol/mg (592.7-2787.5) and 69.1 ± 45.0 pmol/mg (17.8-145.6), respectively. The mean total ceramides and dihydroceramides species in "no or mild enhancement" group were 664.7 ± 120.4pmol/mg (522.5-826.0) and 31.5 ± 13.6 pmol/mg (17.6-53.6), respectively.

Total ceramides and DHCer levels (Fig. 43) were significantly higher in "intense enhancement" chordomas in comparison to the "no/mild enhancement" chordomas (p=0.0290 and p=0.0186, respectively).

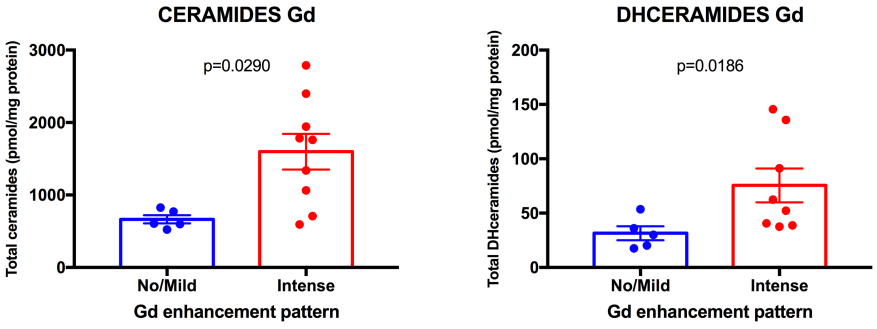

Figure 43. Bar graphs, with SEM, showing the content of total ceramides (left) and dihydroceramides (right) species in chordomas with no/mild contrast and intense contrast enhancement.

Among the single ceramides species (Fig. 44), Cer C16:0 (p=0.0120), Cer C20:0 (p=0.0290), Cer C22:0 (p=0.0120), Cer C24:1 (p=0.0120) and Cer C24:0 (p=0.0120) were significantly different between “intense enhancement” chordomas and “no/mild enhancement” chordomas, whereas Cer C14:0 (p=0.6064) and Cer C18:1 (p=0.3636), Cer C18:0 (p=0.0829) did not reach any statistical significance.

Among the single DHCer species (Fig. 45), DHCer C18:0 (p=0.0385) were the only one significantly different between “intense enhancement” chordomas and “no/mild enhancement” chordomas, whereas DHCer C16:0 (p=0.1469), DHCer C18:1 (p=0.6703), DHCer C24:1 (p=0.0829), DHCer C24:0 (p=0.0829) did not reach any statistical significance.

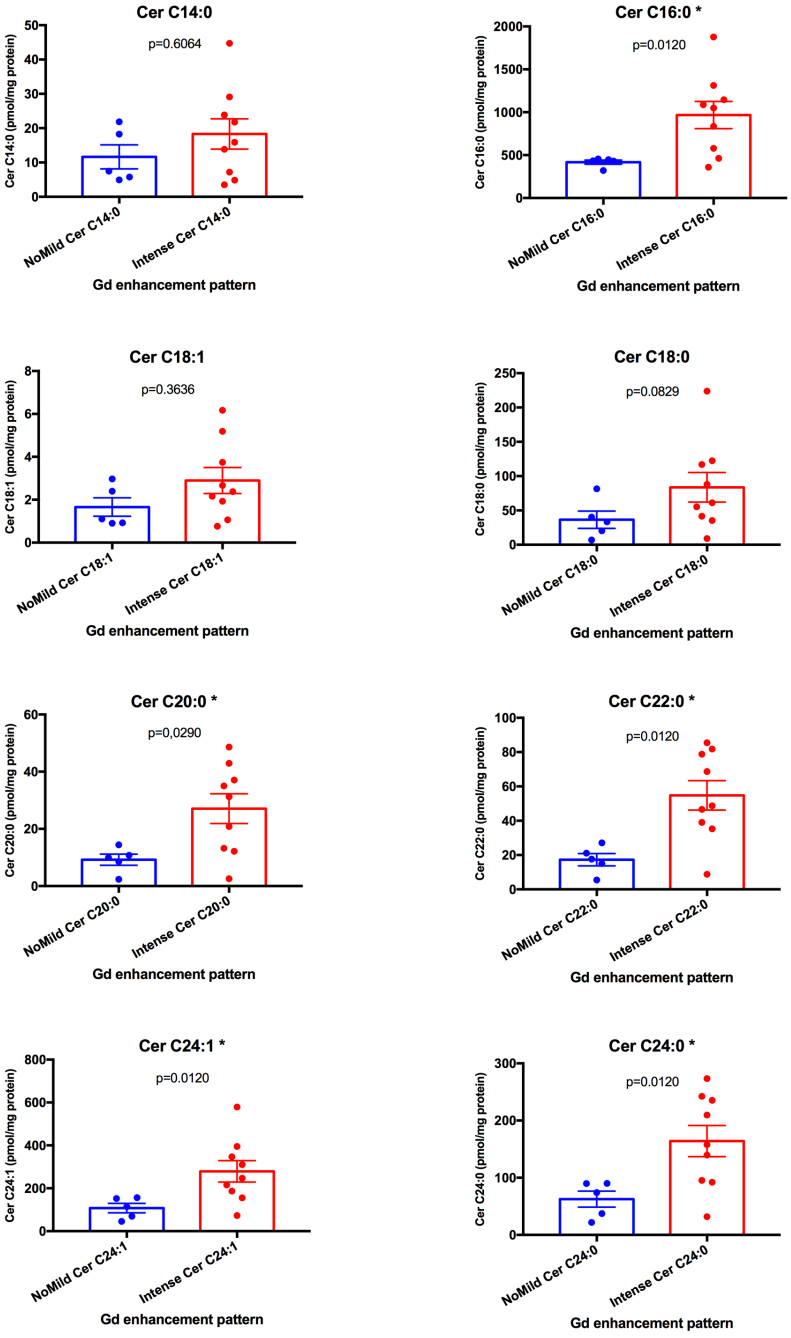

Figure 44. Bar graphs, with SEM, showing the content of single ceramides species in chordomas with no/mild contrast and intense contrast enhancement. *, p≤0.05; **, p≤0.01; ***, p≤0.001, ****, p≤0.0001

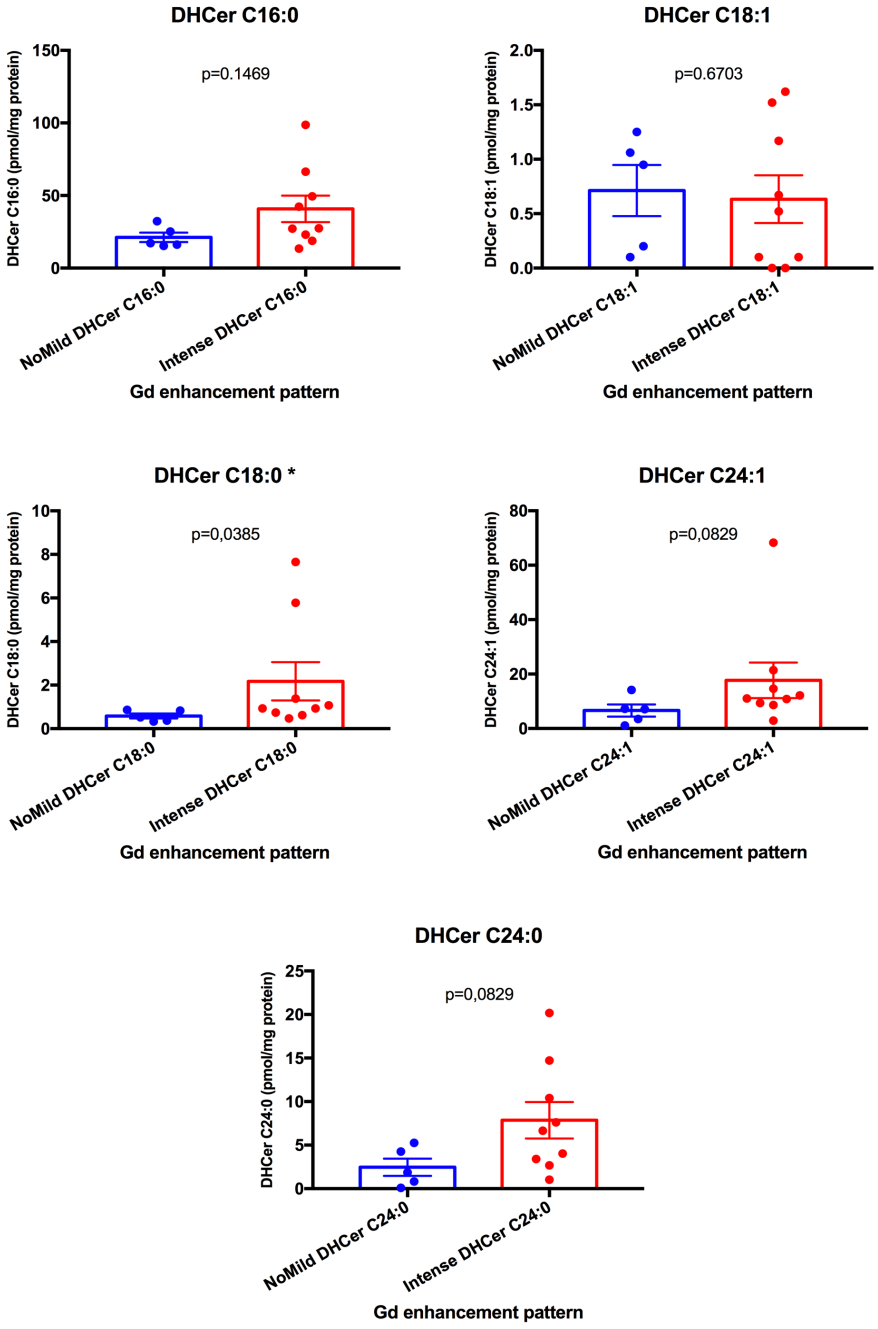

Figure 45. Bar graphs, with SEM, showing the content of single dihydroceramides species in chordomas with no/mild contrast and intense contrast enhancement. *, p≤0.05; **, p≤0.01; ***, p≤0.001, ****, p≤0.0001

Sphingolipids characterization and proliferative index

Following the hypothesis of ceramides as aggressive behaviors bio-markers of skull base chordomas we, therefore, investigated the relationships between ceramides and DHCer levels with tumor proliferation rate, evaluated by MIB-1 staining on IHC slices (Fig. 46). MIB-1 staining information was available in 14/15 of patients (Fig. 47). Analyzing the association between ceramides levels and MIB-1 within each skull base chordoma patient, total ceramides levels showed a strong association ($r=0.7257$, $r^2=0.5267$) with MIB-1 staining ($p=0.0033$). Analyzing the association between DHCer levels and MIB-1 within each skull base chordoma patient, total DHCer levels showed also a strong association ($r=0.6733$, $r^2= 0.4533$) with MIB-1 staining ($p=0.0083$).

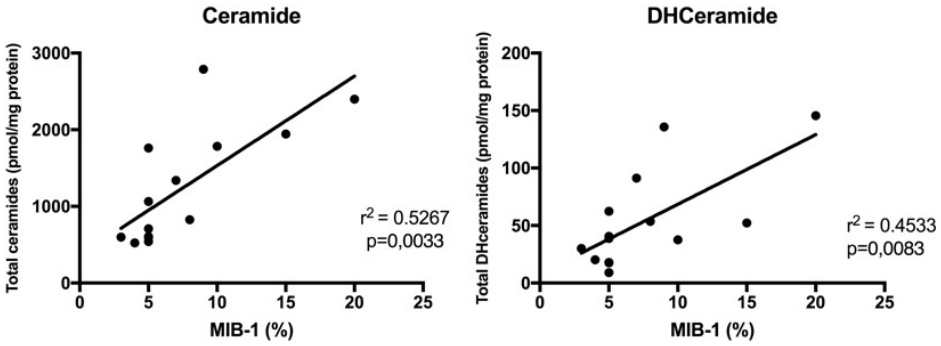

Figure 46. Linear regression graphs showing the correlation between the MIB-1 staining and total ceramide (left) and total dihydroceramides (right).

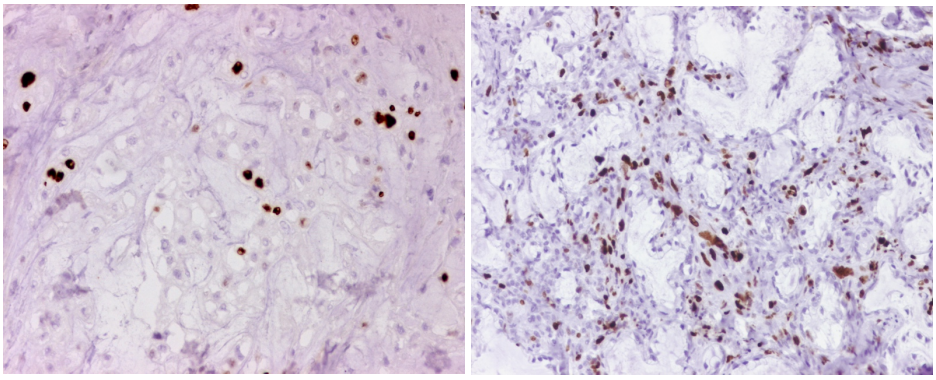

Figure 47. Photomicrographs showing chordoma having a low MIB-1 (left) staining and a high MIB-1 (right) staining (40x).

In particular, we have analyzed any possible association between every single ceramides species and MIB-1 (Fig. 48) and found that Cer C16:0 ($r=0.6338$, $r^2=0.4016$, $p=0.0149$), Cer C18:1 ($r=0.5386$, $r^2=0.2901$, $p=0.0469$), Cer C18:0 ($r=0.6949$, $r^2=0.4829$, $p=0.0058$), Cer C20:0 ($r=0.5665$, $r^2=0.3209$, $p=0.0347$), Cer C22:0 ($r=0.5645$, $r^2=0.3186$, $p=0.0355$), Cer C24:1 ($r=0.8814$, $r^2=0.7769$, $p\leq0.0001$) and Cer C24:0 ($r=0.6125$, $r^2=0.375$, $p=0.0199$), levels showed a significant correlation with MIB-1 staining.

Moreover, we have also analyzed an association between every single dihydroceramides species and MIB-1 (Fig. 49) and found that DHCer C18:0 ($r=0.9426$, $r^2=0.8885$, $p\leq0.0001$), DHCer C24:1 ($r=0.8429$, $r^2=0.7104$, $p=0.0002$) and DHCer C24:0 ($r=0.649$, $r^2=0.4212$, $p=0.0120$) levels showed a significant correlation with MIB-1 staining.

The results of correlation analysis are shown in Table 14.

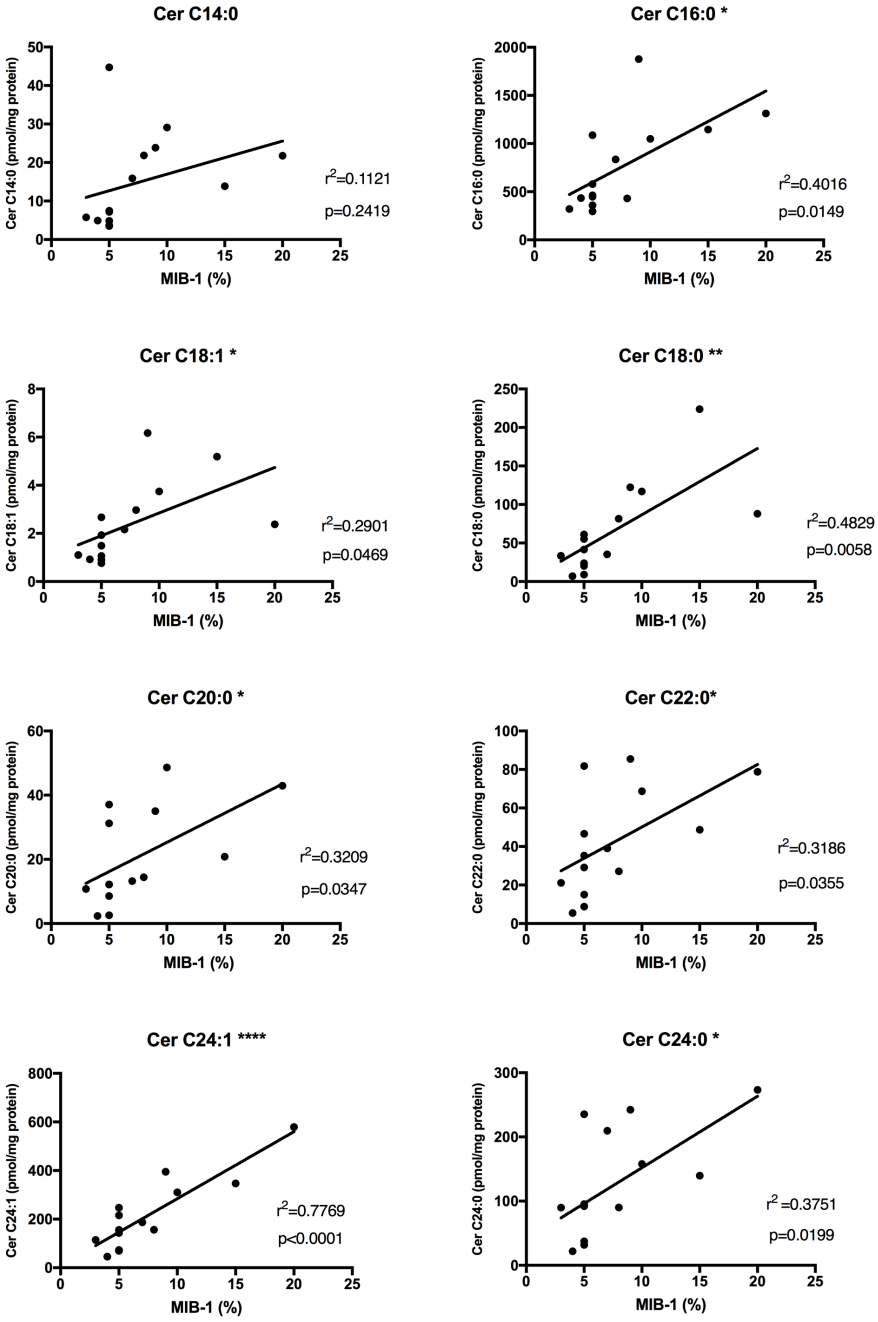

Figure 48. Linear regression graphs showing the correlation between the MIB-1 staining and single ceramides species. *, p≤0.05; **, p≤0.01; ***, p≤0.001, ****, p≤0.0001

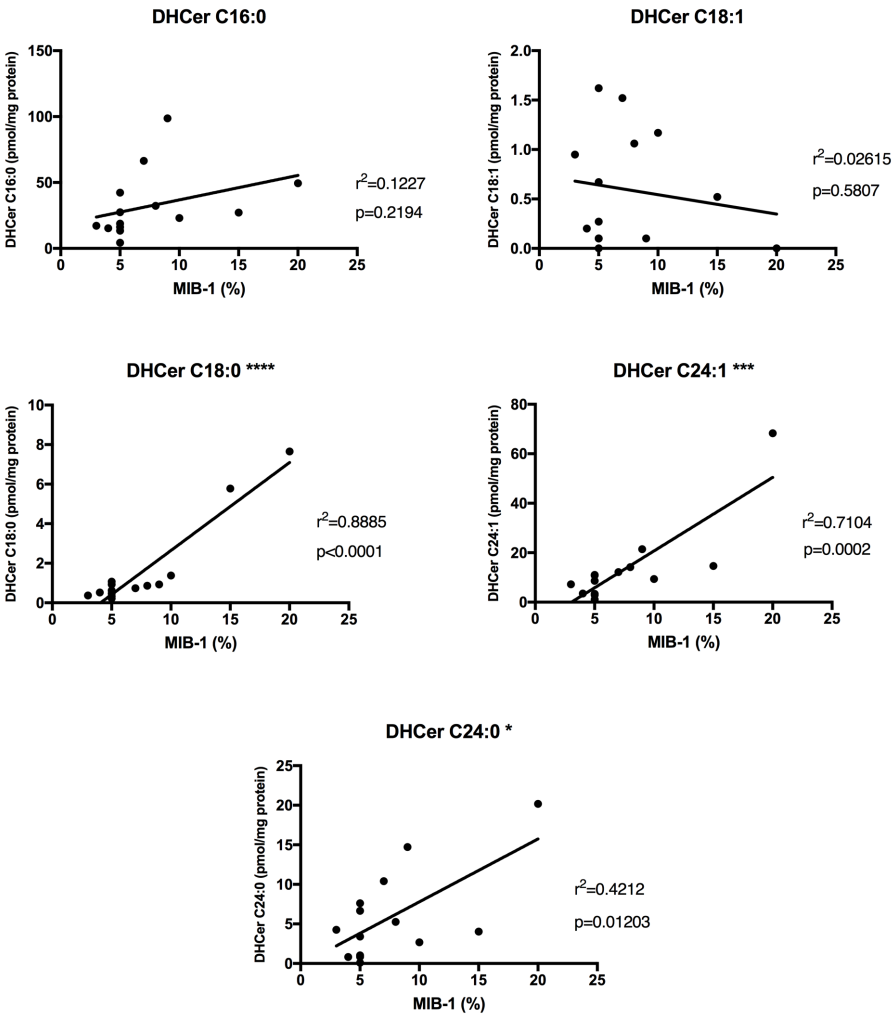

Figure 49. Linear regression graphs showing the correlation between the MIB-1 staining and single dihydroceramides species. *, p≤0.05; **, p≤0.01; ***, p≤0.001, ****, p≤0.0001

Table 14. Summary of the correlation analysis between ceramides and MIB-1.

Variable	r	p-value	
Cer14:0	0,3349	0,2419	ns
Cer16:0	0,6338	0,0149	*
Cer18:1	0,5386	0,0469	*
Cer18:0	0,6949	0,0058	**
Cer20:0	0,5665	0,0347	*
Cer22:0	0,5645	0,0355	*
Cer24:1	0,8814	≤0,0001	****
Cer24:0	0,6125	0,0199	*
DHCer16:0	0,3503	0,2194	ns
DHCer18:1	- 0,1617	0,5807	ns
DHCer18:0	0,9426	≤0,0001	****
DHCer24:1	0,8429	0,0002	***
DHCer24:0	0,6490	0.0120	*

A regression model has been developed to evaluate the role of ceramides and dihydroceramides as independent predictors of MIB-1. The level of significance was set to 0.05/15=0.0033, according to Bonferroni's correction. All the independent variables were entered into the equation first and each one was deleted one at a time if they did not contribute to the regression equation by the backward elimination method. A multi-collinearity test has been used to assess the Variance Inflation Factor (VIF) and tolerance. Final candidate predictive factors that well fitted the model were: Cer C24:1 (r=0.824, $P \leq 0.001$), and DHCer C18:0 (r=0.748, $P=0.002$).

Table. 15 Summary of the results derived from the regression analysis model*

Variable	B (SE)	Beta	p-value	Tolerance	VIF
Constant	2.97 (0.73)		0.002		
Cer C24:1	0.011 (0.004)	0.348	0.025	0.351	2.85
DHCer C18:0	1.40 (0.28)	0.663	≤0.0001	0.351	2.85

*R^2=0.931, Adj-R^2=0.918; F=74.0 (p≤0.001)

Sphingolipids characterization and outcome prediction

On the ground of the retrospective clinical study, a preliminary multivariate analysis has been performed on 13 patients to evaluate if ceramides represent independent predictors of outcome or if they merely correlate with other predictors that have been found to be significant in the first section. The results of the multivariate analysis are shown in Table 14. The analysis showed that Cer C16:0, the most abundant single ceramide, is the only ceramide subspecies that correlated with overall survival (p=0.046) and the presence of any pre-operative CN deficit correlated with PFS (p=0.035). The other analyzed variables did not show any correlation with OS neither with PFS (Table 14). By applying a regression linear model analysis, no Cer C16:0 neither the presence of any pre-operative CN deficit revealed to be significant prognostic factors (p=0.111 and p=0.089, respectively). The non-statistically significance of any predictors into the multivariate analysis outcome model may be explained due to the very small sample size and the relative short mean follow-up of such patients (13.7 months) that were prospectively enrolled from December 2015.

Table 15. Summary of the results derived from the multivariate analysis

Variable	OS	PFS
Cer C14:0	0.928	0.899
Cer C16:0	0.046*	0.083
Cer C18:1	0.787	0.885
Cer C18:0	0.225	0.318
Cer C20:0	0.389	0.269
Cer C22:0	0.249	0.114
Cer C24:1	0.145	0.168
Cer C24:0	0.249	0.130
DHCer C16:0	0.329	0.240
DHCer C18:0	0.329	0.459
DHCer C24:1	0.512	0.482
Cer Tot	0.099	0.114
DHCer Tot	0.500	0.377
Jugular foramen	0.248	0.628
Pre-brainstem cistern	0.684	0.734
Brainstem dislocation	0.676	0.625
Calcifications	0.873	0.873
MR contrast enhancement	0.320	0.231
CN deficits	0.057	0.035*
Motor deficits	0.172	0.290
Complications	0.716	0.708
ΔKPS	0.087	0.074
EOR	0.494	0.096

* $p \leq 0.05$

DISCUSSION

CLINICAL STUDY

Skull base chordoma is a malignant tumor and its behavior is still far away to be completely understood[30,45,115,203]. Since chordoma is a very rare tumor, many small studies have been published in the current literature[12,14,40,52,94,177]. Such findings lead to a big heterogeneity to better disclose which are the main prognostic factors in skull base chordomas patients[50,105,219]. Therefore, the first aim of the present study is to evaluate which clinical factor could be considered a prognostic bio-marker in a large, single-institutional, cohort of surgically treated skull base chordomas.

Skull base chordomas present an intrinsic and locally aggressive behavior because of their intricate relationships with the surrounding neurovascular structures[12,40,177]. The clinical presentation of each patient could be, therefore, an important factor impacting their outcomes and quality of life. Particularly, in our survival analysis, the pre-operative presence of any motor deficits in both primary and recurrent skull base chordomas patients correlated with a shorter PFS. KM analysis regarding OS did not reach any statistical significance. Such finding could be explained by the extensive tumor involvement of the intradural spaces and displacement of the brainstem and, consequently, development of motor deficits. Analogously, the presence of any pre-operative cranial nerve deficits revealed to be a significant prognostic factor related to shorter PFS in our cohort of recurrent patients. According to a recent systematic review and meta-analysis on prognostic factors in skull base chordoma, the presence of pre-operative motor deficit is a completely new prognostic factor never described in the current literature, whereas, the presence of any cranial nerve deficits (such as visual deficit or diplopia) has been already described as significant predictor of PFS and OS[26,50,198,219].

The radiological appearance of chordomas is very heterogeneous and it has been scarcely described and correlated with prognosis in the literature[54,138]. In our univariate analysis, the presence of calcifications and/or bone sequestrations (Fig. 50), identified on CT scan and/or SWI imaging, correlated with a better OS in the cohort of primary skull base chordomas. Although the presence of intratumoral calcifications has been regarded as positive prognostic factor in other tumors, it has never been described in skull base chordomas and its biological correlate should be assessed in future studies[73,85].

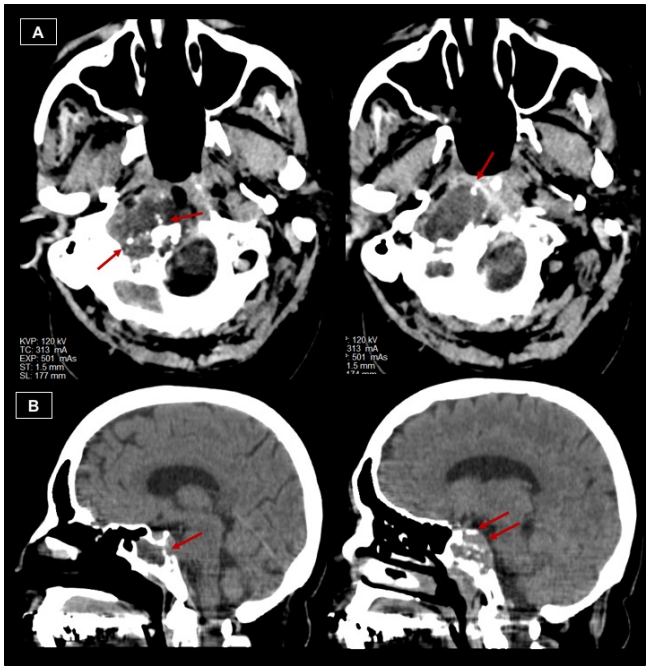

Figure 50. Axial (A) and sagittal (B) CT scan slices of two patients with chordomas presenting with intrinsic calcifications/bone sequestrations (red arrows).

Moreover, there are some recent papers that sought to preliminarily adopt a radiomics approach in skull base chordomas[107,111,182]. Ma JP et al. firstly described a radiomics approach in chordomas using three ratios of signal intensity between the tumor and brainstem on T1-weighed (R_{T1}), T2-weighted (R_{T2}) and post-contrast images (R_{CE}). They have found that $R_{CE}/R_{T1} \geq 1.7$ and $R_{T2}/R_{T1} \leq 4.3$ represented two significant factors correlating with PFS[111]. In 2017, Tian K et al. used a similar approach and proposed a MR grading classification taking into account signal intensity on T1 FLAIR pre- (R_{T1}) and post-contrast enhancement (R_{CE}) and T2 sequences (R_{T2}) and found that a higher R_{T2} correlated with longer PFS, whereas a higher R_{EN} value correlated with a shorter PFS[182]. Moreover, chordomas with a higher MR grade showed a more abundant blood supply than MR grade I tumors[182]. A recent publication, in a retrospective series of patients, showed that there was a difference in terms of PFS between non-enhancing and enhancing chordomas, but the study did not show any statistically significance in terms of PFS and degree of contrast enhancement[107]. On the ground of previous confirmatory quantitative radiomics results, we adopted the following classification of MR enhancement pattern: intense enhancement, mild enhancement and no enhancement that revealed to be very simple to use and fast-forward (Figs. 51-53)[138]. Of note, the degree of Gd enhancement in our cohort of skull base chordomas showed to strongly correlate with both OS and PFS ($p \leq 0.0001$ and 0.0010, respectively). It could, therefore, represents a radiological bio-marker of an aggressive behavior that will be also discussed in a translational view in the following paragraphs of the present dissertation. Although such approach could be easily and routinely applied in the pre-operative stratification of patients with no need of complex measurements on a dedicated and accessorized stations, the main limitation is that such approach should be validated in larger cohorts of patients and intra-observer and inter-observer reliability should be ad-hoc assessed.

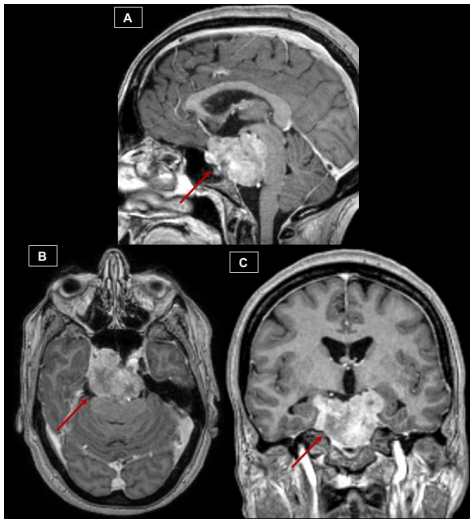

Figure 52. Sagittal (A), axial (B), coronal (C) T1-weighted post-contrast MR images showing a chordoma (red arrows) with intense contrast enhancement.

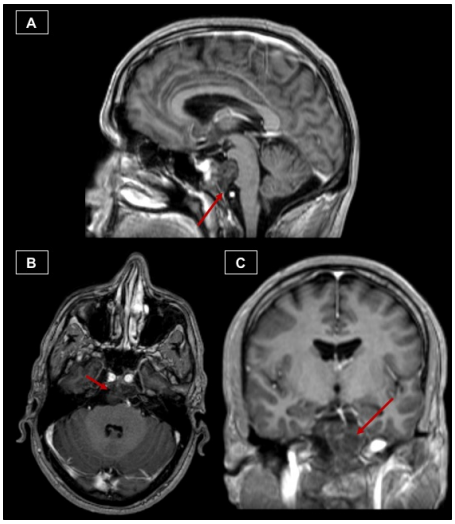

Figure 53. Sagittal (A), axial (B), coronal (C) T1-weighted post-contrast MR images showing a chordoma (red arrows) with mild contrast enhancement.

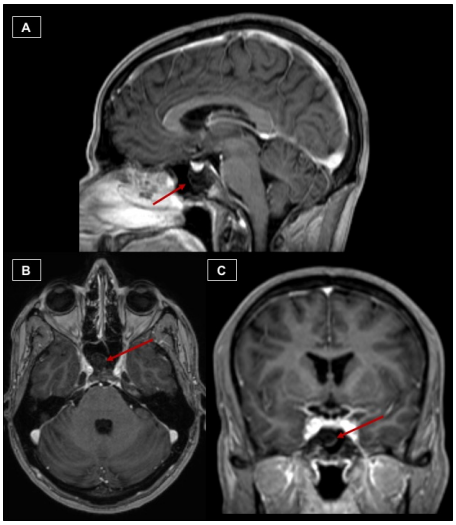

Figure 51. Sagittal (A), axial (B), coronal (C) T1-weighted post-contrast MR images showing a chordoma (red arrows) with no contrast enhancement.

Some other radiological and surgical anatomical location of chordoma that could be act as important prognostic factor were rhynopharynx invasion (PFS and OS)[12], important dural penetration (PFS and OS)[216] and occipito-cervical location (PFS)[183]. In our cohort of primary skull base chordomas, JF involvement (Fig. 54) correlated with a shorter PFS (p=0.0130). Jugular foramen area is a very challenging surgical region, although the great surgical advancements technique in the last decades, and it is still associated with limited surgical resection and higher morbidity rates[40,164]. Residual tumors in JF area are usually treated by adjuvant radiation therapy and seems to be more prone to recur[79,80,86].

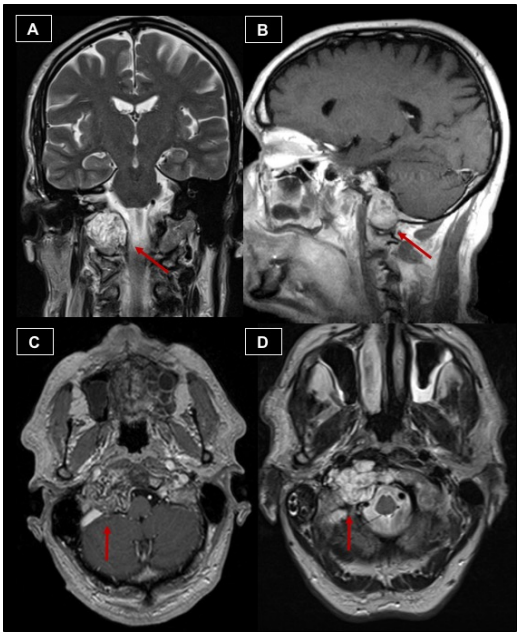

Figure 54. Coronal T2-weighted (A), sagittal T1-weighted post-contrast (B), axial T1-weighted post-contrast (C) and axial T2-weighted (D) MR images showing a chordoma (red arrows) involving jugular foramen.

Moreover, we found that intradural space involvement (Fig. 55), namely pre-brainstem cistern (crural, pre-pontine, pre-medullary cisterns), confirmed to be a significant prognostic factor related to a shorter PFS in the cohort of recurrent skull base chordomas (p=0.0210). Such findings could be explained by the effects of previous treatments (surgery and RT) on inducing the formation of tough adhesions of the tumor to the brainstem, a bad cleavage plan and, therefore, limiting the further amount of tumor extent of resection less treatable by RT and higher rate of post-operative complications[134,200,212]. Similarly, the presence of any brainstem dislocation (Fig. 56, 57) by the tumor itself represented an important prognostic factor correlating with shorter OS and PFS in the cohort of recurrent chordomas (p=0.0060 and 0.0030).

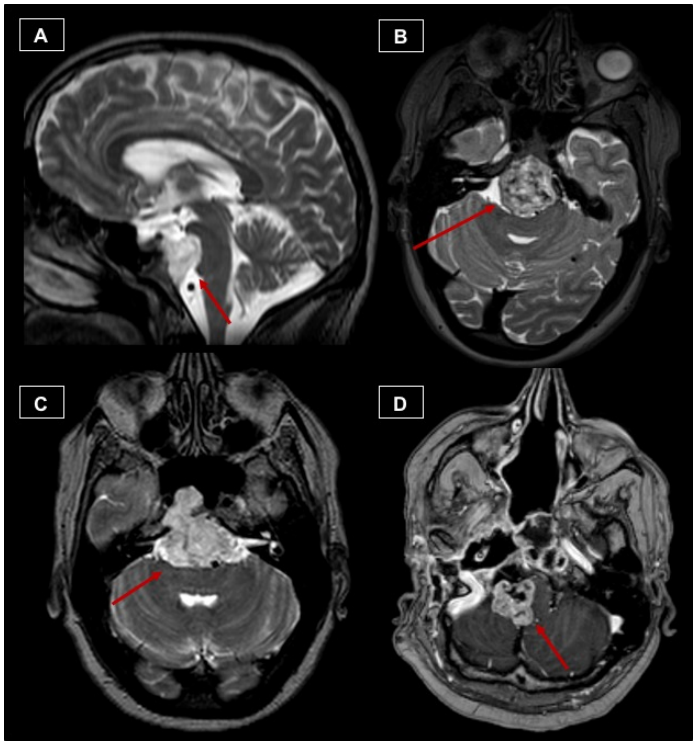

Figure 55. Sagittal T2-weighted (A), axial T2-weighted (B), axial T2-weighted (C) and axial T1-weighted post-contrast (D) MR images showing chordomas (red arrows) extending into the antero-lateral cistern of the brainstem.

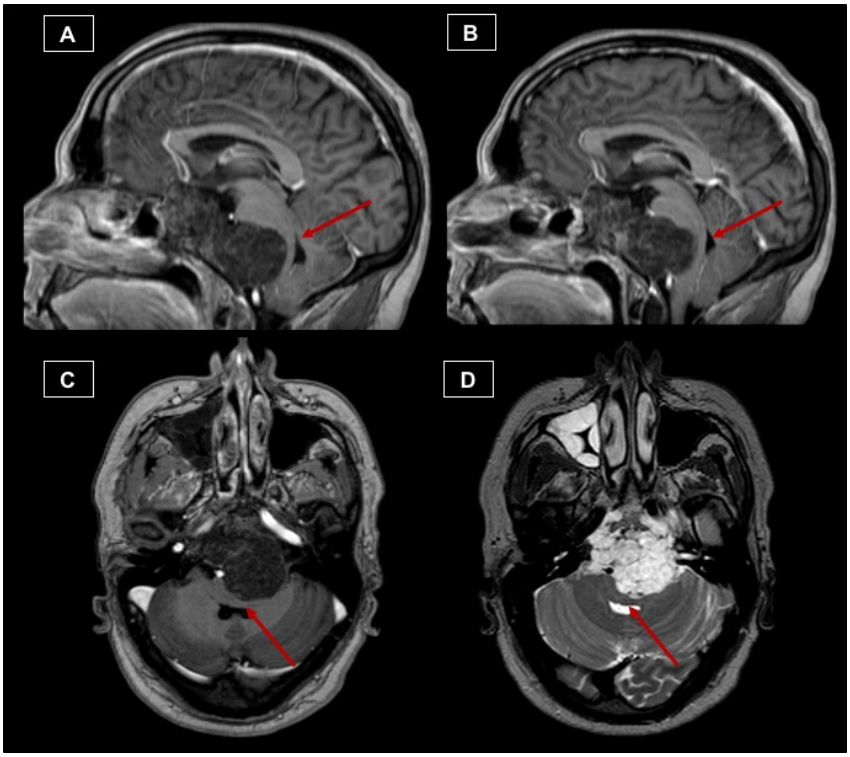

Figure 56. Sagittal (A, B) and axial (C) T1-weighted post-contrast and axial T2-weighted (D) MR images showing chordomas dislocating the brainstem.

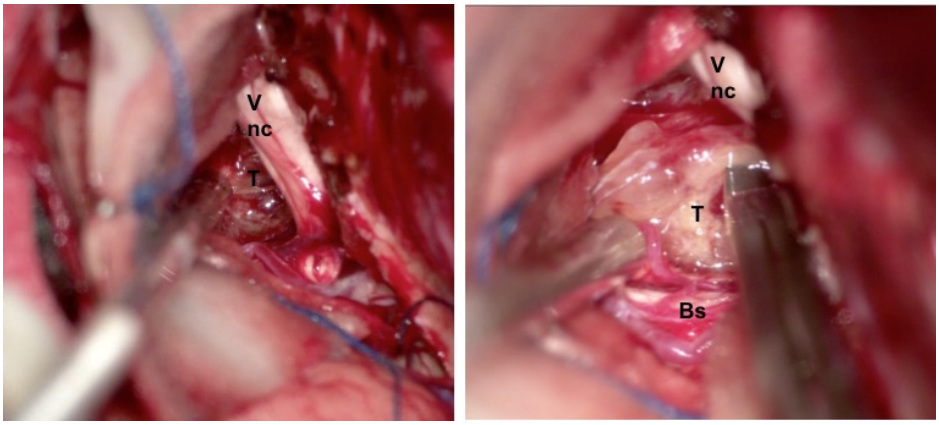

Figure 57. Intraoperative surgical pictures showing the strict relationships between the chordoma tumor and the brainstem. The images refer to the case of figure 59. Bs, *brainstem*, T, *tumor*, V nc, *trigeminal nerve*.

Over the last years, EEA gained wide popularity among skull base chordoma surgeons as a good alternative to open surgery in selected patients because it provided acceptable surgical outcomes with reduced morbidity[24,51,52,177]. Although there were many attempts to perform systematic reviews and meta-analysis in the neurosurgical literature regarding the choice of the approach, it is somewhat difficult to compare outcomes between two different approaches in a so heterogeneous tumor[91,99,100]. In the present cohort, we showed a relevant shift regarding the most common employed approach in our Institution (Fig. 28), from an open surgery-centered selection to a more combined open-endoscopic surgery. Moreover, analyzing the EOR in relation to the two consequential decades (1991-2004 and 2005-2017), the GTR raised from 0% to 27.8%, the STR raised from 45.8% to 50% and PR decreased from 54.2% to 22.2% ($p \leq 0.05$). Our current surgical strategy was represented by the use of endoscopic endonasal approach in the majority of midline-centered skull base chordomas[99]. Some tumors may extend or primarily develop at a lateral site (such as petro-clival and cavernous sinus regions) and through an EEA a complete bilateral exposure of para-clival segments of ICAs is recommended to attempt gross total tumor removal[99,123]. The surgical management of chordoma extending more laterally to the cranial nerves plane is challenging and, in our opinion should be treated by a multi-staged approach combined EEA-craniotomical approach to reduce the risk of postoperative deficits. The only exception of using an anterior open approach, in our hands, are patients with midline-centered skull base chordoma with a very limited inter-carotid distance (Figs. 59 and 60)[99]. To better assess a specific surgical approach in neurosurgery, a valid and reasonable approach is to make the so-called “equipoise”. It is therefore important to select a restricted group of lesions that could be approached by either modality[7,127]. But the rarity of chordoma makes this approach challenging and only multi-institutional studies are needed.

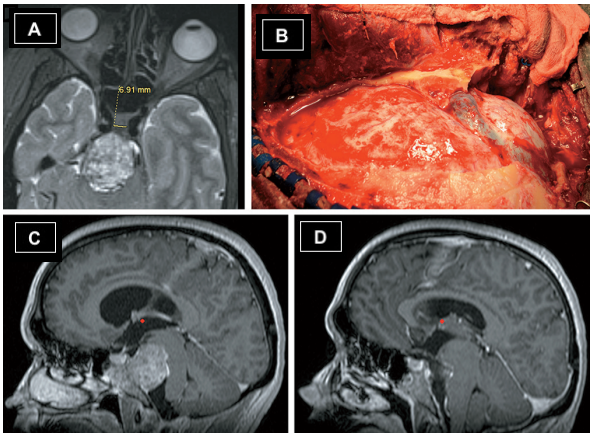

Figure 59. A) Preoperative axial MR T2-weighted image showing a clivus chordoma arising in the midline and displacing posteriorly the brainstem. The sellar inter-carotid distance is barely 7 mm. Due to the short ICA-ICA distance we decided to perform a one-stage combined subtemporal trans tentorial and retrosigmoid approach. B) Intraoperative view of the craniotomy with full-exposition of sovra- and infra-tentorial regions and transverse-sigmoid sinus junction. C) Preoperative sagittal MR T1-weighted image with gadolinium showing the significant chordoma extension rostral to the retro-sellar and inter-penduncular fossa. D) Postoperative sagittal MR T1-weighted image with gadolinium showing gross total tumor removal [adapted from La Corte et al., 2018].

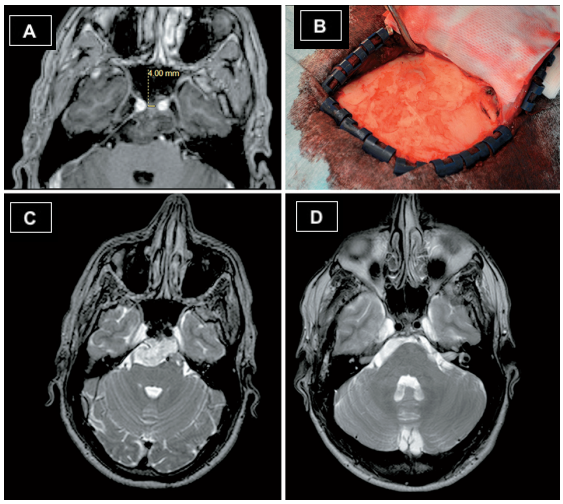

Figure 58. A) Preoperative axial MR T1-weighted image with gadolinium showing a clivus chordoma arising from the midline and displacing posteriorly the brainstem. The para-clival inter-carotid distance is around 4 mm. Due to the short ICA-ICA distance we decided to perform a one-stage sub-temporal trans-tentorial approach. B) Intraoperative view of the temporal bone exposure, from the zygomatic arch root anteriorly to the asterion posteriorly. C) Preoperative axial MR T2-weighted image showing the clivus chordoma extending in the pre-pontine cistern and totally behind the two ICAs. D) Postoperative axial MR T2-weighted image showing gross total tumor removal [adapted from La Corte et al., 2018].

EOR in skull base chordomas represented one of the most important prognostic factors described by many surgical series in the literature[12,26,79,80,86,165,183,184,205,216]. Since no definite guidelines exist to evaluate post-operative tumor removal and different classification are used over different centers, comparing our results with other groups was very difficult. In our cohort of primary skull base chordomas, EOR revealed to be a significant prognostic factor related to PFS (p=0.0200).

Interestingly, the more experienced surgeon, defined as the operator who have performed in the present cohort more than 10 chordoma surgeries, represented a positive prognostic factor with longer PFS in primary patients (p=0.0340). As already stated, this finding supports the need of large-referral center where there is a multi-disciplinary team where chordoma patients can receive the gold standard treatments, reaching better long-term outcomes and reducing surgical-related morbidities.

The development of any post-operative complications represented a significant prognostic factor correlating with both OS and PFS in the cohort of primary skull base chordomas ($p \leq 0.0001$ and p=0.0360, respectively). Similarly, the ΔKPS, defined as the difference between initial and at discharge KPS evaluation, correlated with a shorter OS in primary chordomas and with both reduction in OS and PFS in recurrent chordomas (p=0.0170 and 0.0180, respectively). Post-operative complications and KPS have been already looked as prognostic factors in some papers, and these outcomes could be related to the treatment selection and postponing of adjuvant therapies[184,216].

Post-operative high dose radiation therapy represents the main gold standard treatment in chordoma and showed to be an important factor that correlates with local disease control. Our data confirmed that adjuvant RT prolonged both OS and PFS in chordoma patients (p=0.0020 and 0.0010, respectively). Interestingly, hadron radiation therapy conferred a more prolonged OS than classical photon radiation therapy in chordoma patients.

The effective and beneficial role of carbon ion over proton therapy is still under evaluation and there is a still ongoing clinical trial in Heidelberg[133] (NCT01182779).

Based on the clinical results obtained in the first section on univariate analysis, our aim was to preliminarily build a personalized grading scale, that we called Peri-Operative Chordoma Scale (POCS), for each individualized patient that could be useful for practitioners to determine surgical outcome and, thus, the better management of patients undergoing potential adjuvant therapies[45,197,207]. The three significant factors of the predictive model of POCS were: the degree of MR contrast enhancement, the presence of preoperative motor deficits and the development of any post-operative complications according to CDG[28,138]. POCS strength and performance has been also evaluated in a restricted subgroup of patients having at least a F-UP≥45 months for evaluating PFS and a F-UP≥100 months for evaluating OS. The Peri-Operative Chordoma Scale (POCS) incorporates both pre-operative and peri-operative factors that can aid the surgeon to better manage the skull base chordoma patient immediately at the discharge or at first months after surgery.

There are some limitations to the present clinical analysis. Firstly, the study period spans over 20 years and this may lead to a big heterogeneity of surgical treatments and advanced radiation therapy modalities. We hope that such new prognostic factors could be validated in larger, multi-institutional studies in a prospective fashion.

PATHOLOGICAL STUDY

In the small cohort of retrospectively reviewed specimens, the presence of tumor infiltrating lymphocytes (TILs) revealed to be a factor that correlated with a prolonged survival in primary skull base chordomas (p=0.0170). Some other research groups have showed that the presence of TIL in other cancers, may be favorable. Moreover, a recent study confirmed that TILs correlated with a good prognosis and the expression of PD-1 and PD-L1 and found the basis for the starting a new clinical trial evaluating PD-L1 inhibitors[44,113] (NCT01519817 and NCT02989636). The immunologic tumor surveillance represents a hot topic in the current oncological literature and could be further analyzed prospectively and incorporated as immune-score in future studies[113,218].

In the small cohort of specimens analyzed by IHC there was a positive expression of PDGFR-B showing that this pathway, as observed by other researchers, could potentially be targeted by inhibitors of TKRs such as imatinib[20,68,179]. Moreover, the negative expression of PTEN in mostly of the cases could be interpreted as a genetic inactivation/mutation of the oncosuppresor role of PTEN, as observed in other cancers, leading to increasing signal activity mediated by Akt/PI3K/mTOR pathway, but this hypothesis should be proven[93]. This pathway has been targeted by mTOR inhibitors such as sirolimus in a case series of advanced chordomas.[171]. The significant TERT expression, the protein subunit of the telomerase, in chordomas may play a role in enabling tumor replicative immortality by increasing the length of telomeres or in the recent developed telomerase's telomere-independent functions such as amplification of the Wnt pathway[31,139,190]. Since IHC data have not been validated by other techniques, i.e. q-PCR and/or western blot, we have not performed any survival analysis in relation to the different analyzed markers.

SPHINGOLIPIDS STUDY

This study represents the first combined translational, clinical and sphingolipidomic analysis in skull base chordomas.

Sphingolipids act as bio-active molecular mediators in different cellular functions such as stress-response and downstream-signaling pathways, tumor proliferation and resistance to treatment[66,186]. In particular, ceramides can drive programmed cell death, such as autophagy and apoptosis, in response to several stress and stimuli such as oxidative stress, ionizing radiation and chemotherapeutic agents but also be involved into cell proliferation[60,161]. Previous studies have demonstrated that a delicate equilibrium exists between long-chain (i.e. Cer C16:0, Cer C18:0, Cer C20:0) and very long chain (Cer C24:1, Cer C24:0) ceramides to determine their specific biological role in regulating apoptosis and proliferation pathways[60,61]. Many studies have demonstrated the ceramides involvement in many types of cancers, such as breast, prostate cancers and gliomas, but nothing is known about their possible implication in chordomas[11,158,209]. The specific ultrastructural structure of chordomas consists of many vacuoles and lipid raft-like regions of endoplasmic reticulum tightly linked with mitochondrial membranes, called MAM mitochondria-associated ER membrane[89]. These structures have been found to be involved in lipid synthesis, apoptosis and cell proliferation[34,89,151]. Based on such observations, we decided to perform a thorough sphingolipid analysis in chordoma samples.

Our preliminary targeted analysis showed that recurrent skull base tumors presented a higher level of total ceramides than the primary ones ($p \leq 0.05$). Recurrent patients have undergone previous combined treatments such as surgery and RT and both factors may explain why ceramides are significantly different in the two groups[3,4,76,158]. Since the recurrent tumor type and previous treatments represented a significant negative prognostic factor relating to worse OS and PFS in previous studies, a raising in ceramides

content in skull base chordomas could act as a negative prognostic factor[111,171,182,216]. We showed that there is also a concomitant rise in both ceramides and dihydroceramides and such finding could be related to an activation of the *de novo* pathway, but further analyses are needed. *De novo* pathway represents a strong autophagy inducer[37,66,169,206]. *In vitro*, autophagy could trigger both a cytoprotective action promoting radio-resistance and a cytotoxic function[9,104,106,124]. Autophagy induces the activation of many cellular pathways and damaged organelles and proteins are conveyed to degradation to maintain cellular homeostasis[106,108,122,214]. For example, ionizing radiation induces mitochondrial damage, which triggers autophagy mediated by E3-ubiquitin ligase p62[76]. In our retrospective analysis, we preliminarily evaluated by IHC the presence of p62 that is expressed in around 90% of all chordomas. Such factor could be, therefore, one of the main inducing autophagy mechanisms in chordomas, but further confirmation studies are needed with the evaluation of the other standardized autophagy markers[88].

Different molecules have been developed as inhibitors of serine palmitoyltransferase (SPT), the first enzyme involved in the *de novo* synthesis pathway. Some potent and selective inhibitors have been isolated from microorganisms, such as sphingofungins, lipoxamycins, viridiofungins and myriocin (Myr)[112,121]. Several studies showed the efficacy of Myr treatment, the only commercially available product, either *in vivo* and *in vitro* models and its capacity to irreversibly inhibit SPT[78,121]. Myr showed to have also a potential role in reducing tumor cell proliferation through the SPT inhibition[121,196]. The involvement of *de novo* ceramide synthesis has been shown in different immunometabolic diseases clusters such as obesity, diabetes and neurodegeneration, cystic fibrosis and retinitis pigmentosa[17,70,72,141,187]. Several recent studies showed that intra-tracheal administration of Myr in CF mouse model infected with Pseudomonas aeruginosa or Aspergillus fumigatus showed an anti-inflammatory role due

to the inhibition of *de novo* sphingolipid synthesis[16–19]. Therefore, Myr may have a significant role in the future therapeutical innovation and application in chordoma patients where a *de novo* ceramide synthesis seems to be over activated. More studies are needed to firstly confirm the deregulation of such ceramide biosynthesis pathway in chordoma and to assess the pharmacokinetics and pharmacodynamics of Myr.

Moreover, single ceramides species have never been correlated with clinical variables and no definitive biological role could be hypothesized in chordomas. The regression and correlation analyses showed that very long chain ceramides (such as Cer C24:1) were significantly different between primary and recurrent chordomas (p=0.0076). Also, the very long chain DHCer C24:1 (p=0.0120) was the only species that was significantly different related to tumor type.

To furtherly support ceramides as a bio-marker of aggressive behavior of chordomas, we tried to make some correlation analysis in relation to the gadolinium enhancement pattern (Fig. 43-45). On the ground of our previous clinical analysis, such radiological feature represented an aggressive feature to be considered in the proper management of chordomas patients (Fig. 60). Firstly, total ceramides and dihydroceramides levels were significantly higher in intense gadolinium enhancement group than no/mild enhancement group (p=0.0290). Moreover, very long chain single ceramides species were significantly different between the two radiological categories (p=0.0120). Such results confirmed that very long chain ceramides and dihydroceramides may represent an intrinsic biological feature of more aggressive chordomas.

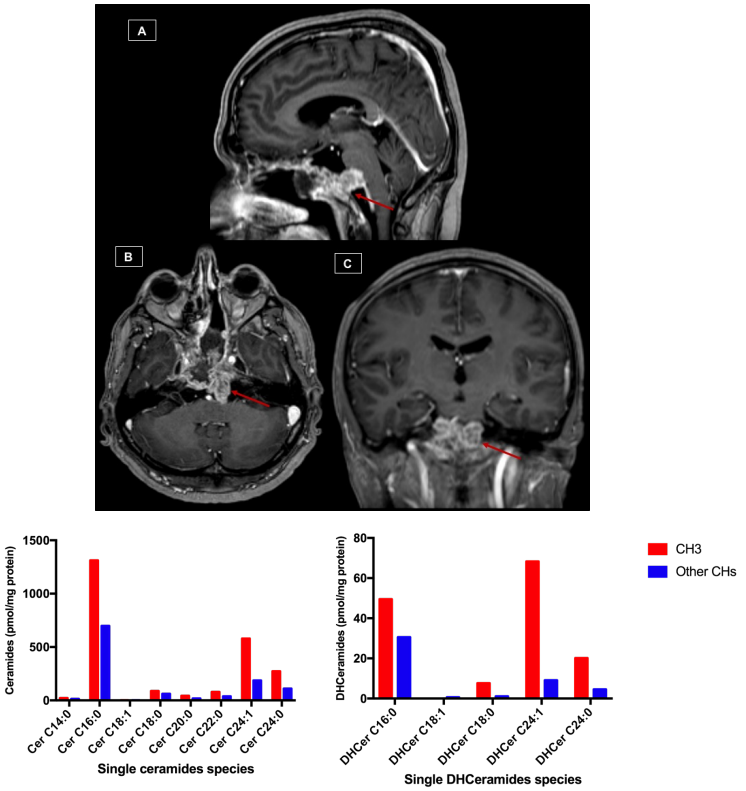

Figure 60. Above, Sagittal (A), axial (B), coronal (C) T1-weighted post-contrast MR images showing a chordoma (red arrows) with intense contrast enhancement. Pathology showed a de-differentiated chordoma. Below, sphingolipid analysis showed the highest content in ceramides and dihydroceramides. Bar graphs showing the ceramide content of the present case (CH3) in comparison with the average of ceramide levels of other chordomas.

We, then, correlated the Cer and DHCer levels with tumor proliferation rate MIB-1 marker (Fig. 46) and found that were strongly correlated (r=0.7257, p=0.0033 and r=0.6733, p=0.0083, respectively). Higher levels of sphingolipids were associated with higher MIB-1 values and, therefore, to high proliferating tumors. The single ceramides and dihydroceramides species that were more correlated to high proliferative tumors were Cer 24:1 and its respective DHCer24:1 (r=0.8814, p≤0.0001 and r=0.8429, p=0.0002, respectively). Moreover, the final candidate predictive factors that well fitted the regression model were Cer C24:1 (beta=0.348, *P*=0.025), and DHCer C18:0 (beta=0.663, *P*≤0.001).

A paper showed, in an *in vitro* HeLa cells model, that ceramides produced by CerS5 (mainly Cer C16:0) following radiation have a pro-apoptotic role, whereas ceramides produced by CerS2 (mainly very long chain, Cer C24:1 and C24:0) act as a pro-tumor survival[118]. These explained the delicate interplay among the different CerS isoforms and the different ceramides production into the stress-induced response and that tumoral cells can activate pro-survival mechanism that could be related to chordoma radio-resistance[118]. Interestingly, Kolb et al. also showed through a lipid targeted analysis, that a chordoma cell line presented a massive upregulation of glucosylceramides GlyCer C24:0 and GlyCer C24:1 compared with other health and pathological cell lines and postulated that these species could be related to chordoma radio-resistance[89].

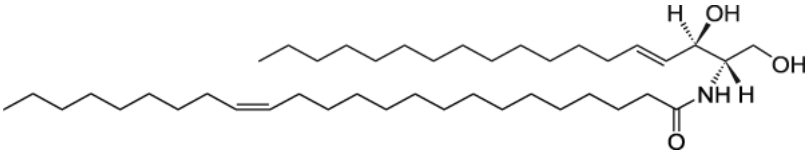

Figure 61. Chemical structure of Cer C24:1, also called N-nervonoyl-D-erythro-sphingosine.

Based on our results, Cer C24:1 (Fig. 61[5]) and DHCer C18:0 may represent aggressiveness bio-markers of skull base chordomas. The concomitantly rise of DHCer C24:1 may be also explained by an exaggerated upregulation of the *de novo* pathway that, in turn, may be the inducer of cytoprotective autophagy concurring to cell survival and resistance to different treatments[81]. Since it is a preliminary study, larger samples are needed to confirm and externally validate our results. To better asses if *de novo* pathway is actually activated, the specific involved enzyme should be *ad hoc* analyzed[60,126].

CONCLUSIONS AND FUTURE PERSPECTIVES

The current project presents an innovative translational approach to study skull base chordoma, a rare intracranial tumor that enormously affects the quality of life of our patients. Our clinical analysis showed that pre-operative clinical symptoms (motor and cranial nerve deficits), anatomical location (jugular foramen, pre-brainstem cisterns and brainstem dislocation), surgical features (extent of tumor resection and surgeon's experience), development of post-operative complications and KPS decline represented significant prognostic factors. The pattern of MR contrast enhancement significantly correlated to both OS and PFS. The Peri-Operative Chordoma Scale (POCS) has been devised for practitioners to determine surgical outcome and the better management of patients undergoing potential adjuvant therapies. Such clinical bio-markers should be validated in multi-institutional and prospective studies. Pathological and immunohistochemical data should be also validated by other techniques in a larger sample population involving more than one Institution.

Sphingolipids analysis represents a really new approach in chordomas and future studies are needed. Our analysis showed ceramides as promising tumoral bio-markers in chordomas. Long and very long chain ceramides, such as Cer C24:1 and DHCer C18:0, may be related to a more prolonged tumor survival, aggressiveness and the understanding of their effective biological role will hopefully shed lights on the mechanisms of chordoma radio-resistance and tendency to recur. To better determine which pathway of ceramides synthesis is involved in chordoma biology it will be useful to specifically evaluate different enzymes, such as ceramides synthases and desaturases. *In vitro* studies would be useful to determine the direct relationship between hadron-therapy and ceramides formation and analysis of programmed cell-death mechanisms. *In vitro* and *in vivo* models could be also employed to evaluate the potential therapeutic effects of specific molecules, such as Myriocin, targeting sphingolipids metabolism.

REFERENCES

1. Almefty KK, Pravdenkova S, Sawyer JR, Al-Mefty O: Impact of cytogenetic abnormalities on the management of skull base chordomas. **J Neurosurg 110**:715–724, 2009
2. Amichetti M, Cianchetti M, Amelio D, Enrici RM, Minniti G: Proton therapy in chordoma of the base of the skull: a systematic review. **Neurosurg Rev 32**:403–16, 2009
3. Aureli M, Bassi R, Prinetti A, Chiricozzi E, Pappalardi B, Chigorno V, et al: Ionizing radiations increase the activity of the cell surface glycohydrolases and the plasma membrane ceramide content. **Glycoconj J 29**:585–597, 2012
4. Aureli M, Murdica V, Loberto N, Samarani M, Prinetti A, Bassi R, et al: Exploring the link between ceramide and ionizing radiation. **Glycoconj J 31**:449–459, 2014
5. Avantilipids CC: 860525- Cer C24:1 Web-Structure.gif Available: https://avantilipids.com/assets/products/images/860525-Web-Structure.gif.
6. Bambakidis NC: **Surgery of the Craniovertebral Junction**. Thieme, 2012
7. Bander ED, Singh H, Ogilvie CB, Cusic RC, Pisapia DJ, Tsiouris AJ, et al: Endoscopic endonasal versus transcranial approach to tuberculum sellae and planum sphenoidale meningiomas in a similar cohort of patients. **J Neurosurg 128**:40–48, 2018
8. Bartke N, Hannun YA: Bioactive sphingolipids: metabolism and function. **J Lipid Res 50**:S91–S96, 2009
9. Bedia C, Levade T, Codogno P: Regulation of Autophagy by Sphingolipids. **Anticancer Agents Med Chem 11**:844–853, 2011
10. Benndorf M, Neubauer J, Langer M, Kotter E: Bayesian pretest probability estimation for primary malignant bone tumors based on the Surveillance, Epidemiology and End Results Program (SEER) database. **Int J Comput Assist Radiol Surg 12**:485–491, 2017

11. Bernhart E, Damm S, Wintersperger A, Nusshold C, Brunner AM, Plastira I, et al: Interference with distinct steps of sphingolipid synthesis and signaling attenuates proliferation of U87MG glioma cells. **Biochem Pharmacol 96**:119–30, 2015
12. Boari N, Gagliardi F, Cavalli A, Ferrari L, Riva P, Mortini, Md P: Skull base chordomas: clinical outcome in a consecutive series of 45 patients with long-term follow-up and evaluation of clinical and biological prognostic factors. **J Neurosurg 125**:450–460, 2016
13. Brandal P, Bjerkehagen B, Danielsen H, Heim S: Chromosome 7 abnormalities are common in chordomas. **Cancer Genet Cytogenet 160**:15–21, 2005
14. Brito da Silva H, Straus D, Barber JK, Rostomily RC, Ferreira M, Sekhar LN: Cranial Chordoma: A New Preoperative Grading System. **Neurosurgery 83**:403–415, 2018
15. Burrow J le F, Stewart MJ: Malignant Spheno-Occipital Chordoma. **J Neurol Psychopathol 4**:205–17, 1923
16. Campisi GM, Signorelli P, Rizzo J, Ghilardi C, Antognetti J, Caretti A, et al: Determination of the serine palmitoyl transferase inhibitor myriocin by electrospray and Q-trap mass spectrometry. **Biomed Chromatogr 31**:e4026, 2017
17. Caretti A, Bragonzi A, Facchini M, De Fino I, Riva C, Gasco P, et al: Anti-inflammatory action of lipid nanocarrier-delivered myriocin: therapeutic potential in cystic fibrosis. **Biochim Biophys Acta - Gen Subj 1840**:586–594, 2014
18. Caretti A, Torelli R, Perdoni F, Falleni M, Tosi D, Zulueta A, et al: Inhibition of ceramide de novo synthesis by myriocin produces the double effect of reducing pathological inflammation and exerting antifungal activity against A. fumigatus airways infection. **Biochim Biophys Acta - Gen Subj 1860**:1089–1097, 2016
19. Caretti A, Vasso M, Bonezzi FT, Gallina A, Trinchera M, Rossi A, et al: Myriocin treatment of CF lung infection and inflammation: complex analyses for enigmatic lipids. **Naunyn Schmiedebergs Arch Pharmacol 390**:775–790, 2017

20. Casali PG, Messina A, Stacchiotti S, Tamborini E, Crippa F, Gronchi A, et al: Imatinib mesylate in chordoma. **Cancer 101**:2086–2097, 2004
21. Casali PG, Stacchiotti S, Sangalli C, Olmi P, Gronchi A: Chordoma. **Curr Opin Oncol 19**:367–70, 2007
22. Cates JMM, Itani DM, Coffin CM, Harfe BD: The sonic hedgehog pathway in chordoid tumours. **Histopathology 56**:978–979, 2010
23. Chambers KJ, Lin DT, Meier J, Remenschneider A, Herr M, Gray ST: Incidence and survival patterns of cranial chordoma in the United States. **Laryngoscope 124**:1097–1102, 2014
24. Chibbaro S, Cornelius JF, Froelich S, Tigan L, Kehrli P, Debry C, et al: Endoscopic endonasal approach in the management of skull base chordomas--clinical experience on a large series, technique, outcome, and pitfalls. **Neurosurg Rev 37**:217-24; discussion 224–5, 2014
25. Choi K-S, Lee C, Harfe BD: Sonic hedgehog in the notochord is sufficient for patterning of the intervertebral discs. **Mech Dev 129**:255–262, 2012
26. Choy W, Terterov S, Kaprealian TB, Trang A, Ung N, DeSalles A, et al: Predictors of recurrence following resection of intracranial chordomas. **J Clin Neurosci 22**:1792–1796, 2015
27. Chugh R, Tawbi H, Lucas DR, Biermann JS, Schuetze SM, Baker LH: Chordoma: The Nonsarcoma Primary Bone Tumor. **Oncologist 12**:1344–1350, 2007
28. Clavien PA, Barkun J, de Oliveira ML, Vauthey JN, Dindo D, Schulick RD, et al: The Clavien-Dindo Classification of Surgical Complications. **Ann Surg 250**:187–196, 2009
29. Clinical trials - Chordoma Foundation: Available: https://www.chordomafoundation.org/clinical-trials/.
30. Colia V, Stacchiotti S: Medical treatment of advanced chordomas. **Eur J Cancer 83**:220–228, 2017
31. Cong Y, Shay JW: Actions of human telomerase beyond telomeres. **Cell Res 18**:725–732, 2008
32. Conger AR, M.S. J, Lucas J, Zada G, Schwartz TH, Cohen-Gadol AA: Endoscopic extended transsphenoidal resection of craniopharyngiomas: nuances of neurosurgical technique. **Neurosurg Focus 37**:E10, 2014

33. Crockard HA: The transoral approach to the base of the brain and upper cervical cord. **Ann R Coll Surg Engl 67**:321–5, 1985
34. Csordás G, Renken C, Várnai P, Walter L, Weaver D, Buttle KF, et al: Structural and functional features and significance of the physical linkage between ER and mitochondria. **J Cell Biol 174**:915–21, 2006
35. Cushing H: **The Pituitary Body and Its Disorders, Clinical States Produced by Disorders of the Hypophysis Cerebri**. 1912
36. Dalprà L, Malgara R, Miozzo M, Riva P, Volontè M, Larizza L, et al: First cytogenetic study of a recurrent familial chordoma of the clivus. **Int J Cancer 81**:24–30, 1999
37. Devlin CM, Lahm T, Hubbard WC, Van Demark M, Wang KC, Wu X, et al: Dihydroceramide-based Response to Hypoxia. **J Biol Chem 286**:38069–38078, 2011
38. Dhall G, Traverso M, Finlay JL, Shane L, Gonzalez-Gomez I, Jubran R: The role of chemotherapy in pediatric clival chordomas. **J Neurooncol 103**:657–62, 2011
39. Di Maio S, Kong E, Yip S, Rostomily R: Converging paths to progress for skull base chordoma: Review of current therapy and future molecular targets. **Surg Neurol Int 4**:72, 2013
40. Di Maio S, Rostomily R, Sekhar LN: Current surgical outcomes for cranial base chordomas: cohort study of 95 patients. **Neurosurgery 70**:1355–60; discussion 1360, 2012
41. Di Maio S, Yip S, Al Zhrani GA, Alotaibi FE, Al Turki A, Kong E, et al: Novel targeted therapies in chordoma: an update. **Ther Clin Risk Manag 11**:873–83, 2015
42. Dorfman HD, Czerniak B: Bone cancers. **Cancer 75**:203–10, 1995
43. Fasig JH, Dupont WD, LaFleur BJ, Olson SJ, Cates JMM: Immunohistochemical analysis of receptor tyrosine kinase signal transduction activity in chordoma. **Neuropathol Appl Neurobiol 34**:95–104, 2008
44. Feng Y, Shen J, Gao Y, Liao Y, Cote G, Choy E, et al: Expression of programmed cell death ligand 1 (PD-L1) and prevalence of tumor-infiltrating lymphocytes (TILs) in chordoma. **Oncotarget 6**:11139–49, 2015

45. Fernandez-Miranda JC, Gardner PA, Snyderman CH, Devaney KO, Mendenhall WM, Suárez C, et al: Clival chordomas: A pathological, surgical, and radiotherapeutic review. **Head Neck 36**:892–906, 2014
46. Ferraresi V, Nuzzo C, Zoccali C, Marandino F, Vidiri A, Salducca N, et al: Chordoma: clinical characteristics, management and prognosis of a case series of 25 patients. **BMC Cancer 10**:22, 2010
47. File:BraggPeak.png - Wikimedia Commons: Available: https://commons.wikimedia.org/wiki/File:BraggPeak.png.
48. File:Sphingolipids general structures.png - Wikimedia Commons: Available: https://commons.wikimedia.org/wiki/File:Sphingolipids_general_structures.png.
49. Fleming GF, Heimann PS, Stephens JK, Simon M a, Ferguson MK, Benjamin RS, et al: Dedifferentiated chordoma. Response to aggressive chemotherapy in two cases. **Cancer 72**:714–8, 1993
50. Forsyth PA, Cascino TL, Shaw EG, Scheithauer BW, O'Fallon JR, Dozier JC, et al: Intracranial chordomas: a clinicopathological and prognostic study of 51 cases. **J Neurosurg 78**:741–747, 1993
51. Fraser JF, Nyquist GG, Moore N, Anand VK, Schwartz TH: Endoscopic Endonasal Minimal Access Approach to the Clivus. **Oper Neurosurg 67**:ons150-ons158, 2010
52. Fraser JF, Nyquist GG, Moore N, Anand VK, Schwartz TH: Endoscopic endonasal transclival resection of chordomas: operative technique, clinical outcome, and review of the literature. **J Neurosurg 112**:1061–1069, 2010
53. Frempong-Boadu AK, Faunce WA, Fessler RG: Endoscopically assisted transoral-transpharyngeal approach to the craniovertebral junction. **Neurosurgery 51**:S60-6, 2002
54. George B, Bresson D, Bouazza S, Froelich S, Mandonnet E, Hamdi S, et al: [Chordoma]. **Neurochirurgie 60**:63–140, 2014
55. George B, Bresson D, Herman P, Froelich S: Chordomas: A Review. **Neurosurg Clin N Am 26**:437–52, 2015
56. Ginat DT, Mangla R, Yeaney G, Johnson M, Ekholm S: Diffusion-Weighted Imaging for Differentiating Benign From Malignant Skull Lesions and Correlation With Cell Density. **Am J Roentgenol 198**:W597–W601, 2012

57. Hallor KH, Staaf J, Jönsson G, Heidenblad M, Vult von Steyern F, Bauer HCF, et al: Frequent deletion of the CDKN2A locus in chordoma: analysis of chromosomal imbalances using array comparative genomic hybridisation. **Br J Cancer 98**:434–442, 2008
58. Hannun YA, Obeid LM: Many ceramides. **J Biol Chem 286**:27855–62, 2011
59. Hannun YA, Obeid LM: Principles of bioactive lipid signalling: Lessons from sphingolipids. **Nat Rev Mol Cell Biol 9**:139–150, 2008
60. Hartmann D, Lucks J, Fuchs S, Schiffmann S, Schreiber Y, Ferreirós N, et al: Long chain ceramides and very long chain ceramides have opposite effects on human breast and colon cancer cell growth. **Int J Biochem Cell Biol 44**:620–628, 2012
61. Hartmann D, Wegner M-S, Wanger RA, Ferreirós N, Schreiber Y, Lucks J, et al: The equilibrium between long and very long chain ceramides is important for the fate of the cell and can be influenced by co-expression of CerS. **Int J Biochem Cell Biol 45**:1195–1203, 2013
62. Harvald EB, Olsen ASB, Færgeman NJ: Autophagy in the light of sphingolipid metabolism. **Apoptosis 20**:658–670, 2015
63. Hasse H: Ein neuer Fall von Schleimgeschwulst am Clivus. **Virchows Arch 11**:1857
64. Hasselblatt M, Thomas C, Hovestadt V, Schrimpf D, Johann P, Bens S, et al: Poorly differentiated chordoma with SMARCB1/INI1 loss: a distinct molecular entity with dismal prognosis. **Acta Neuropathol 132**:149–151, 2016
65. Henderson SR, Guiliano D, Presneau N, McLean S, Frow R, Vujovic S, et al: A molecular map of mesenchymal tumors. **Genome Biol 6**:R76, 2005
66. Henry B, Möller C, Dimanche-Boitrel M-T, Gulbins E, Becker KA: Targeting the ceramide system in cancer. **Cancer Lett 332**:286–294, 2013
67. Herrmann BG, Labeit S, Poustka A, King TR, Lehrach H: Cloning of the T gene required in mesoderm formation in the mouse. **Nature 343**:617–622, 1990
68. Hindi N, Casali PG, Morosi C, Messina A, Palassini E, Pilotti S, et al: Imatinib in advanced chordoma: A retrospective case series analysis. **Eur J Cancer 51**:2609–14, 2015

69. Hoch BL, Nielsen GP, Liebsch NJ, Rosenberg AE: Base of Skull Chordomas in Children and Adolescents. **Am J Surg Pathol 30**:811–818, 2006
70. Holland WL, Bikman BT, Wang L-P, Yuguang G, Sargent KM, Bulchand S, et al: Lipid-induced insulin resistance mediated by the proinflammatory receptor TLR4 requires saturated fatty acid–induced ceramide biosynthesis in mice. **J Clin Invest 121**:1858–1870, 2011
71. Horbinski C, Oakley GJ, Cieply K, Mantha GS, Nikiforova MN, Dacic S, et al: The prognostic value of Ki-67, p53, epidermal growth factor receptor, 1p36, 9p21, 10q23, and 17p13 in skull base chordomas. **Arch Pathol Lab Med 134**:1170–6, 2010
72. Hotamisligil GS: Inflammation, metaflammation and immunometabolic disorders. **Nature 542**:177–185, 2017
73. Hsu CC-T, Watkins TW, Kwan GNC, Haacke EM: Susceptibility-Weighted Imaging of Glioma: Update on Current Imaging Status and Future Directions. **J Neuroimaging 26**:383–390, 2016
74. Hsu W, Mohyeldin A, Shah SR, ap Rhys CM, Johnson LF, Sedora-Roman NI, et al: Generation of chordoma cell line JHC7 and the identification of Brachyury as a novel molecular target. **J Neurosurg 115**:760–9, 2011
75. Hsu W, Wolinsky J-P, Gokaslan ZL, Sciubba DM: Transoral Approaches to the Cervical Spine. **Neurosurgery 66**:A119–A125, 2010
76. Hu L, Wang H, Huang L, Zhao Y, Wang J: Crosstalk between autophagy and intracellular radiation response (Review). **Int J Oncol 49**:2217–2226, 2016
77. Hug EB: Review of skull base chordomas: prognostic factors and long-term results of proton-beam radiotherapy. **Neurosurg Focus 10**:E11, 2001
78. Ikushiro H, Hayashi H, Kagamiyama H: Reactions of Serine Palmitoyltransferase with Serine and Molecular Mechanisms of the Actions of Serine Derivatives as Inhibitors. **Biochemistry 43**:1082–1092, 2004
79. Ito E, Saito K, Okada T, Nagatani T, Nagasaka T: Long-term control of clival chordoma with initial aggressive surgical resection and gamma knife radiosurgery for recurrence. **Acta Neurochir (Wien) 152**:57–67, 2010

80. Jahangiri A, Chin AT, Wagner JR, Kunwar S, Ames C, Chou D, et al: Factors predicting recurrence after resection of clival chordoma using variable surgical approaches and radiation modalities. **Neurosurgery 76**:179–185, 2015

81. Jiang W, Ogretmen B: Autophagy paradox and ceramide. **Biochim Biophys Acta 1841**:783–92, 2014

82. Jones DC, Hayter JP, Vaughan ED, Findlay GF: Oropharyngeal morbidity following transoral approaches to the upper cervical spine. **Int J Oral Maxillofac Surg 27**:295–8, 1998

83. Kassam AB, Vescan AD, Carrau RL, Prevedello DM, Gardner P, Mintz AH, et al: Expanded endonasal approach: vidian canal as a landmark to the petrous internal carotid artery. **J Neurosurg 108**:177–183, 2008

84. Kelley MJ, Shi J, Ballew B, Hyland PL, Li W-Q, Rotunno M, et al: Characterization of T gene sequence variants and germline duplications in familial and sporadic chordoma. **Hum Genet 133**:1289–1297, 2014

85. Kikuchi K, Hiwatashi A, Togao O, Yamashita K, Kamei R, Kitajima M, et al: Usefulness of perfusion- and diffusion-weighted imaging to differentiate between pilocytic astrocytomas and high-grade gliomas: a multicenter study in Japan. **Neuroradiology 60**:391–401, 2018

86. Kitamura Y, Sasaki H, Kimura T, Miwa T, Takahashi S, Kawase T, et al: Molecular and clinical risk factors for recurrence of skull base chordomas: gain on chromosome 2p, expression of brachyury, and lack of irradiation negatively correlate with patient prognosis. **J Neuropathol Exp Neurol 72**:816–23, 2013

87. Klebs E: Ein Fall von Ecchocondrosis spheno-occipitalase amylace. **Virchows Arch Pathol Anat 31**:396–399, 1864

88. Klionsky DJ, Abdelmohsen K, Abe A, Abedin MJ, Abeliovich H, Arozena AA, et al: Guidelines for the use and interpretation of assays for monitoring autophagy (3rd edition). **Autophagy 12**:1–222, 2016

89. Kolb D, Pritz E, Steinecker-Frohnwieser B, Lohberger B, Deutsch A, Kroneis T, et al: Extended Ultrastructural Characterization of Chordoma Cells: The Link to New Therapeutic Options. **PLoS One 9**:e114251, 2014

90. Kolesnick R, Hannun YA: Ceramide and apoptosis. **Trends Biochem Sci 24**:224–5; author reply 227, 1999
91. Komotar RJ, Starke RM, Raper DMSS, Anand VK, Schwartz TH: The endoscope-assisted ventral approach compared with open microscope-assisted surgery for clival chordomas. **World Neurosurg 76**:318–327, 2011
92. Korzh V, Grunwald D: Nadine Dobrovolskaïa-Zavadskaïa and the dawn of developmental genetics. **BioEssays 23**:365–371, 2001
93. Koul D: PTEN signaling pathways in glioblastoma. **Cancer Biol Ther 7**:1321–1325, 2008
94. Koutourousiou M, Gardner P a, Fernandez-Miranda JC, Tyler-Kabara EC, Wang EW, Snyderman CH: Endoscopic endonasal surgery for craniopharyngiomas: surgical outcome in 64 patients. **J Neurosurg 119**:1194–207, 2013
95. Kroemer G, Mariño G, Levine B: Autophagy and the Integrated Stress Response. **Mol Cell 40**:280–293, 2010
96. La Corte E, Aldana PR: Endoscopic approach to the upper cervical spine and clivus: an anatomical study of the upper limits of the transoral corridor. **Acta Neurochir (Wien) 159**:2017
97. La Corte E, Aldana PR, Ferroli P, Greenfield JP, Härtl R, Anand VK, et al: The rhinopalatine line as a reliable predictor of the inferior extent of endonasal odontoidectomies. **Neurosurg Focus 38**:2015
98. La Corte E, Aldana PR, Schiariti M, Maccari A, Ferroli P: Endoscopic approaches to the craniovertebral junction. **Acta Neurochir (Wien) 156**:2014
99. La Corte E, Broggi M, Bosio L, Danesi G, Ferroli P: Tailored surgical strategy in clival chordomas: an extraordinary selection bias that limits approach comparison. **J Neurosurg Sci 62**:519–521, 2018
100. Labidi M, Watanabe K, Bouazza S, Bresson D, Bernat AL, George B, et al: Clivus chordomas: a systematic review and meta-analysis of contemporary surgical management. **J Neurosurg Sci**:2016

101. Lau CSM, Mahendraraj K, Ward A, Chamberlain RS: Pediatric Chordomas: A Population-Based Clinical Outcome Study Involving 86 Patients from the Surveillance, Epidemiology, and End Result (SEER) Database (1973-2011). **Pediatr Neurosurg 51**:127–36, 2016
102. Lee IJ, Lee RJ, Fahim DK: Prognostic Factors and Survival Outcome in Patients with Chordoma in the United States: A Population-Based Analysis. **World Neurosurg 104**:346–355, 2017
103. Lee RWY, Tierney E: Hypothesis: The Role of Sterols in Autism Spectrum Disorder. **Autism Res Treat 2011**:1–7, 2011
104. Levine B: Autophagy and cancer. **Nature 446**:745–747, 2007
105. Li M, Zhai Y, Bai J, Wang S, Gao H, Li C, et al: SNF5 as a prognostic factor in skull base chordoma. **J Neurooncol 137**:139–146, 2018
106. Li Y, Li S, Qin X, Hou W, Dong H, Yao L, et al: The pleiotropic roles of sphingolipid signaling in autophagy. **Cell Death Dis 5**:e1245–e1245, 2014
107. Lin E, Scognamiglio T, Zhao Y, Schwartz TH, Phillips CD: Prognostic implications of gadolinium enhancement of skull base chordomas. **Am J Neuroradiol 39**:1509–1514, 2018
108. Liu WJ, Ye L, Huang WF, Guo LJ, Xu ZG, Wu HL, et al: P62 Links the Autophagy Pathway and the Ubiqutin-Proteasome System Upon Ubiquitinated Protein Degradation. **Cell Mol Biol Lett 21**:1–14, 2016
109. Longoni M, Orzan F, Stroppi M, Boari N, Mortini P, Riva P: Evaluation of 1p36 markers and clinical outcome in a skull base chordoma study. **Neuro Oncol 10**:52–60, 2008
110. Luschka H: Ueber gallertartige Auswüchse am Clivus Blumenbachii. **Virchows Arch 11**:8–12, 1857
111. Ma JP, Tian KB, Wang L, Wang K, Li D, Yang Y, et al: Proposal and Validation of a Basic Progression Scoring System for Patients with Skull Base Chordoma. **World Neurosurg 91**:409–418, 2016
112. Mandala SM, Harris GH: [35] Isolation and characterization of novel inhibitors of sphingolipid synthesis: Australifungin, viridiofungins, rustmicin, and khafrefungin. **Methods Enzymol 311**:335–348, 2000

113. Mathios D, Ruzevick J, Jackson CM, Xu H, Shah SR, Taube JM, et al: PD-1, PD-L1, PD-L2 expression in the chordoma microenvironment. **J Neurooncol 121**:251–9, 2015
114. McCann MR, Tamplin OJ, Rossant J, Séguin CA: Tracing notochord-derived cells using a Noto-cre mouse: implications for intervertebral disc development. **Dis Model Mech 5**:73–82, 2012
115. McMaster ML, Goldstein AM, Bromley CM, Ishibe N, Parry DM: Chordoma: Incidence and survival patterns in the United States, 1973-1995. **Cancer Causes Control 12**:1–11, 2001
116. Menezes AH: Surgical approaches: postoperative care and complications "transoral–transpalatopharyngeal approach to the craniocervical junction." **Child's Nerv Syst 24**:1187–1193, 2008
117. Merrill Jr. AH, Sullards MC, Allegood JC, Kelly S, Wang E: Sphingolipidomics: High-throughput, structure-specific, and quantitative analysis of sphingolipids by liquid chromatography tandem mass spectrometry. **Methods 36**:207–224, 2005
118. Mesicek J, Lee H, Feldman T, Jiang X, Skobeleva A, Berdyshev E V., et al: Ceramide synthases 2, 5, and 6 confer distinct roles in radiation-induced apoptosis in HeLa cells. **Cell Signal 22**:1300–1307, 2010
119. Miettinen M (Markku M., Fetsch JF, Antonescu CR, Folpe AL, Wakely PE, American Registry of Pathology: **Tumors of the Soft Tissues**.
120. Miozzo M, Dalprà L, Riva P, Volontà M, Macciardi F, Pericotti S, et al: A tumor suppressor locus in familial and sporadic chordoma maps to 1p36. **Int J Cancer 87**:68–72, 2000
121. Miyake Y, Kozutsumi Y, Nakamura S, Fujita T, Kawasaki T: Serine Palmitoyltransferase Is the Primary Target of a Sphingosine-like Immunosuppressant, ISP-1/Myriocin. **Biochem Biophys Res Commun 211**:396–403, 1995
122. Mizushima N, Levine B, Cuervo AM, Klionsky DJ: Autophagy fights disease through cellular self-digestion. **Nature 451**:1069–1075, 2008
123. Mohyeldin A, Prevedello D, Jamshidi A, Filho L, Carrau R: Nuances in the Treatment of Malignant Tumors of the Clival and Petroclival Region. **Int Arch Otorhinolaryngol 18**:S157–S172, 2014

124. Morad SAF, Cabot MC: Ceramide-orchestrated signalling in cancer cells. **Nat Rev Cancer 13**:51–65, 2013
125. Morera VA, Fernandez-Miranda JC, Prevedello DM, Madhok R, Barges-Coll J, Gardner P, et al: “Far-Medial” Expanded Endonasal Approach to the Inferior Third of the Clivus. **Oper Neurosurg 66**:ons211-ons220, 2010
126. Moro K, Kawaguchi T, Tsuchida J, Gabriel E, Qi Q, Yan L, et al: Ceramide species are elevated in human breast cancer and are associated with less aggressiveness. **Oncotarget 9**:19874–19890, 2018
127. Moussazadeh N, Prabhu V, Bander ED, Cusic RC, Tsiouris AJ, Anand VK, et al: Endoscopic endonasal versus open transcranial resection of craniopharyngiomas: a case-matched single-institution analysis. **Neurosurg Focus 41**:E7, 2016
128. Müller J: Ueber das Vorkommen von Resten der Chorda dorsalis bei Menschen nach der Geburt und über ihr Verhaltnis zu den Gallertgeschewülsten am Clivus. **Z Rat Med 2**:1858
129. Müller U, Kubik-Huch RA, Ares C, Hug EB, Löw R, Valavanis A, et al: Is there a role for conventional MRI and MR diffusion-weighted imaging for distinction of skull base chordoma and chondrosarcoma? **Acta radiol 57**:225–232, 2016
130. Munzenrider JE, Liebsch NJ: Proton therapy for tumors of the skull base. **Strahlenther Onkol 175 Suppl 2**:57–63, 1999
131. Nelson AC, Pillay N, Henderson S, Presneau N, Tirabosco R, Halai D, et al: An integrated functional genomics approach identifies the regulatory network directed by brachyury (T) in chordoma. **J Pathol 228**:274–285, 2012
132. Nibu Y, José-Edwards DS, Di Gregorio A: From notochord formation to hereditary chordoma: the many roles of Brachyury. **Biomed Res Int 2013**:826435, 2013
133. Nikoghosyan A V, Karapanagiotou-Schenkel I, Münter MW, Jensen AD, Combs SE, Debus J: Randomised trial of proton vs. carbon ion radiation therapy in patients with chordoma of the skull base, clinical phase III study HIT-1-Study. **BMC Cancer 10**:607, 2010
134. Noel G, Gondi V: Proton therapy for tumors of the base of the skull. **Chinese Clin Oncol 5**:51–51, 2016

135. O'Connell JX, Renard LG, Liebsch NJ, Efird JT, Munzenrider JE, Rosenberg AE: Base of skull chordoma: A correlative study of histologic and clinical features of 62 cases. **Cancer 74**:2261–2267, 1994
136. Oakley GJ, Fuhrer K, Seethala RR: Brachyury, SOX-9 and podoplanin, new markers in the skull base chordoma vs chondrosarcoma differential: a tissue microarray-based comparative analysis. **Mod Pathol 21**:1461–1469, 2008
137. Ora il Cnao di Pavia «esporta» l'alta tecnologia per battere i tumori - Il Sole 24 ORE: Available: https://www.ilsole24ore.com/art/impresa-e-territori/2017-10-20/ora-cnao-pavia-esporta-l-alta-tecnologia-battere-tumori-131806.shtml?uuid=AEO7qhsC&refresh_ce=1.
138. Pamir MN, Özduman K: Analysis of radiological features relative to histopathology in 42 skull-base chordomas and chondrosarcomas. **Eur J Radiol 58**:461–470, 2006
139. Park J-I, Venteicher AS, Hong JY, Choi J, Jun S, Shkreli M, et al: Telomerase modulates Wnt signalling by association with target gene chromatin. **Nature 460**:66–72, 2009
140. Park J-B, Lee C-K, Koh J-S, Lee J-K, Park E-Y, Riew KD: Overexpressions of nerve growth factor and its tropomyosin-related kinase A receptor on chordoma cells. **Spine (Phila Pa 1976) 32**:1969–73, 2007
141. Posse de Chaves EI: Sphingolipids in apoptosis, survival and regeneration in the nervous system. **Biochim Biophys Acta - Biomembr 1758**:1995–2015, 2006
142. Presneau N, Shalaby A, Idowu B, Gikas P, Cannon SR, Gout I, et al: Potential therapeutic targets for chordoma: PI3K/AKT/TSC1/TSC2/mTOR pathway. **Br J Cancer 100**:1406–1414, 2009
143. Prevedello DM, Pinheiro-Neto CD, Fernandez-Miranda JC, Carrau RL, Snyderman CH, Gardner PA, et al: Vidian Nerve Transposition for Endoscopic Endonasal Middle Fossa Approaches. **Oper Neurosurg 67**:ons478-ons484, 2010
144. Ramesh T, Nagula S V, Tardieu GG, Saker E, Shoja M, Loukas M, et al: Update on the Notochord Including its Embryology, Molecular Development, and Pathology: A Primer for the Clinician. **Cureus 9**:e1137, 2017

145. RARECARE - Surveillance of Rare Cancers in Europe: Available: http://www.rarecare.eu/rarecancers/rarecancers.asp.
146. Ravikumar B, Sarkar S, Davies JE, Futter M, Garcia-Arencibia M, Green-Thompson ZW, et al: Regulation of Mammalian Autophagy in Physiology and Pathophysiology. **Physiol Rev 90**:1383–1435, 2010
147. Rhoton A: **Rhoton Cranial Anatomy and Surgical Approaches**. Congress of Neurological Surgeons (ed), Schaumburg, IL, 2003
148. Ribbert H: Ueber die e Ecchondrosis physaliphora sphenooccipitalis. **Zentralbl Allg Pathol Anat 5**:457–61, 1894
149. Ribbert H: Ueber die experimentelle Erzeugung einer Ecchondrosis physaliphora. **Verh Dtsch Kongr Inn Med 13**:455–64, 1895
150. Riva P, Crosti F, Orzan F, Dalprà L, Mortini P, Parafioriti A, et al: Mapping of candidate region for chordoma development to 1p36.13 by LOH analysis. **Int J Cancer 107**:493–497, 2003
151. Rizzuto R, Pinton P, Carrington W, Fay FS, Fogarty KE, Lifshitz LM, et al: Close contacts with the endoplasmic reticulum as determinants of mitochondrial Ca2+ responses. **Science 280**:1763–6, 1998
152. Russo SB, Tidhar R, Futerman AH, Cowart LA: Myristate-derived d16:0 sphingolipids constitute a cardiac sphingolipid pool with distinct synthetic routes and functional properties. **J Biol Chem 288**:13397–409, 2013
153. Sa JK, Lee I-H, Hong SD, Kong D-S, Nam D-H, Sa JK, et al: Genomic and transcriptomic characterization of skull base chordoma. **Oncotarget 8**:1321–1328, 2017
154. Sadler TW (Thomas W.: **Langman's Medical Embryology**.
155. Sahyouni R, Goshtasbi K, Mahmoodi A, Chen JW: A historical recount of chordoma. **J Neurosurg Spine 28**:422–428, 2018
156. Santegoeds RGC, Temel Y, Beckervordersandforth JC, Van Overbeeke JJ, Hoeberigs CM: State-of-the-Art Imaging in Human Chordoma of the Skull Base. **Curr Radiol Rep 6**:16, 2018
157. Santos P, Peck KK, Arevalo-Perez J, Karimi S, Lis E, Yamada Y, et al: T1-Weighted Dynamic Contrast-Enhanced MR Perfusion Imaging Characterizes Tumor Response to Radiation Therapy in Chordoma. **Am J Neuroradiol 38**:2210–2216, 2017

158. Scarlatti F, Sala G, Ricci C, Maioli C, Milani F, Minella M, et al: Resveratrol sensitization of DU145 prostate cancer cells to ionizing radiation is associated to ceramide increase. **Cancer Lett 253**:124–30, 2007

159. Scheil S, Brüderlein S, Liehr T, Starke H, Herms J, Schulte M, et al: Genome-wide analysis of sixteen chordomas by comparative genomic hybridization and cytogenetics of the first human chordoma cell line, U-CH1. **Genes Chromosomes Cancer 32**:203–11, 2001

160. Scheipl S, Barnard M, Cottone L, Jorgensen M, Drewry DH, Zuercher WJ, et al: EGFR inhibitors identified as a potential treatment for chordoma in a focused compound screen. **J Pathol 239**:320–34, 2016

161. Schenck M, Carpinteiro A, Grassmé H, Lang F, Gulbins E: Ceramide: Physiological and pathophysiological aspects. **Arch Biochem Biophys 462**:171–175, 2007

162. Schwab J, Antonescu C, Boland P, Healey J, Rosenberg A, Nielsen P, et al: Combination of PI3K/mTOR inhibition demonstrates efficacy in human chordoma. **Anticancer Res 29**:1867–71, 2009

163. Schwab JH, Boland PJ, Agaram NP, Socci ND, Guo T, O'Toole GC, et al: Chordoma and chondrosarcoma gene profile: implications for immunotherapy. **Cancer Immunol Immunother 58**:339–349, 2009

164. Sekhar LN, Fessler RG: **Atlas of Neurosurgical Techniques. Brain**. Thieme

165. Sen C, Triana AI, Berglind N, Godbold J, Shrivastava RK: Clival chordomas: clinical management, results, and complications in 71 patients. **J Neurosurg 113**:1059–1071, 2010

166. Sentelle RD, Senkal CE, Jiang W, Ponnusamy S, Gencer S, Panneer Selvam S, et al: Ceramide targets autophagosomes to mitochondria and induces lethal mitophagy. **Nat Chem Biol 8**:831–838, 2012

167. Shah SR, David JM, Tippens ND, Mohyeldin A, Martinez-Gutierrez JC, Ganaha S, et al: Brachyury-YAP Regulatory Axis Drives Stemness and Growth in Cancer. **Cell Rep 21**:495–507, 2017

168. Shimizu S, Kanaseki T, Mizushima N, Mizuta T, Arakawa-Kobayashi S, Thompson CB, et al: Role of Bcl-2 family proteins in a non-apoptotic programmed cell death dependent on autophagy genes. **Nat Cell Biol 6**:1221–1228, 2004

169. Sims K, Haynes CA, Kelly S, Allegood JC, Wang E, Momin A, et al: Kdo2-lipid A, a TLR4-specific agonist, induces de novo sphingolipid biosynthesis in RAW264.7 macrophages, which is essential for induction of autophagy. **J Biol Chem 285**:38568–79, 2010

170. Spiegel S, Milstien S: Sphingosine-1-phosphate: an enigmatic signalling lipid. **Nat Rev Mol Cell Biol 4**:397–407, 2003

171. Stacchiotti S, Marrari A, Tamborini E, Palassini E, Virdis E, Messina A, et al: Response to imatinib plus sirolimus in advanced chordoma. **Ann Oncol 20**:1886–94, 2009

172. Stacchiotti S, Tamborini E, Lo Vullo S, Bozzi F, Messina A, Morosi C, et al: Phase II study on lapatinib in advanced EGFR-positive chordoma. **Ann Oncol 24**:1931–6, 2013

173. Stacchiotti S, Longhi A, Ferraresi V, Grignani G, Comandone A, Stupp R, et al: Phase II study of imatinib in advanced chordoma. **J Clin Oncol 30**:914–20, 2012

174. Stacchiotti S, Sommer J, Chordoma Global Consensus Group: Building a global consensus approach to chordoma: A position paper from the medical and patient community. **Lancet Oncol 16**:e71–e83, 2015

175. Stemple DL: Structure and function of the notochord: an essential organ for chordate development. **Development 132**:2503–12, 2005

176. Stiban J, Fistere D, Colombini M: Dihydroceramide hinders ceramide channel formation: Implications on apoptosis. **Apoptosis 11**:773–780, 2006

177. Stippler M, Gardner PA, Snyderman CH, Carrau RL, Prevedello DM, Kassam AB: ENDOSCOPIC ENDONASAL APPROACH FOR CLIVAL CHORDOMAS. **Neurosurgery 64**:268–278, 2009

178. Sun X, Hornicek F, Schwab JH: Chordoma: an update on the pathophysiology and molecular mechanisms. **Curr Rev Musculoskelet Med 8**:344–52, 2015

179. Tamborini E, Miselli F, Negri T, Lagonigro MS, Staurengo S, Dagrada GP, et al: Molecular and biochemical analyses of platelet-derived growth factor receptor (PDGFR) B, PDGFRA, and KIT receptors in chordomas. **Clin Cancer Res 12**:6920–8, 2006

180. Tamborini E, Virdis E, Negri T, Orsenigo M, Brich S, Conca E, et al: Analysis of receptor tyrosine kinases (RTKs) and downstream pathways in chordomas. **Neuro Oncol 12**:776–89, 2010

181. Tauziéde-Espariat A, Bresson D, Polivka M, Bouazza S, Labrousse F, Aronica E, et al: Prognostic and Therapeutic Markers in Chordomas: A Study of 287 Tumors. **J Neuropathol Exp Neurol 75**:111–20, 2016

182. Tian K, Wang L, Ma J, Wang K, Li D, Du J, et al: MR Imaging Grading System for Skull Base Chordoma. **AJNR Am J Neuroradiol 38**:1206–1211, 2017

183. Tian K, Wang L, Wang K, Ma J, Li D, Hao S, et al: Analysis of Clinical Features and Outcomes of Skull Base Chordoma in Different Age-Groups. **World Neurosurg 92**:407–417, 2016

184. Tian K, Zhang H, Ma J, Wang K, Ru X, Du J, et al: Factors for Overall Survival in Patients with Skull Base Chordoma: A Retrospective Analysis of 225 Patients. **World Neurosurg 97**:39–48, 2017

185. Triana A, Sen C, Wolfe D, Hazan R: Cadherins and catenins in clival chordomas: correlation of expression with tumor aggressiveness. **Am J Surg Pathol 29**:1422–34, 2005

186. Truman J-P, García-Barros M, Obeid LM, Hannun YA: Evolving concepts in cancer therapy through targeting sphingolipid metabolism. **Biochim Biophys Acta - Mol Cell Biol Lipids 1841**:1174–1188, 2014

187. Tuson M, Marfany G, Gonzàlez-Duarte R: Mutation of CERKL, a novel human ceramide kinase gene, causes autosomal recessive retinitis pigmentosa (RP26). **Am J Hum Genet 74**:128–38, 2004

188. van Straaten HW, Hekking JW, Thors F, Wiertz-Hoessels EL, Drukker J: Induction of an additional floor plate in the neural tube. **Acta Morphol Neerl Scand 23**:91–7, 1985

189. Vaz-Guimaraes F, Nakassa ACI, Gardner PA, Wang EW, Snyderman CH, Fernandez-Miranda JC: Endoscopic Endonasal Approach to the Ventral Jugular Foramen: Anatomical Basis, Technical Considerations, and Clinical Series. **Oper Neurosurg 13**:482–491, 2017

190. Vinagre J, Pinto V, Celestino R, Reis M, Pópulo H, Boaventura P, et al: Telomerase promoter mutations in cancer: An emerging molecular biomarker? **Virchows Arch 465**:119–133, 2014

191. Virchow R: **Untersuchungen Ueber Die Entwicklung Des Schaedelgrundes**. Berlin: G Rimer, 1857

192. Visocchi M, Pappalardo G, Pileggi M, Signorelli F, Paludetti G, La Rocca G: Experimental Endoscopic Angular Domains of Transnasal and Transoral Routes to the Craniovertebral Junction. **Spine (Phila Pa 1976) 41**:669–677, 2016

193. Visocchi M, Della Pepa GM, Doglietto F, Esposito G, La Rocca G, Massimi L: Video-assisted microsurgical transoral approach to the craniovertebral junction: personal experience in childhood. **Child's Nerv Syst 27**:825–831, 2011

194. Visocchi M, Doglietto F, Della Pepa GM, Esposito G, La Rocca G, Di Rocco C, et al: Endoscope-assisted microsurgical transoral approach to the anterior craniovertebral junction compressive pathologies. **Eur Spine J 20**:1518–25, 2011

195. Vujovic S, Henderson S, Presneau N, Odell E, Jacques T, Tirabosco R, et al: Brachyury, a crucial regulator of notochordal development, is a novel biomarker for chordomas. **J Pathol 209**:157–165, 2006

196. Wadsworth JM, Clarke DJ, McMahon SA, Lowther JP, Beattie AE, Langridge-Smith PRR, et al: The Chemical Basis of Serine Palmitoyltransferase Inhibition by Myriocin. **J Am Chem Soc 135**:14276–14285, 2013

197. Walcott BP, Nahed B V, Mohyeldin A, Coumans J-V, Kahle KT, Ferreira MJ: Chordoma: current concepts, management, and future directions. **Lancet Oncol 13**:e69-76, 2012

198. Wang L, Tian K, Wang K, Ma J, Ru X, Du J, et al: Factors for tumor progression in patients with skull base chordoma. **Cancer Med 5**:2368–2377, 2016
199. Wasserman JK, Gravel D, Purgina B: Chordoma of the Head and Neck: A Review. **Head Neck Pathol 12**:261–268, 2018
200. Weber DC, Malyapa R, Albertini F, Bolsi A, Kliebsch U, Walser M, et al: Long term outcomes of patients with skull-base low-grade chondrosarcoma and chordoma patients treated with pencil beam scanning proton therapy. **Radiother Oncol 120**:169–174, 2016
201. Weber DC, Rutz HP, Pedroni ES, Bolsi A, Timmermann B, Verwey J, et al: Results of spot-scanning proton radiation therapy for chordoma and chondrosarcoma of the skull base: The Paul Scherrer Institut experience. **Int J Radiat Oncol 63**:401–409, 2005
202. Weinberger PM, Yu Z, Kowalski D, Joe J, Manger P, Psyrri A, et al: Differential expression of epidermal growth factor receptor, c-Met, and HER2/neu in chordoma compared with 17 other malignancies. **Arch Otolaryngol Head Neck Surg 131**:707–11, 2005
203. Who: WHO classification of tumours of soft tissue. **WHO Classif Tumours Soft Tissue Bone Fourth Ed 46**:10–12, 2013
204. Winn HR: **Youmans and Winn Neurological Surgery**.
205. Wu Z, Zhang J, Zhang L, Jia G, Tang J, Wang L, et al: Prognostic factors for long-term outcome of patients with surgical resection of skull base chordomas—106 cases review in one institution. **Neurosurg Rev 33**:451–456, 2010
206. Xu Z, Zhou J, McCoy DM, Mallampalli RK: LASS5 is the predominant ceramide synthase isoform involved in de novo sphingolipid synthesis in lung epithelia. **J Lipid Res 46**:1229–38, 2005
207. Yakkioui Y, van Overbeeke JJ, Santegoeds R, van Engeland M, Temel Y: Chordoma: the entity. **Biochim Biophys Acta 1846**:655–69, 2014
208. Yamagata M, Obara K, Kihara A: Sphingolipid synthesis is involved in autophagy in Saccharomyces cerevisiae. **Biochem Biophys Res Commun 410**:786–791, 2011

209. Yang L, Zheng L-Y, Tian Y, Zhang Z-Q, Dong W-L, Wang X-F, et al: C6 ceramide dramatically enhances docetaxel-induced growth inhibition and apoptosis in cultured breast cancer cells: a mechanism study. **Exp Cell Res 332**:47–59, 2015

210. Yang XR, Ng D, Alcorta D a, Liebsch NJ, Sheridan E, Li S, et al: T (brachyury) gene duplication confers major susceptibility to familial chordoma. **Nat Genet 41**:1176–8, 2009

211. Yeom KW, Lober RM, Mobley BC, Harsh G, Vogel H, Allagio R, et al: Diffusion-Weighted MRI: Distinction of Skull Base Chordoma from Chondrosarcoma. **Am J Neuroradiol 34**:1056–1061, 2013

212. Younus I, Forbes JA, Ordóñez-Rubiano EG, Avendano-Pradel R, la Corte E, Anand VK, et al: Radiation therapy rather than prior surgery reduces extent of resection during endonasal endoscopic reoperation for craniopharyngioma. **Acta Neurochir (Wien)**:2018

213. Youssef AS, Sloan AE: Extended Transoral Approaches. **Neurosurgery 66**:A126–A134, 2010

214. Yu L, Alva A, Su H, Dutt P, Freundt E, Welsh S, et al: Regulation of an ATG7-beclin 1 Program of Autophagic Cell Death by Caspase-8. **Science (80-) 304**:1500–1502, 2004

215. Zenker F: Ueber die gallertgeschwulste des Clivus Blumenbachii (Ecchondro- sis prolifera, Virchow). **Virchows Arch 12**:407–412, 1857

216. Zhai Y, Bai J, Wang S, Du J, Wang J, Li C, et al: Differences in Dural Penetration of Clival Chordomas Are Associated with Different Prognosis and Expression of Platelet-Derived Growth Factor Receptor-β. **World Neurosurg 98**:288–295, 2017

217. Zheng W, Kollmeyer J, Symolon H, Momin A, Munter E, Wang E, et al: Ceramides and other bioactive sphingolipid backbones in health and disease: Lipidomic analysis, metabolism and roles in membrane structure, dynamics, signaling and autophagy. **Biochim Biophys Acta - Biomembr 1758**:1864–1884, 2006

218. Zou M-X, Lv G-H, Wang X-B, Huang W, Li J, Jiang Y, et al: Clinical Impact of the Immune Microenvironment in Spinal Chordoma: Immunoscore as an Independent Favorable Prognostic Factor. **Neurosurgery 0**:1–16, 2018

219. Zou MX, Lv GH, Zhang QS, Wang SF, Li J, Wang X Bin: Prognostic Factors in Skull Base Chordoma: A Systematic Literature Review and Meta-Analysis. **World Neurosurg 109**:307–327, 2018

220. Zuckerman SL, Bilsky MH, Laufer I: Chordomas of the Skull Base, Mobile Spine, and Sacrum: An Epidemiologic Investigation of Presentation, Treatment, and Survival. **World Neurosurg 113**:e618–e627, 2018

SCIENTIFIC PRODUCTS

PEER-REVIEWED PUBLICATIONS

[***** denotes the scientific product strictly related to the present PhD thesis work]

1. La Corte Emanuele, Younus I, Pivari F, Selimi A, Ottenhausen M, Forbes JA, Pisapia DJ, Dobri GA, Anand VK, Schwartz TH. **BRAF V600E mutant papillary craniopharyngiomas: a single-institutional case series.** Pituitary. 2018 Dec;21(6):571-583. doi: 10.1007/s11102-018-0909-z.

2. La Corte Emanuele, Selimi A, Ottenhausen M, Forbes JA, Arnaout MM, Ferroli P, Serrao G, Anand VK, Schwartz TH. **Anterior communicating artery division in the endoscopic endonasal translamina terminalis approach to the third ventricle: an anatomical feasibility study.** Acta Neurochir (Wien). 2018 Nov 14. doi: 10.1007/s00701-018-3709-3. [Epub ahead of print]

3. Zattra C, Schiariti MP, La Corte Emanuele, Broggi M, Acerbi F, Ferroli P. **Atlanto-axial rotatory fixation complicating ventriculo-peritoneal shunt surgery: a case report and literature review.** Childs Nerv Syst. 2018 Oct 1. doi: 10.1007/s00381-018-3983-7. [Epub ahead of print]

4. ***** La Corte Emanuele, Broggi M, Bosio L, Danesi G, Ferroli P, **Tailored Surgical Strategy in Clival Chordomas: an Extraordinary Selection Bias that Limits Approach Comparison.** *J Neurosurg Sci. 2018 Aug;62(4):519-521. doi: 10.23736/S0390-5616.17.03986-8. Epub 2017 Oct 23.*

5. Ferroli P, La Corte Emanuele, Bertolini G, Serrao G, Acerbi F, **Anterior cerebral artery revascularization: superficial temporal artery-callosomarginal artery bypass using a contralateral superficial temporal artery interposition graft**. *J Neurosurg Sci*. 2018 Aug;62(4):529-531. doi: 10.23736/S0390-5616.16.03936-9. Epub 2016 Dec 16.

6. Younus I, Forbes JA, Ordóñez-Rubiano EG, Avendano-Pradel R, La Corte Emanuele, Anand VK, Schwartz TH, **Radiation therapy rather than prior surgery reduces extent of resection during endonasal endoscopic reoperation for craniopharyngioma.** *Acta Neurochir* (Wien). 2018 Jul;160(7):1425-1431. doi: 10.1007/s00701-018-3567-z. Epub 2018 May 25.

7. Forbes JA, Banu M, Lehner K, Ottenhausen M, La Corte Emanuele, Alalade AF, Ordóñez-Rubiano EG, Greenfield JP, Anand VK, Schwartz TH. **Endoscopic endonasal resection of epidermoid cysts involving the ventral cranial base.** *J Neurosurg*. 2018 Jun 8:1-10. doi: 10.3171/2017.12.JNS172575. [Epub ahead of print]

8. Ottenhausen M, Rumalla K, Alalade AF, Nair P, La Corte Emanuele, Younus I, Forbes JA, Ben Nsir A, Banu MA, Tsiouris AJ, Schwartz TH, **Decision-making algorithm for minimally invasive approaches to anterior skull base meningiomas.** *Neurosurg Focus*. 2018 Apr;44(4):E7. doi: 10.3171/2018.1.FOCUS17734

9. Acerbi F, Broggi M, Schebesch KM, Höhne J, Cavallo C, De Laurentis C, Eoli M, Anghileri E, Servida M, Boffano C, Pollo B, Schiariti M, Visintini S, Montomoli C, Bosio L, La Corte Emanuele, Broggi G, Brawanski A, Ferroli P. **Fluorescein-guided surgery for resection of high-grade gliomas: A multicentric prospective phase II study (FLUOGLIO).** *Clin Cancer Res*. 2018 Jan 1;24(1):52-61. doi: 10.1158/1078-0432.CCR-17-1184.

10. Ottenhausen M, Rumalla K, La Corte Emanuele, Alalade A, Nair P, Forbes J, Ben Nsir A, Schwartz TH. **Treatment strategies for craniopharyngiomas.** *J Neurosurg Sci*. 2017 Sep 4. doi: 10.23736/S0390-5616.17.04171-6. [Epub ahead of print]

11. * La Corte Emanuele, Aldana PR, **Endoscopic Approach to the Upper Cervical Spine and Clivus: An Anatomical Study of the Transoral Corridor.** *Acta Neurochir (Wien)*. 2017 Apr;159(4):633-639. doi: 10.1007/s00701-017-3103-6.

12. Ferroli P, Broggi M, Schiavolin S, Acerbi F, Bettamio V, Caldiroli D, Cusin A, La Corte Emanuele, Leonardi M, Raggi A, Schiariti M, Visintini S, Franzini A, Broggi G, **Predicting functional impairment in brain tumor surgery: the Big Five and the Milan Complexity Scale** *Neurosurg Focus.* 2015 Dec;39(6):E14. doi: 10.3171/2015.9.FOCUS15339

PUBLISHED ABSTRACTS, ORAL & POSTER PRESENTATIONS

1. * La Corte Emanuele, Patanè M, Calatozzolo C, Maderna E, Raggi A, Dei Cas M, Paroni R, Ghidoni R, Ferroli P, Pollo B *De-novo* **ceramide synthesis in skull base chordomas suggests a correlation with tumor proliferation**, *Neuro-Oncology*, Volume 20, Issue suppl_3, 19 September 2018, Pages iii273, https://doi.org/10.1093/neuonc/noy139.216 (Oral presentation, October 2018, Stocholm, Sweden)

2. * Dei Cas M, La Corte Emanuele, Patanè M, Calatozzolo C, Maderna E, Raggi A, Ferroli P, Pollo B, Ghidoni R, Paroni R *Chordoma Sphingolipidomics* (Oral presentation, Sphingolipid Italian Day, October 2018, Milan, Italy)

3. * Patanè M, La Corte Emanuele, Calatozzolo C, Paterra R, Campisi GM, Dei Cas M, Ghidoni R, Ferroli P, Pollo B, **A multimodal approach to study skull-base chordomas and their tendency to recur** *Clinical Neuropathology*, 2018 Vol. 37– No. 3/2018 (112-145) DOI 10.5414/NPP37112 e-pub: May 3, 2018 Joint meeting: 54th Congress of the Italian Association of Neuropathology and Clinical Neurobiology (AINPeNC) / 44th Congress of the Italian Association for Cerebral Aging Research (AIRIC), (Oral presentation, May 17 – 19 2018, Milan, Italy) ISSN 0722-5091

4. * La Corte Emanuele, Patanè M, Campisi GM, Paroni RC, Serrao G, Milanesi I, Visintini S, Ferroli P, Ghidoni R, Pollo B, **Molecular and clinical bio-markers in a series of 48 consecutive skull base chordoma patients** *Neuro-Oncology.* 2017 May;19 (suppl_3):iii36. DOI:10.193/neuonc/nox036.128 (Poster presentation, 5th Quadrennial WFNOS Meeting, Zurich). ISSN 1522-8517

5. Schiariti MP, Monti E, Bertolini B, Restelli F, Pollo B, Broggi M, Acerbi F, La Corte Emanuele, Ferroli P, **Treatment of thalamic glial lesions: surgery versus biopsy** *Neuro-Oncology.* 2017 May;19 (suppl_3):iii112. DOI:10.193/neuonc/nox036.430 (Poster presentation, 5th Quadrennial WFNOS Meeting, Zurich). ISSN 1522-8517

6. La Corte Emanuele, Acerbi F, Maccari A, Serrao G, Felisati G, Ferroli P, **The use of a peel-away catheter as a working channel in pediatric endoscopic endonasal surgery: a technical note**. *Journal of Neurological Surgery Part B*. 2016; Issue S02, 77 (Oral presentation, European Skull Base Society Congress, Berlin, May 2016).

7. Villa SL, Broggi M, Bosio L, La Corte Emanuele, Restelli, F Ferroli P, **How to Avoid Complication in Endoscopic Trans-Nasal Skull Base Surgery: Lesson Learned from the Last 129 Consecutive Cases,** *Journal of Neurological Surgery Part B*. 2016; Issue S02, 77 (Oral presentation, European Skull Base Society Congress, Berlin, May 2016).

FUNDINGS

PhD School of Molecular and Translational Medicine, Department of Health Sciences, University of Milan.

LIST OF FIGURES

LIST OF TABLES

LIST OF VIDEOS